Master's thesis

NTNU
Norwegian University of Science and Technology
Faculty of Natural Sciences
Department of Chemical Engineering

Emma Solheim Cornell

A Techno-Economic Evaluation of Solvents in Biogas Upgrading

Master's thesis in Chemical Engineering and Biotechnology
Supervisor: Diego Di Domenico Pinto
Co-supervisor: Hanna Knuutila
June 2023

NTNU
Norwegian University of
Science and Technology

Emma Solheim Cornell

A Techno-Economic Evaluation of Solvents in Biogas Upgrading

Master's thesis in Chemical Engineering and Biotechnology
Supervisor: Diego Di Domenico Pinto
Co-supervisor: Hanna Knuutila
June 2023

Norwegian University of Science and Technology
Faculty of Natural Sciences
Department of Chemical Engineering

NTNU
Norwegian University of
Science and Technology

Declaration of Compliance

I, Emma Solheim Cornell, hereby declare that this is independent work according to the exam regulations of the Norwegian University of Science and Technology.

Place and Date: Trondheim, June 7th, 2023

Signature:

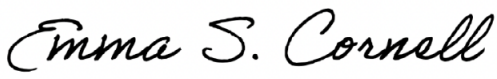

Emma Solheim Cornell

Preface

This thesis was completed in the spring of 2023 as the concluding component of the Industrial Chemistry and Biotechnology program at the Norwegian University of Science and Technology. This report was produced in partnership with the Environmental Engineering and Reactor Technology group as part of the TKP4900 Chemical Process Technology - Master's thesis course.

I would like to extend my sincere appreciation to my supervisors, Dr. Diego Di Domenico Pinto and Prof. Hanna K. Knuutila, for their invaluable guidance and support throughout this process.

Abstract

Anthropogenic greenhouse gas emissions are widely recognized as the primary contributor to global climate change. To address this issue, the integration of renewable energy sources into the energy mix is essential. Biomethane has emerged as a possible substitute for natural gas, with potential use as clean vehicle fuel and injection into the gas grid. However, the cleaning and upgrading process of biogas to biomethane can be costly and energy-intensive.

Various carbon dioxide (CO_2) removal processes, including chemical scrubbing, are available for biogas treatment. The solvent for chemical scrubbing has to meet a number of requirements, including low degradation rate, high CO_2 capacity, and low regeneration energy demand. Amines, despite being effective, pose challenges in terms of cost and potential environmental impacts associated with emissions and degradation. Amino acid salts have been proposed as a solution to mitigate amine-related issues due to their ionic nature and high biodegradability, which offers potential benefits compared to amines.

This thesis evaluates two solvents, namely sodium glycinate (NaGly) and piperazine-promoted methyl diethanolamine, known as aMDEA, for chemical scrubbing in terms of regeneration energy requirements. Process modifications including intercooled absorber were implemented. A comparison was made with previous work on piperazine-promoted aminomethyl propanol, known as CESAR1, and monoethanolamine (MEA). Simulations using the ProTreat® software tool, along with experimental data, were conducted to investigate the performance of the solvents.

The validation of the models revealed large deviations between datasets and the NaGly model. Precipitation experiments were conducted with 45 wt% and 35 wt% NaGly, demonstrating precipitation occurrence at low loadings. Simulation results showed a minimum specific reboiler duty of 2.83 MJ/kg CO_2 for NaGly, comparable to that obtained with MEA (2.77 MJ/kg CO_2). Activated MDEA exhibited the lowest energy requirements at 1.716 MJ/kg CO_2 before CESAR1 (2.06 MJ/kg CO_2).

Furthermore, an economic analysis was performed for two aMDEA cases at atmospheric and 8 bar pressures. Subsidies covering up to 45% of CAPEX, and the potential for selling carbon credits were evaluated. Although the 8 bar case had lower regeneration energy requirements, the economic analysis indicated a shorter payback period for the 1.05 bar case. Depending on subsidy levels and carbon credit sales, the payback time ranged from three to nine years.

Sammendrag

Antropogene klimagassutslipp er anerkjent som hovedårsaken til globale klimaendringer. For å begrense virkningene av klimaendringer er integrasjonen av fornybare energikilder i energisammensetningen avgjørende. Biometan har vist seg å være en lovende erstatning for naturgass, men rensing av biogass står ovenfor utfordringer knyttet til kostnad og energiforbruk, og er en flaskehals for økt produksjon av biometan.

Det finnes ulike prosesser for fjerning av karbondioksid (CO_2) fra biogass, inkludert kjemisk absorpsjon. Løsningsmidlene for kjemisk absorpsjon må innfri en rekke krav, inkludert lav nedbrytningsrate, høy CO_2-kapasitet og lave energibehov ved regenerering. Aminer, til tross for sin effektivitet, utfordres med hensyn til kostnader og potensielle miljøpåvirkninger knyttet til utslipp og nedbrytning. Aminosyre-salter er foreslått som en løsning for å redusere problemer knyttet til aminer, på grunn av deres ioniske egenskaper og høye nedbrytbarhet, som tilbyr potensielle fordeler sammenlignet med aminer.

Denne mastergradsavhandlingen vurderer to løsningsmidler, nemlig aminosyre-saltet natriumglycinat (NaGly) og aminbladingen piperazin-aktivert metyldietanolamin (aMDEA), for kjemisk skrubbing i forhold til energibehov ved regenerering. Ulike prosessmodifikasjoner, inkludert kjølt absorber ble evaluert. En sammenligning blir gjort med forfatterens tidligere arbeid med piperazin-aktivert aminometylpropanol, kjent som CESAR1, og monoetanolamin (MEA). Simuleringer ved hjelp av programvareverktøyet ProTreat®, sammen med eksperimentelle data, ble utført for å undersøke ytelsen til løsningsmidlene.

Validering av modeller viste høye avvik mellom datasettene og NaGly-modellen. Eksperimenter ble utført med 45 wt% og 35 wt% NaGly og viste at utfelling skjedde ved lave CO_2-konsentrasjoner. Simuleringsresultatene viste et minimum energibehov på 2.83 MJ/kg CO_2, som er sammenlignbart med MEAs(2.77 MJ/kg CO_2). Aktivert MDEA viste de laveste energibehovene på 1.716 MJ/kg CO_2, foran CESAR1 (2.06 MJ/kg CO_2).

En økonomisk analyse ble utført av to studier med aMDEA, ved atmosfærisk trykk og åtte bars trykk. Muligheten for salg av CO_2 kvoter, samt subsidier som dekket inntil 45% av investringskostnader, ble vurdert. Til tross for at studiet med åtte bars trykk hadde lavere energibehov, indikerte den økonomiske analysen kortere tilbakebetalingstid for studiet med 1.05 bars trykk. Avhengig av subsidiegrad og kvotesalg varierte tilbakebetalingstiden fra tre til ni år.

Table of Contents

List of Figures

List of Tables

Abbreviations

AARD Absolute Average Relative Deviation.
AAS amino acid salt.
aMDEA Activated MDEA.
AMP 2-amino-2-methyl-1-propanol.
ARD Average Relative Deviation.

CCS Carbon Capture and Storage.
CEPCI Chemical engineering Plant Cost Index.
CH_4 methane.
CO_2 Carbon dioxide.

D&E Design and Engineering.

GHG greenhouse gas.

H_2O water.
H_2S Hydrogen sulfide.
HHV higher heating value.
HSE Health, safety and environment.

IC intercooler.
IPCC Intergovernmental Panel of Climate Change.
ISBL inside battery limits.

KGly potassium glycinate.
KOH Potassium hydroxide.

LHV lower heating value.
LVR Lean vapor recompression.

MDEA Methyldiethanolamine.
MEA Monoethanolamine.

NaGly Sodium glycinate.
NaOH Sodium hydroxide.
NTNU Norwegian University of Science and Technology.

OSBL outside battery limits.

PCC Post-combustion capture.
ppm parts per million.
PSA pressure swing adsorption.
PZ Piperazine.

TOC Total Organic Carbon.

VLE vapor-liquid equilibrium.
VOC volatile organic compound.

WI Wobbe index.
wt% Weight percentage.

X Contingency.

Chapter 1

Introduction

In this chapter the background and motivation for studying biogas is given, as well as the scope and an outline of the thesis.

1.1 Background and Motivation

Climate change is defined by The American Meterological Society as any systematic change in the long-term statistics of climate elements (such as temperature, pressure or winds) sustained over several decades or longer, and is recognized as one of the most significant challenges confronting humanity today[7]. While the Earth has undergone natural climatic changes historically, the rapid increase in global average temperature is largely attributed to human activities[8]. The concentration of the so-called greenhouse gases (GHGs), with carbon dioxide (CO_2) being the most significant, has risen dramatically in recent decades, primarily due to industrial processes and burning of fossil fuels. Figure 1 shows the global atmospheric CO_2 concentration over the past 2000 years, clearly indicating a rapid increase from around the industrial revolution (1850s). Increased concentrations of GHGs in the atmosphere have led to observable changes in

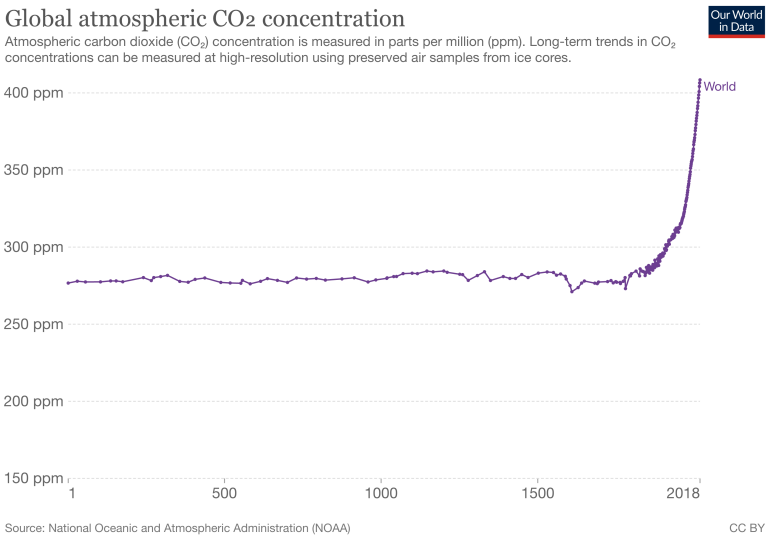

Figure 1: Global atmospheric CO_2 concentration, from Our World in Data[1]

the Earth's climate across all climatic regions[9]. This includes increased frequency of extreme weather events, such as droughts, rising sea levels, heat waves and tropical storms, creating

problems and threatening both human and animal life. It is crucial that efforts are made to mitigate climate change as it poses a significant threat to the well-being of future generations.

To address this issue, various international agreements have been made in order to try to mitigate climate change. In 1997, the Kyoto protocol was adopted, legally binding emission reduction targets for developed countries[10]. In 2015, the Paris Agreement set the goal to limit the global temperature increase to well below 2 °C before the end of the 21. century[11].

One of the major challenges in mitigating climate change, is the transition to carbon-neutral energy, which requires a move away from the use of fossil-based energy sources. However, as of 2021, fossil-based energy sources still accounted for 86% of the global primary energy mix, and with economic growth, the demand for energy is expected to increase further[12]. In order to succeed with the energy transition, renewable energy must become a larger share of the energy mix. Natural gas currently accounts for 25% of the global energy consumption, and one promising alternative that can become a potential direct replacement, is biomethane.

Biogas is a renewable energy source, produced by anaerobic digestion of organic matter such as food and agricultural waste, as well as sludge. Biogas is a gaseous mixture mainly composed of CO_2 and methane (CH_4), as well as impurities such as hydrogen sulfide (H_2S), ammonium (NH_4) and water vapor. Currently, biogas is primarily used for electricity generation through direct combustion, or in combined heat and power plants[13]. However, these methods do not fully exploit its potential resulting in reduced conversion efficiencies and limited heat recovery. Biogas upgrading refers to the process of removing CO_2, and ensuring a biomethane that meets the regulations for its intended use. Biomethane can be utilized as vehicle fuel or as a substitute in the natural gas grid. Technologies for upgrading biogas include water scrubbing, membrane separation, pressure swing adsorption (PSA) and chemical scrubbing. The main challenge connected to wider adoption of biomethane is the availability of low-cost and energy-efficient technologies for processing biogas, and the development of such technologies is necessary to make biomethane economically viable for the aforementioned purposes without the need for subsidies[13]. This thesis focuses on solvent based CO_2 scrubbing processes.

Chemical scrubbing is a commonly used technique for natural gas sweetening and flue gas CO_2 capture, and has recently been gaining attention as a biogas upgrading technology. However, biogas has a higher partial pressure of CO_2 compared to flue gas, with CO_2 concentration around 40 vol%[14]. In chemical scrubbing the choice of solvent is crucial. Although amines such as MEA, have traditionally been preferred, they face challenges in commercialisation due to high energy requirements for regeneration, as well as problems related to emissions and degradation. While other second generation solvents, such as CESAR1 and activated MDEA (aMDEA) have

shown lower energy requirements than MEA, they still face problems with amine emissions and degradation. Amino acid salts (AAS) show potential as a substitute for amines, due to their similar reactive groups, lack of emissions and high biodegradability. However, the potential of precipitation and low reactivity may hinder the implementation of amino acid salts.

1.2 Scope

The aim of this study is to determine the most appropriate design and solvent for a chemical scrubbing facility for biogas upgrading, considering both energy requirements and cost. The study will compare earlier obtained simulation results using CESAR1 and MEA, with those obtained from the amine blend known as activated MDEA, and the AAS sodium glycinate (NaGly), exploring the potential of an AAS as an alternative to amines. Additionally, various process modifications will be investigated to identify the optimal configuration. The study will determine the minimum energy requirements for a fixed removal target. Finally, an economic analysis will be conducted to assess the feasibility of the optimal case.

1.3 Outline of Thesis

Chapter 1 provides an introduction to the study of biogas upgrading, as well as the objectives of the project and an outline of the thesis. In Chapter 2, the theory of biogas upgrading with chemical absorption is discussed, including an introduction of the different solvents and a review of earlier research on the subject. Chapter 3 presents a thermodynamic validation of the model used in ProTreat®, while Chapter 4 outlines the methodology of the study, including details on the design basis of the simulations and experimental work. Chapter 5 presents the results and discussion, and Chapter 6 presents the conclusions, along with suggestions for further work.

Chapter 2

Theory

2.1 Biogas Upgrading

The process of removing contaminants from biogas is commonly referred to as biogas cleaning, which is an essential treatment step to ensure the gas is of appropriate quality and to protect against equipment damage and comply with Health, Safety and Environment (HSE) regulations. Raw biogas contains a significant amount of water vapor, which can cause damage to equipment if it solidifies or reacts with other contaminants[15]. The presence of acid gases such as CO_2 and H_2S, may result in production of acids when in contact with water. The concentration of CO_2 in biogas has been reported to reach levels as high as 50 vol%, according to literature[16]. In contrast, natural gas usually exhibits a lower CO_2 concentration, typically ranging from 1-2 vol%. However, it is important to note that the partial pressure of CO_2 in natural gas can be higher due to the overall higher pressure of the gas, which in turn influences the separation process employed for CO_2 removal. Other contaminants, such as NH_3, volatile organic compounds (VOCs), siloxanes, and hydrogenated hydrocarbons, must also be removed during the cleaning process. However, the biogas cleaning process adds to the cost of biogas, making it crucial to achieve an optimized process that delivers highly concentrated biomethane with the lowest possible energy consumption. Depending on the cleaning technique, pre-treatment may be required.

One way of measuring the quality of any gas is by using the Wobbe Index (WI), which indicates the heat generated per cubic meter of gas. The WI is given by:

$$I_W = \frac{\mathrm{V_C}}{\sqrt{\mathrm{G_S}}}, \tag{1}$$

where V_C is the higher heating value (HHV), and G_s is the relative density. The HHV is a measure of the energy per volume of gas, and includes the heat of vaporization of water content in the gas. Monitoring the WI is important for gases used as fuels, as it determines the quality and influences the market price. The index also gives an indication of the gases relative ability to deliver energy, as well as the interchangeability of the fuel[17]. Often, the WI sets the standard for gas quality for the grid system, rather than the concentration of CH_4. The lower heating value (LHV) in biogas varies with the CH_4 concentration, typically ranging from 45-75%, with a LHV between 16-28 MJ/m^3. In comparison, biomethane has a LHV of 36 MJ/m^3[18]. One

benefit of increasing the WI is that it allows for a higher energy content to be delivered in a smaller volume, which can result in a higher market price for the gas. Increasing the WI is achieved by increasing the CH_4 concentration, through removal of CO_2, or by mixing in another hydrocarbon.

2.2 Different Upgrading Techniques

Figure 2 presents the distribution of technologies used for biogas upgrading in the countries: Australia, Austria, Brazil, China, Finland, Germany, Ireland, Norway, Sweden, Switzerland and the United Kingdom[2]. It can be observed that the most commonly used methods are pressure swing adsorption, membrane separation, water scrubbing, and chemical absorption[19]. All techniques can deliver a methane purity of 97%, which is the required purity for use as vehicle fuel. Most techniques require a certain degree of pre-treatment, especially removal of H_2S. Additionally, all techniques require drying, either before or after upgrading[19].

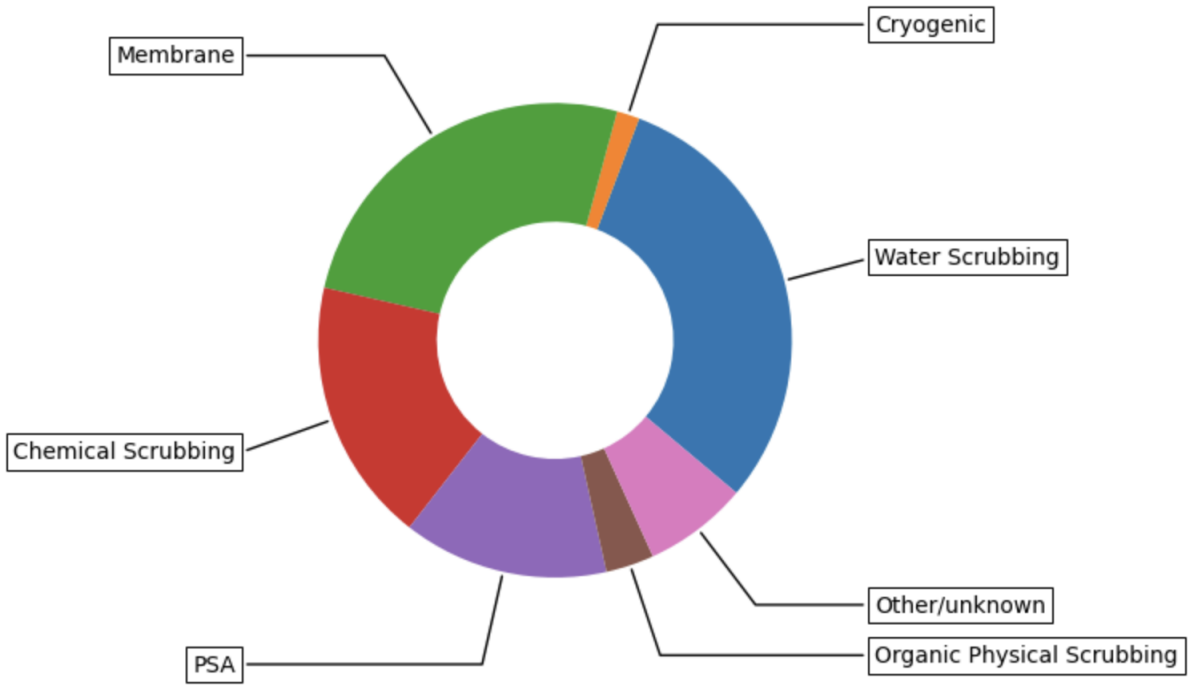

Figure 2: The allocation of technologies for biogas upgrading in operational units reported by member countries of IEA Bioenergy Task 37 is presented above[2]

The process of Pressure Swing Adsorption (PSA) utilizes the property that certain gases have a tendency to adsorb onto a surface under high pressure. When the pressure is reduced, the adsorbed molecules detach from the surface. Adsorption in PSA takes place at temperatures of around 50-60 °C, and pressures ranging from 3-7 bars. The typical adsorbents used in this

process are zeolites or activated carbon[15]. In the case of biogas upgrading, the CO_2 molecules are adsorbed at high pressures, while most of the CH_4 flows through the column. At reduced pressures, the CO_2 desorbs.

Membrane separation is a widely used technique for upgrading biogas that involves the selective transfer of certain gases across a semipermeable membrane, while retaining other gases on the same side. The separation process can be based on various properties, including chemical potential, size of molecule, or affinity for a specific molecule, and has proven to be an effective method for gas separation. In biogas upgrading, CO_2 molecules permeate the membrane, while the most of CH_4 molecules remain on the feed side. The system typically operates at around 8 bar[19].

Water scrubbing is a technique that utilizes the high solubility of CO_2, as well as other contaminants such as H_2S and NH_3 in water. Thus, H_2S removal is not a required pre-treatment step, but potentially a post-treatment step. Biogas is introduced at the bottom of a column, while water is introduced from the top, and a packed tower is used to ensure a large gas-liquid contact area. While some CH_4 may dissolve in water, its solubility is lower than that of CO_2, enabling most of the CH_4 to rise to the top of the column without dissolving. CO_2 dissolves in the water, leading to the formation of CO_2-rich water. In the presence of air or steam, the CO_2 desorbs from the water and is released, and the water can be recycled[15].

Amine scrubbing is a technique that involves absorption of CO_2 into an amine solution, where the CO_2 reacts with the amines present. This process is similar to water scrubbing, but requires regeneration of the amine solvent. The regeneration step is highly energy-intense, and is the largest challenge associated with this technology. Additionally, the choice of amines has to be carefully considered, taking into account factors such as physiochemical properties, energy requirements and environmental impact[2].

According to Bauer et al. (2013) the specific investment costs of biogas plants are largely dependent on their capacity. For plants with lower capacities (500 Nm^3/h), membrane technology is the most cost-efficient option, while for higher capacity plants (1500 Nm^3/h), there is little difference in cost between the various technologies[20]. However, the specific investment costs do not account for extra investment options or site-specific circumstances.

The specific energy demands of biogas upgrading technologies generally decrease with increasing capacity[20], but this trend is also affected by factors like operating temperature and pressure, as well as ambient temperature. Both water scrubbing and amine scrubbing have varying electricity requirements throughout different seasons, due to increased cooling water requirements

during hotter temperatures. For membranes and PSA technologies, the energy demands are highly dependent on purity level, allowable methane slip and configuration.

Compared to other technologies, amine scrubbing processes require less electricity. However, they require additional heat for the stripping of CO_2, and regeneration of amines, which is often supplied by on-site combustion of biogas. The excess heat can be used in connection with the biogas production[20].

Methane slippage from biogas upgrading facilities has two environmental impacts. Firstly, CH_4 is a potent GHG, with a global warming potential 28 times higher than CO_2[21]. Secondly, when methane is lost, it represents a loss of energy that could otherwise replace natural gas, demanding the production of additional heat. Table 1 shows the methane slippage from the most common technologies. While it might seem simple to chose a technology solely based

Table 1: Typical methane losses in different technologies[3]

Technology	Methane losses [%]
PSA	1-3.5
Water Scrubbing	1.5-1.97
Membrane	0.5-20
Amine scrubbing	0.04-0.1

on methane slips, there are additional factors that needs to be taken into account, for instance available heat, available cooling water, and size of site[22].

The European Union's Emissions Trading System (EU ETS) operates as a carbon market, allowing for trading of CO_2 quotas[23]. The European Biogas Association aims to link the sale of biomethane sale to the EU ETS sector[24], since biomethane, as a renewable energy source, can generate carbon credits through the reduction of greenhouse gas emissions from fossil fuels. When biomethane is produced and used as a substitute for fossil fuels, the resulting reduction in emissions can be quantified as carbon credits, which can be sold to businesses that need them to meet their emissions targets under the ETS. This increases the demand for biomethane, as well as being a way to support the transition to a low-carbon economy.

2.3 Chemical Scrubbing CO_2 capture

The chemical scrubbing process was patented by R.R. Bottoms in 1930, and can be observed in Figure 3[25]. The process relies on CO_2 affinity for the solvent at low temperatures, and the reverse at higher temperatures. Chemical scrubbing is applicable for capturing CO_2 from different gas mixtures including natural gas, flue gas, and biogas. In the case of biogas upgrading, the gas is inserted at the bottom of the absorber column at temperatures ranging from 30-45 °C. The lean solvent is introduced at the top of the column also at relatively low temperatures, with an operating temperature typically around 30-40 °C. Countercurrent flow through the column ensures efficient absorption of CO_2 into the solvent[26]. The absorber is a packed column with

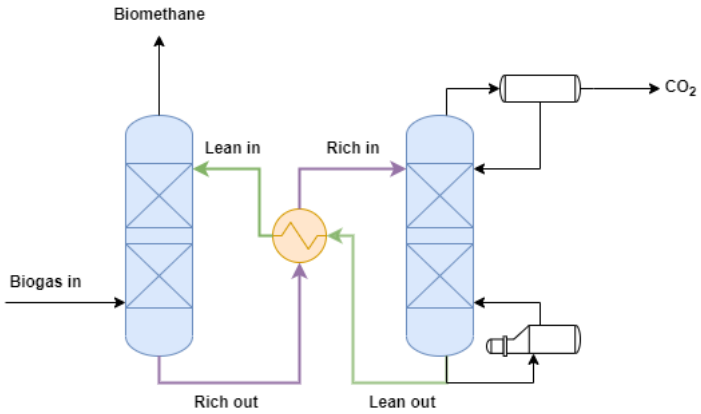

Figure 3: Absorption and stripper process in biogas upgrading

either random or structured packing, and is normally rings of stainless steel, glass or ceramic material. The purpose of the packing is to create a large surface area for maximal CO_2 absorption by the absorbent[26]. The CO_2 concentration at the top of the column is low, allowing the lean solvent to absorb most of the remaining CO_2. At the bottom of the column the solution is rich in CO_2. The rich solution is partially heated in a heat exchanger, before being fed to the top of the stripper where the solvent is regenerated by steam from a reboiler, causing the CO_2 to desorb from the solvent. The operating temperature of the stripper is normally between 100-140 °C. The CO_2 gas rises to the top of the stripper, and is condensed, while the lean solution is cooled in the heat exchanger and returned to the absorber. The pressure in the system is relatively low, approximately 1 bar[27]. The selectivity of amines towards CO_2 is very high, and the upgraded gas can have a quality of at least 99.5% CH_4 on dry basis[19].

To improve the performance of the process, various strategies can be used to increase energy efficiency, reduce emissions, and improve cost-effectiveness. There are two main approaches for enhancing the process: solvent optimization and process modifications. Process modifications

involve altering process parameters such as temperature and pressure, or by implementing additional equipment to the process. According to Moullec & Neveux (2016) the most advanced modifications can reduce energy consumption up to 30%[28]. Solvent optimization focuses on modifying the chemical properties, concentration, or mixture of solvent to increase absorption capacities, and reduce energy requirements and emissions.

2.3.1 Process Modification - Intercooled Absorber

Implementation of an intercooled absorber involves extracting a fraction of the liquid solvent from the column and reducing its temperature, before reintroducing it back into the absorber, as can be observed in Figure 4a. As absorption rates are higher at lower temperature, intercooling causes a shift in the thermodynamic gas-liquid equilibrium, resulting in a higher rich loading at the bottom of the column. The increased solvent loading results in reduced solvent circulation, thereby reducing the amount of liquid that needs to be heated in the reboiler[28]. Research suggests that intercoolers (IC) are more efficient on low-kinetic systems, like tertiary amines compared to primary.

Various parameters like split fraction and positioning of the intercooler needs to be optimized. Karimi et al. (2011) suggested that the optimal position for minimizing the specific regeneration energy was to place the IC within a quarter of the absorber height from the bottom[29]. However, Plaza et al. (2010) concluded that the positioning of the intercooler was not critical when the packing was over 20 meters, when using cascade mini-rings random packing[30]. Le Moullec & Kanniche (2011) reported that the intercooler appeared more efficient if placed in the lower half of the column, leading to a reduction in reboiler duty of 3.8% when using MEA. Positioning the IC in the lower half of the column reduces cooling water demands, as the temperature is lower in this region[31].

The temperature at the top of the column, where the solvent is lightly loaded with CO_2, encourages rapid transfer due to a high driving force of absorption. Lowering the temperature in this region could limit the mass transfer rate. However, at the bottom of the column, where the solvent is highly loaded with CO_2, lowering the temperature increases the driving force of absorption, thus loading the solvent with more CO_2. At a certain temperature transfer would not occur, regardless of the transfer rate. However, optimal intercooling position is dependent on the solvent's properties and the column's internals.

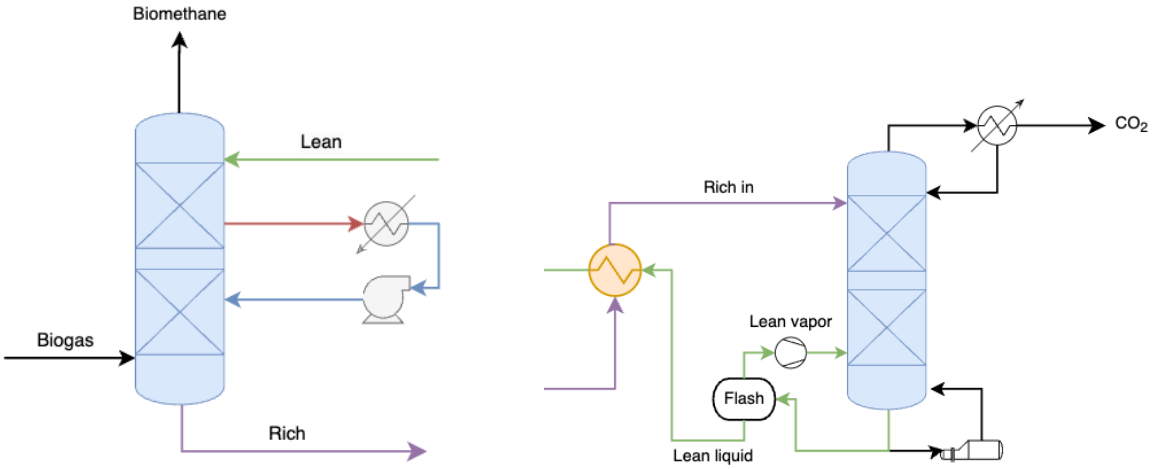

(a) Intercooled absorber **(b)** Lean vapor recompression

Figure 4: Possible process modifications for chemical absorption

2.3.2 Process Modification - Lean Vapor Recompression

In Figure 4b the lean vapor recompression (LVR) modification is illustrated. LVR involves flashing the lean solution, and compressing the resulting vapor, while returning the liquid fraction to the absorber, maximizing the absorption process[28]. The LVR process utilizes sensible heat from the top of the stripper and transfers it to latent heat in the bottom of the stripper[32]. The vapor phase mainly consists of H_2O and CO_2. By compressing the gas, the temperature of the gas increases, and it acts as stripping steam when reintroduced to the stripper, thereby reducing the steam requirements. Furthermore, the lean liquid leaving the flash has a lower temperature than when exiting the stripper directly. This results in less heat being exchanged with the rich stream, resulting in lower cooling requirements for the condenser.

Research on carbon capture from flue gas has shown that the LVR process can reduce the energy requirements up to 11.5%[28], depending on the flash temperature. Karimi et al. (2011) reported energy savings between 8.39-9.36% depending on the pressure. Le Moullec and Kannike (2011) found 7.78% energy savings, when using MEA, but recommended further investigation of other solvents, such as aMDEA and AMP[33][31]. Amrollahi (2012) investigated the combination of intercooled absorption and LVR with MEA, and achieved a reduction in reboiler energy consumption of 27%[34]. Knudsen et al. (2011) investigated MEA, CESAR1 and CESAR2 in pilot scale with different process modifications, including LVR. They concluded that LVR has a more significant impact on solvents with higher reboiler duties, such as MEA and CESAR2, as these are the solvents experience greater heat losses due to water evaporation[32].

2.4 Solvents for Chemical Scrubbing

The chemical scrubbing process can also be optimized through solvent optimization, which involves selecting the appropriate solvent for CO_2 capture. The solvent used must meet a number of requirements, including[35]:

- Low cost
- High CO_2 capacity
- High reaction rate
- Low degradation rate
- Low corrosivity
- Low vapor pressure
- Low regeneration energy
- Low volatility

Among these requirements, the regeneration energy requirements have the most significant impact on operational costs. The regeneration energy can be estimated by adding three terms: the heat of evaporation required to generate stripping steam in the reboiler, the heat needed for desorption of CO_2 from the solvent, and the heat needed to increase the solvent temperature from absorber to desorber temperature[35]. It is essential to carefully consider these requirements when selecting a solvent for CO_2 capture to optimize the chemical scrubbing process.

2.4.1 Amines

Amines are organic compounds containing a nitrogen atom bonded to one or more carbon atoms. Depending on the number of carbon atoms attached to the amine-nitrogen, amines are classified as primary (RNH_2), secondary (RRNH) or tertiary amine (RRRN) as can be seen in Figure 5. The reactivity of amines towards CO_2 and the formation of carbamate salts depend on the type of amine, with primary amines being more reactive than secondary and tertiary amines[26]. The reactions that occur in a CO_2 absorption process with amines can be found in Table 2. It is crucial that all reactions are reversible, as the objective is to capture and subsequently release CO_2, since

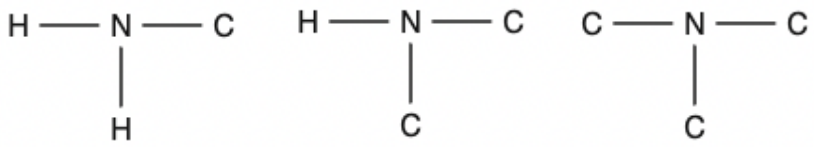

Figure 5: Illustration of primary, secondary and tertiary amines respectively

it is too costly not to regenerate the amine solution[19]. The reactions are highly exothermic, leading to increased temperature inside the absorber. However, the heat of absorption varies with the specific amines used.

Table 2: Chemical reactions taking place in the absorber/stripper system

$H^+ + OH^- \longleftrightarrow H_2O$
$CO_2 + H_2O \longleftrightarrow H_2CO_3$
$CO_2 + OH^- \longleftrightarrow HCO_3^-$
$CO_3^{2-} + H^+ \longleftrightarrow HCO_3$
$HCO_3^- + H^+ \longleftrightarrow H_2CO_3$
$RNH_2 + H^+ \longleftrightarrow NRH_3^+$
$CO_2 + RNH_2 \longleftrightarrow RNHCO_2H$
$RNH_2CO_2^- + H^+ \longleftrightarrow RNH_2CO_2H$

The overall reaction for primary amines is:

$$CO_2 + 2RNH_2 \longleftrightarrow RHNCO_2 + RNH_3^+, \tag{2}$$

whilst for tertiary and sterically hindered amines the overall reaction is:

$$CO_2 + R_3N(+H_2O) \longleftrightarrow HCO_3 + R_3NH^+. \tag{3}$$

One can observe from the reactions presented above that primary amines (Equation 2) require two moles of amines (RNH_2) per mole of CO_2, while for Equation 3 the molar ratio between amine and CO_2 is one. Therefore, processes with primary amines require twice the amount of solvent for removal of the same amount of CO_2, compared to tertiary or sterically hindered amines. However, the choice of amine can also be influenced by the reaction rate which differ among the types of amine[26].

The regeneration of the amine solvent is driven by CO_2 affinity, and temperature swing. At low temperatures, the solvent has a high affinity for CO_2, leading to higher absorption capacity. At higher temperatures, the affinity for CO_2 decreases, which causes a shift in the reaction equilibrium, and drives the reactions towards desorption[26]. The amount of CO_2 absorbed by

the solvent can be measured as the loading (α), which is the ratio of absorbed CO_2 to solvent concentration. The cyclic capacity is a measure of the solvents effectiveness, and is calculated as the difference between the rich and the lean CO_2 loading[26]. A higher cyclic capacity means that more CO_2 can be absorbed using less absorbent.

Since the 1950s, amines have been the leading solvent for chemical absorption[36]. Monoethanolamine (MEA) has been benchmark solvent for amine-based CO_2 capture processes due to its high selectivity, fast reaction, low cost, and easy accessibility[26]. Despite these favourable properties, MEA still suffers from several operational challenges, including high regeneration energy demand and low absorption capacity[37]. To address these issues, researchers have studied other amines and amine blends, such as the ones composing CESAR1 and activated methyl diethanolamine (aMDEA), which have shown to require less energy and exhibit higher absorption capacities. Nevertheless, the use of amines poses significant challenges due to amine losses and amine degradation, which can result in environmental and economic impact[38][37].

There are mainly two types of amine degradation found in CO_2 capture processes, namely oxidative and thermal degradation. Oxidative degradation occurs when oxygen in the gas mixture reacts with the amines present in the system, resulting in various degradation compounds. Thermal degradation, on the other hand, is caused by the heat generated during the regeneration process when the amine is loaded with CO_2. Amine degradation can lead to production of harmful degradation products which can impact both human health and the environment[39]. Furthermore, it can cause operational challenges such as fouling, corrosion, and foaming. Amine degradation has been estimated to account for up to 10% of the total CO_2 capture cost[39].

Amine losses mainly happen through amine degradation, volatility and aerosol formation. Gas phase emissions of either the solvent itself or degradation products mainly happens in the absorber, and the amines are released with the sweet gas at the column exit[40]. Efforts have been made to reduce amine emissions, including the implementation of a water wash section. The water wash section has been shown to significantly decrease volatile emissions[41][40].

When amines are released into the atmosphere they can react with nitrous oxides to form nitrosamines and nitramines. These compounds, along with others such as ammonia, alkylamines, ketones and aldehydes have been identified as degradation products[42]. Some of these compounds have the potential to cause severe long-term effects, such as mutagenicity, genotoxicity and reproduction effects[37]. In addition, amines pose a threat to the environment by contaminating drinking water and crop contamination, particularly for biogas plants, as they often are geographically connected to farms or crop production. However, the extent of these impacts has yet to be determined[37].

2.4.2 Activated MDEA and CESAR1

Both aMDEA and CESAR1 are examples of amine blends, which are mixtures of different amines. Activated MDEA consists of the tertiary amine, MDEA and an activator with fast reaction kinetics, typically the cyclic amine Piperazine (PZ), which can be observed in Figure 6. CESAR1 is an amine blend of the sterically hindered 2-amino-2-methyl-1-propanol (AMP) and PZ. Tertiary and sterically hindered amines offer advantages over primary amines in CO_2 capture processes, such as higher absorption capacities and lower degradation rates. However, these types of amines suffer from reduced reaction rates[43].

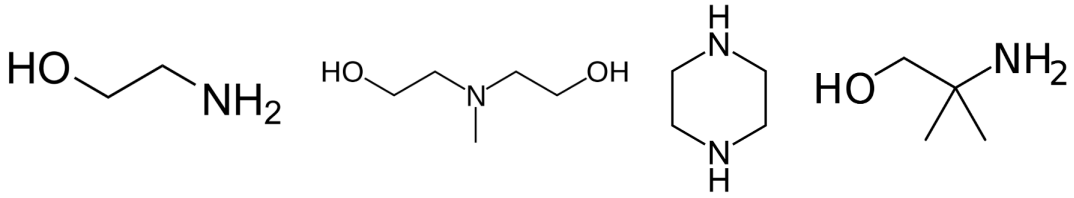

Figure 6: Amines from the left: MEA, MDEA, PZ, AMP

To address the challenge associated with low reaction rate, an activator or promoter can be added. A promoter is a reactive substance that reacts with another molecule to produce a chemical compound with enhanced properties compared to the individual reagents. Combining a promoter amine with a sterically hindered or tertiary amine, can significantly improve the uptake kinetics and reaction rates. The activation of MDEA using PZ enhances CO_2 absorption capacity, with the kinetics even improved at low PZ concentrations[44]. The presence of a primary or secondary amine, such as PZ, can increase the rate for CO_2 absorption and promote further reaction of CO_2 with the sterically hindered or tertiary amine. This can result in a relatively low heat of absorption for sterically hindered or tertiary amines, making the regeneration process more energy-efficient[4]. Activated MDEA has shown to have lower degradation rates compared to MEA[45]. In CESAR1, the sterically hindering prevents the formation of the stable carbamate ions, which increases the effectiveness of the process[46][47]. Because AMP and MDEA are sterically hindered and tertiary amines, respectively, and therefore react with CO_2 in 1:1 molar ratio (Equation 3), they do not suffer from the maximum theoretical loading of 0.5 that primary and secondary amines, which carbamate (RNHCOO) formers, like MEA, do.

The reaction rate constants in Table 3 provide a clear indication of why PZ is an effective promoter, and also shows the need for promotion of both AMP and MDEA. A downside of using PZ, is the possibility of amine losses as it has a high volatility compared to other amines. However, implementation of a water wash section can drastically reduce PZ losses[4].

Table 3: Reaction rate constants[4] and heat of absorption. Table is based on second order kinetics at 25 °C.

Amine	Reaction rate constant [L/mol s]	Heat of absorption[kJ/mol]
AMP	600	85
MEA	6000	84
MDEA	4	58
PZ	59000	76
NaGly	8000	85

2.4.3 Amino Acid Salts

Amino acids are naturally occurring organic compounds found in living organisms. They are fundamental building blocks of proteins, and play a crucial role in many biological processes[48]. Due to their natural occurrence they have excellent biodegradability, making them easy to dispose and thereby reducing environmental pollution. All amino acids contain at least one carboxylic functional group (-COOH), and one basic amine group (-NH_2). A generic representation of an amino acid can be observed in Figure 7a. Amino acids can be distinguished by their -R group, which defines each unique acid and its properties[49]. The basic amino group contains a free electron pair on the N-atom, allowing it to accept a proton from the -COOH group. This proton transfer occurs when amino acids are dissolved in water, resulting in a zwitterion (Figure 7b): The zwitterion molecule has one positively and one negatively charged functional group, leaving

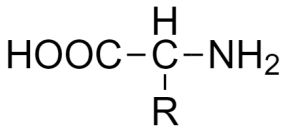

(a) Generic amino acid

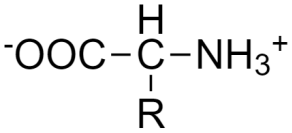

(b) Zwitterion

Figure 7: Generic and zwitterionic amino acid

the molecule as a whole electrically neutral[49]. As the amino group has been protonated it is completely non-reactive towards CO_2. However, when a strong base like potassium hydroxide (KOH) or sodium hydroxide (NaOH) is added to the zwitterionic amino acid, the amine group is deprotonated, and the primary amine is formed again. The reaction between the simplest amino acid, glycine, in its zwitterionic form, and NaOH can be observed in Figure 8.

AASs have a similar reaction mechanism with CO_2 as primary amines due to having the same functional group (NH_2). Studies have shown that the absorption capacities are comparable to those of primary amines[50][51][4]. The non-volatile, ionic nature of AAS makes them an attractive

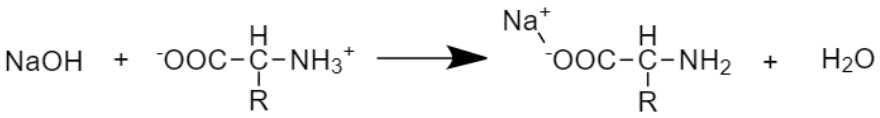

Figure 8: Formation of amino acid salt

option for CO_2 capture since gas-phase emissions are eliminated. Furthermore, as amino acids are naturally occurring in oxygen-rich environments, oxidative degradation is potentially not a concern when using AAS for gas treating, and AAS are therefore known as green solvents.

The absorption of CO_2 can either be by formation of carbamate (Equation 4) or bicarbonate (Equation 5). However, research show that based on reaction rates the formation of carbamate is the initial absorption step[52]. Equation 4 shows that CO_2 and AAS react in 1:2 ratio, like primary amines, limiting them to the maximum theoretical loading of 0.5.

$$CO_2 + 2AAS \rightarrow AASCOO^- + AASH^+ \tag{4}$$

$$CO_2 + OH^- \rightarrow HCO_3^- \tag{5}$$

AASs have been used for co-current removal of H_2S and CO_2 from refineries, coke ovens and natural gas since the 1930s[51].The Alkazid® process was licensed by BASF, and the process consisted of three separate steps with different amino acid solvents in each step, where the solvent was chosen depending on the composition of the gas stream, and the acid gases to be removed[36].

When AAS reacts with CO_2, precipitation may occur. Both the amino acid itself and different carbonate species have been reported to precipitate[53][54]. The boundary between non-precipitating and precipitating systems was investigated by Majchrowicz (2014), who found a strong dependency on the process conditions[49]. Precipitation leads to a constant equilibrium acid gas partial pressure while increasing the solution loading. Moreover, the slurry generated by precipitation can enable new ways of handling and storing CO_2[54]. According to Fernandez et al. (2013), precipitation can reduce energy consumption by 35% compared to the MEA baseline[55]. However, operating a process under salt precipitation conditions may be challenging.

Yan et al. (2015) studied the performance of five different potassium AASs as potential solvents

for biogas upgrading[56]. The results showed that both the initial and maximal absorption rates are higher for all AAS than for MEA, which may be due to higher CO_2 reaction rate constants. The heat of absorption was also reported lower for all AASs than MEA. Furthermore, the regeneration efficiency of MEA and potassium glycinate (KGly) was 46.48% and 50.98%, respectively, suggesting that KGly has a higher recoverability of CO_2 absorption than MEA. Yan et al. (2015) suggested that when selecting which AAS to use, there might be a trade off between loading capacities and high molecular weight, which can result in larger column sizes.

Rabensteiner et al. (2014) conducted a pilot plant study to evaluate NaGly as a solvent for post-combustion capture (PCC) using 15, 25 and 40 wt% of NaGly[51]. For 40 wt% the specific reboiler duty was 5.7 GJ/t CO_2, and they reported that 25 wt% NaGly had a 40% higher regeneration energy requirement compared to 30 wt% MEA. In addition, high solvent flow rates were required to meet removal targets, and for 25 wt% NaGly the flow rate was two to three times higher than for 30 wt% MEA[51]. It is worth noting that no precipitation was reported in the study. Also, Song et al. (2008) estimated the regeneration energy of NaGly by experimentally measuring the sensible heat, heat of vaporization and reaction enthalpy for 30 wt% NaGly and 30 wt% MEA. The results showed that the regeneration energy for NaGly was approximately 1 MJ/kg CO_2 higher than that of MEA[50]. A possible reason for these significant energy demands is the combined effect of slow kinetics and low required partial pressures at the top of the desorber[51]. The heat capacity of NaGly (30 wt%) is lower than that of MEA (30 wt%), requiring less sensible heat to raise the temperature of the rich solvent. It was also proven that CO_2 loadings could not exceed 0.5, resulting in increased steam requirements and energy demands[51].

Simulations done with NaGly have been carried out by different authors, like Weiland et al. (2010a, 2010b), Optimized Gas Treatment (2010), Lee et al. (2008), Ogawa (2013) and Song et al.(2008)[57][4][58][50]. All, except Song, reported using ProTreat® for simulations, with an inlet CO_2 concentration between 4.72 and 13 vol%, and a separation efficiency of 80-90%. The results showed that the regeneration energy for the optimal operating point was between 2.8 and 4.0 GJ/t CO_2. Only Song et al. reported higher specific regeneration energy (5.7 GJ/t CO_2) compared to MEA[51].

Moioli et al. (2018) examined the techno-economic aspects of potassium taurate as a solvent for CO_2 capture compared to conventional MEA, using Aspen Plus simulations[59]. Although the flowrate were higher for the AAS case, the estimations for both operational and capital costs were lower. This was mainly due the use of carbon steel in the AAS case, but stainless steel in MEA case, which was chosen based on corrosion data available for potassium taurate, as well as lower reboiler steam requirements for the AAS case.

As mentioned previously, the degradation of amines is a major challenge when using them as solvents for CO_2 capture. Some literature suggests that NaGly is somewhat resistant to thermal degradation due to its small, stable molecule size[57]. However, Huang et al. (2013) conducted a study on the thermal degradation of NaGly at temperatures of 125, 135, and 145°C. The results showed that NaGly degrades at a much faster rate than MEA at all temperatures, with the amine molar concentration being more than one order of magnitude lower than that of MEA[60].

The existing literature on AASs as solvent for CO_2 capture primarily focuses on flue gas capture, and is typically compared to MEA. As other amines and amine blends, such as CESAR1 and aMDEA has been shown to outperform MEA in terms of energy requirements, the comparison of AAS to these blends are not well documented.

In Table 4 a comparison of important solvent properties for amines and amino acid salts is given.

Table 4: Comparison of solvent properties for amino acid salts and amines

Property	**Amines**	**Amino acid salts**
Toxicity	Varying, some are toxic on their own, some become toxic after chemical reactions, resulting in carcinogenicity, mutagenicity, and possible crop and water contamination	Non-toxic
Corrosivity	Not by themselves, but degradation products like oxalates and formates can cause corrosion. Type of amine and acid gas loading may affect degree of corrosion[61]	NaGly has similar corrosion rates to MEA at higher molarities[62]
Degradation	Prone to both thermal and oxidative degradation	Not prone to oxidative degradation as amino acids are found in oxygen containing environments. Thermal degradation may occur
Stability	Varying, MEA is less stable than amine blends like CESAR1 and aMDEA	Stable
Cost	Varying with complexity of amine, reduced material cost due to increased stability	Similar to amines
Regeneration Energy	Varying between the different amines, high for 30 wt% MEA. Lower for CESAR1 and aMDEA	Varying results from literature, mostly similar or higher than 30 wt% MEA
Cyclic Capacities	Dependant on amine type, primary amines normally have low absorption capacity	NaGly has shown to have low absorption capacity, cannot reach high rich loadings
Absorption rate	High	Similar to amines
Volatilty	High volatility	Non-volatile
Reaction Rate	Dependant on amine(s) and use of promoter.	Data indicate NaGLy has 1/3 to 3 times the reaction rate of MEA, depending on concentration[57] [4]

Chapter 3

Materials and Methods

In the following chapter the materials and methods are presented. The design specifications for the simulations are described, as well as the experimental procedure. Additionally, the basis for the economic analysis is presented. A validation of the model used in ProTreat® is also performed, with the detailed procedure provided in Chapter 4.

3.1 Defining a Base Case

The simulation software used for this thesis is OGT ProTreat®, version 7.0. As a mass and heat transfer rate-based simulation tool, ProTreat® accurately predicts solvent performance by utilizing a set of equations to calculate mass and energy transfer across the interface through rate equations and mass transfer coefficients. The model accounts for non-idealities by allowing long and short-range interactions between the species present in the solvent, and employs Guggenheim's equation to represent activity coefficients[63].

A flowsheet based on a conventional absorber/stripper CO_2 capture process was implemented in ProTreat®, and used as a base for all simulations. The flowsheet for this process can be observed in Figure 9. The specification of the simulations was 1 mol% of CO_2 in the sweet gas (stream 6), which corresponds to a 97.5% removal rate of CO_2.

3.1.1 Inlet

The inlet (stream 1) is assumed to only contain CH_4, CO_2, and water, with all other contaminants removed prior. The gas has a CH_4 concentration of 60 mol%, a CO_2 concentration of 40 mol%, and is saturated with water. To ensure that the gas flows upwards through the absorber, the gas is compressed to 1.05 bara with an efficiency of 80% and cooled to 35 °C before entering a flash tank to remove condensate. Stream 4 is set to be 100% vapor.

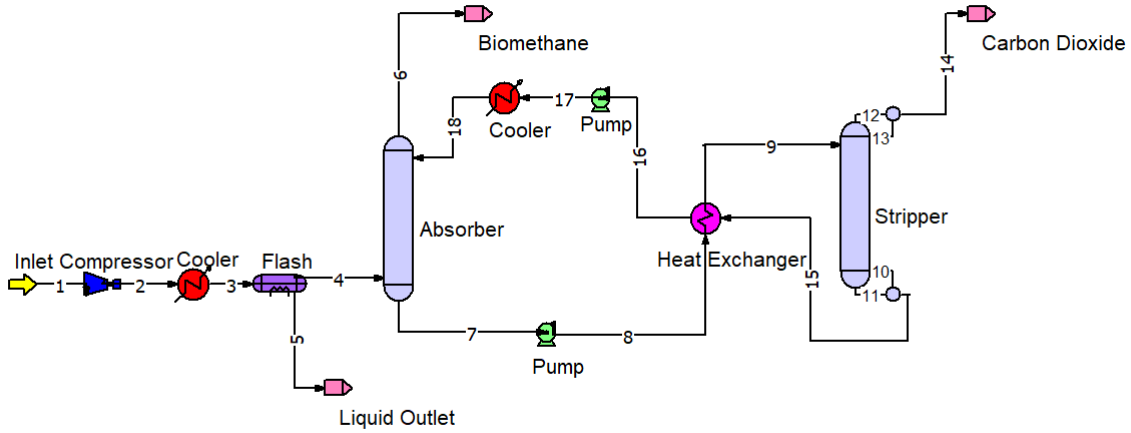

Figure 9: Flowsheet for base case

3.1.2 Absorber

Table 5 shows the absorber design specifications.

Table 5: Absorber parameters

Packing	Mellapak Plus 352Y
Height of packing	22 m as a base
Flooding	70 %
Stream 4 connection	bottom of packing
Stream 18 connection	top of packing
Stream 7 connection	bottom of absorber
Sump residence time	7 min

The packing chosen gives a high surface area, and ensures a low column height compared to more open packings. The sweet gas (stream 6) has a specification of 1 mol% CO_2, and the circulation rate is adjusted by a solver block to meet this specification. In ProTreat® one can either specify the diameter or the percentage of flooding, and the software will calculate the other value accordingly. However, setting the flooding simplifies conversion, and reduces the running time of simulations. Therefore, the flooding was set to 70% in all simulations. However, when optimizing the best cases, the diameter was determined such that the volume of the absorber could be calculated. Initially, the packing height was set to 22 meters to ensure no mass transfer limitations. However, during optimizing this value was minimized.

The rich solution (stream 7) is pressurized to 5 bara, and passed through a heat exchanger, and introduced at the top of the stripper (stream 9). The heat exchanger is designed to have

a minimum temperature approach of 5 °C, and uses a heat transfer coefficient number of 800 W/m^3K[64]. The height of the sump was calculated during optimization, based on a seven minute residence time.

3.1.3 Stripper

The parameters for the stripper are given in Table 6. The rich solution enters the stripper through stream 9, and the lean solution exits as stream 15. Stream 14 is the CO_2 captured in the process. The lean solution, is sent through the heat exchanger to be cooled by the rich stream, before being further cooled by a cooler set to 35 °C.

Table 6: Stripper parameters

Packing	Mellapak M352Y
Flooding	70%
Pressure (bottom of packing)	1.8 bara
Temperature Condenser	40 °C
Pressure drop Condenser	0 Pa
Reflux Return to Column	100%
Reboiler Molar Boilup Ratio	Varying

The molar boilup ratio represents the ratio between the molar flow rate of vapor entering the stripper and the molar flow rate of liquid leaving, and is a function of the amount of heat supplied by the reboiler. The boilup ratio was used as a variable to examine the energy requirements at different solvent circulation rates.

The base case presented above was used as a base for all simulations. Further, different process modifications were introduced in an attempt to reduce energy requirements.

3.1.4 Solvents

Table 7 presents the solvents and their corresponding concentrations used in the simulations for this thesis, as well as the ones from previous work performed during autumn 2022. The chosen NaGly concentration was selected to correspond with 30 wt% MEA in molar equivalents, while aMDEA concentration was selected to match CESAR1 molar ratio (1.5M PZ + 3M MDEA).

Table 7: Solvents and weight percentages used in thesis and previous work

Solvent	Concentration	Simulations done
NaGly	45 wt%	This thesis
Activated MDEA	35wt% MDEA + 13 wt% PZ	This thesis
MEA	30 wt%	Previous work
CESAR1	27 wt% AMP + 13 wt% PZ	Previous work

3.2 Process Modifications for NaGly cases

After conducting simulations with NaGly as the solvent in the base case, various process modifications were made to reduce the regeneration energy requirements. The boilup ratio was used as a variable, to try to find the minimum reboiler duty for each configuration.

3.2.1 Intercooled Absorber

An IC was implemented in order to reduce the temperature inside the absorber, and to ensure absorption throughout the column. The optimal location for the IC was determined by installing it at various heights along the column, including 2 m, 4.5 m, 7 m, 12 m, and 16.5 m from the top. The fraction of solvent to be cooled was set to one, and the solvent was cooled to 25°C. A flowsheet of the process with IC can be found in Appendix K, Figure 43.

3.2.2 Split Absorber

Further, the absorber was split into two columns in series, as shown in Appendix K Figure 46. This attempt was done to use the first column for bulk CO_2 removal, and the second column to adjust the CO_2 concentration to the target. The first column, *40-20*, was designed to reduce the CO_2 concentration from 40 mol% to 20 mol%, while the second absorber, *20-1*, aimed to reduce it further to 1 mol%. A splitter was used to divide the lean stream between the two absorbers, and a mixer combined the rich streams. Since nested solvers are not supported in ProTreat®, the split fraction was manually adjusted until targets were met.

3.2.3 Lean Vapor Recompression

A flash tank and a compressor were implemented after the reboiler, as can be seen from Appendix K, Figure 45. The flash tank parameters are given in Table 8. The vapor fraction from the flash was then further compressed to 1.8 bara, the same as the stripper operating pressure, before being returned to the stripper.

Table 8: Flash tank parameters for LVR

Parameter	Value
Flash type	QP (Enthalpy & Pressure)
Heat duty	0 kW
Outlet Pressure	1 bara
Stream 23 connected	Bottom of Packing

3.2.4 Time line of simulations

At the beginning of the working period of the thesis, simulations using NaGly were conducted. However, as the study progressed, and the ProTreat model was validated using experimental data, the researchers began to question the possibility of precipitation occurring in the system. Since there was limited experimental data on the precipitation behaviour of NaGly and CO_2 available, particularly at 45 wt% NaGly, it was decided that precipitation experiments should be conducted to verify the feasibility of the simulation results.

3.3 Experimental Procedure

As data for precipitation with 45 wt% NaGly was limited in literature, experiments were conducted in the laboratory in relation to this thesis to confirm the reliability of the results from simulations using NaGly as solvent. Precipitation with 35 and 45 wt% NaGly were investigated.

100 grams of solution was prepared by mixing the chemicals, *VRW Sodium Hydroxide pellets (≥98.8%)* and *Sigma-Aldrich Glycine, (≥98.5%)*, with distilled water in a beaker. The exact measurements can be found in Appendix L. The solution was heated and stirred on a magnetic stirrer, until completely dissolved. Further, the solution was transferred to a flask with a gas-injecting cork as shown in Figure 10. The weight of the flask with solution was measured before connecting the gas tube. CO_2 gas (100%) was injected into the solution for different time intervals, which can be observed in Table 9. The time of sampling was determined during the experiments based on visual observations. After every gas injection, the tube was disconnected, and the weight of the solution was measured. A sample of the solution was taken with a pipette into a 1 mL glass vial, before the weight was measured again. The samples were diluted with deionized water before being analysed using a *Shimadzu TOC-L series* TOC analyser. After all the samples were taken, the flask was left for 24 hours, and then reweighed. Precipitation occurred in all experiments. For the 35 wt% experiments the flasks were heated on a magnetic stirrer, while monitoring the temperature to determine the temperature at which precipitation was solubilized. The results are given in the results and discussion section (Chapter 5.2) to justify the choice of further simulations with aMDEA.

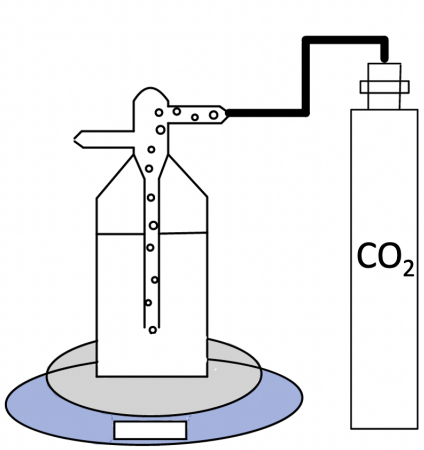

Figure 10: Illustration of experimental set up

The CO_2 loading of the solutions could be determined over time by calculating the weight

Table 9: Solution and time sampling

45 wt%		Sample time [min]	No. of samples
	Round 1	1-10	10
	Round 2	1-8, 17, 27	10
35 wt%			
	Round 1	1-9, 12, 15, 20, 30, 40, 50	15
	Round 2	10, 20, 30, 40, 50, 60	6

increase between each sample and using the TOC results.

3.4 Activated MDEA with IC

As mentioned earlier, a concentration of 35 wt% MDEA, and 13 wt% PZ was chosen for aMDEA simulations[65]. The simulations were conducted using the base case presented in Chapter 3.1. However, after analyzing the results from the experimental work and simulations using NaGly, as well as the simulation results from previous work by the author, it was determined that implementing an absorber intercooler was necessary. The intercooler was placed at 16 meters from the top, based on the previous results from Chapter 3.2.1. The minimum reboiler duty was investigated.

3.4.1 Pressurized system

To study the impact of a pressurized system on energy requirements, several pressurized systems were studied. The gas was cooled to 35 °C between stages using intercoolers, as is shown in Figure 44. The pressure levels studied were 3, 5 and 8 bara, and the minimum reboiler duty was found in each case.

3.5 Economic Analysis

After analyzing the energy requirements for the different solvents, an economic analysis was performed on the configuration with the most favourable results. Two different configurations were analyzed to compare whether the energy benefits outweighed the economic advantages. The economic analysis considered capital expenditure (CAPEX), operational expenditure (OPEX), and revenue based on sale of biomethane, potential subsidies and sale of carbon credits. Conversion factors were required due to the use of different currencies in the calculations. The calculations were based on USD, with a euro to USD exchange rate used of 1.1, and a NOK to USD rate of 10.

In order to conduct the economic analysis, certain assumptions have been made. Firstly, it was assumed that the plant is located in the southern part of Norway, making it easily accessible for connection to the gas grid and close to the sea, allowing for the use of sea water for cooling purposes. Secondly, it was assumed that the biogas facility was already designed and operating. It is important to note that these assumptions introduce uncertainties and deviations in the calculations. Nevertheless, the analysis provides an estimate of the time required to achieve payback, and the feasibility of a upgrading plant of this size.

3.5.1 CAPEX

The CAPEX calculations are based on *Chapter 6 - Costing and Project Evaluation* in Sinnott & Towlers Chemical Engineering Design, *Table 6.6 - Purchased Equipment Cost for Common Plant Equipment*[66].

The equation used to determine the cost of each piece of equipment is:

$$C = a + bS^n \tag{6}$$

where *a* and *b* are cost constants obtained from Table 6.6, *n* is the exponent for that particular type of equipment, and *S* is the size parameter which must be calculated for each process unit. The cost constants, specified in the fifth edition of the book, are based on the January 2007 Chemical Engineering Plant Cost Index (CEPCI). To adjust to 2021 CEPCI Index, Equation 7 was used:

$$C_A = C_B \frac{I_A}{I_B}, \tag{7}$$

where C_A and C_B is the cost in respectively year A and B, and I_A and I_B is the CEPCI indexes in year A and B. The 2007 CEPCI Index is 507.9, while the index for 2021 is 720.2. Table 10 provides the type and cost constants for each process unit used in the economic analysis. Note that, in some cases multiple units of the same process unit were required, however this is given in the results. Both the reboiler and condenser were modeled as a heat exchanger combined with a flash tank, while the coolers were modeled as heat exchangers with cooling water on the tube side.

Table 10: Process Units with cost constants

Process Unit	Type	Unit for S	a	b	n
Heat Exchanger	Plate and frame	area, m^2	1350	180	0.95
Reboiler- flash	U-tube kettle reboiler	shell mass, kg	25000	340	09
Reboiler - exchanger	U-tube kettle reboiler	area, m^2	25000	340	0.9
Packing, absorber	304 ss structured packing	m^3	0	6900	1
Packing, stripper	304 ss structured packing	m^3	0	6900	1
Absorber shell	Pressure vessel, vertical 304 ss	shell mass, kg	15000	68	0.85
Stripper shell	Pressure vessel, vertical 304 ss	shell mass, kg	15000	68	0.85
Condenser - exchanger	Plate and frame	area, m^2	1350	180	0.95
Condenser - flash	Pressure vessel, horizontal 304 ss	shell mass, kg	11000	63	0.85
Compressor	Blower	m^3/h	3800	49	0.8
Flash	Pressure vessel, horizontal 304 ss	shell mass, kg	11000	63	0.85
Pump	Centrifugal	kW	490000	16800	0.6
Lean cooler	Plate and frame	m^2	1350	180	0.95
Intercooler	Plate and frame	m^2	1350	180	0.95
Cooler,	Plate and frame	m^2	1350	180	0.95

Further, an estimation of the projects fixed capital costs were conducted using Table 6.4, under the *Fluids*-column. The inside battery limit investment (ISBL), the cost of the plant itself, is calculated by the equation:

$$\text{ISBL} = \sum C_{CS}[(1 + f_p)f_m + (f_{er} + f_{el} + f_i + f_c + f_f + f_l)] \tag{8}$$

where the factors and values are given in Table 11. The equation for calculating the fixed capital cost (FCC) was given by:

$$\text{FCC} = \text{ISBL} + \text{OSBL} + \text{D\&E} + \text{X} \tag{9}$$

From the reference book the outside battery limits (OSBL) is typically estimated as a fraction of the ISBL costs, and range from 10-100% of the ISBL. For this plant it is assumed to be 15%,

Table 11: Installation factors for fixed capital costs

Symbol	Meaning	Value
C_{CS}	purchased equipment cost in carbon steel	
f_p	installation factor for piping	0.8
f_{eq}	installation factor for equipment erection	0.3
f_{el}	installation factor for electrical work	0.2
f_c	installation factor for civil engineering work	0.3
f_i	installation factor for instrumentation and process control	0.3
f_s	installation factor for structures and buildings	0.2
f_l	installation factor for lagging, insulation or paint	0.1
f_m	$\frac{\text{purchased cost of item in exotic material}}{\text{purchased cost of item in carbon steel}}$	

as the biogas facility is already operating. The engineering costs (D&E) are assumed to be 30% of the ISBL + OSBL, and the contingency (X) is assumed to be 10% of the ISBL[67].

To increase robustness of the plant, 304 stainless steel (SS) is used, as there is available data on costs with 304 SS in the reference book. However, in actual practice, 316 SS would be used, as this is better for acid gas treatment. The conversion factor from carbon steel to stainless steel of 1.3 was used, which is the same factor for 316 SS, thus the cost estimation remains the same.

3.5.2 OPEX

It is assumed that the plant operates 8000 hours per year. The main operational costs connected to the plant are given in Table 12.

Table 12: Operational costs and values

Cost	Unit	Value
Electricity[68]	\$/MWh	132
Operators, 3 shifts[67]	\$/operator/year	60000
MDEA[69]	\$/ton	56760
PZ[69]	\$/ton	75570
Cooling water[70]	\$/m^3	0.02
Steam[68]	\$/MWh	32

The salaries of the operators are estimated to be \$60 000 pr year as per Chemical Engineering Design[67]. However, this amount will vary on the region and level of experience. The amine prices are estimates from Gomes et al. (2015)[69], and the electricity and steam prices are from Aromada et al. (2015)[68]. Depending on the geographical location of the plant the price of

electricity can vary significantly.

3.5.3 Revenue

The produced biomethane is assumed to be sold as natural gas, with an estimated price of 60$/MWh based on numbers from Dutch TTF Natural Gas Futures, for the first quarter of 2023[71]. The calorific value of biomethane is assumed to be 36 MJ/m^3, as per International Energy Agency[72]. The possibility of selling carbon credits was also considered. As the EU-ETS carbon pricing is a very dynamic price, an estimate of €90 pr metric ton has been assumed[73]. In addition, subsidies were considered. According to Innovation Norway subsidies for promoting renewable energy sources or reuse of waste can be up to 45% of CAPEX, depending on the size of the plant[74][75]. Net cash flow diagram was prepared for three hypothetical subsidy scenarios, 20%, 30% and 45% of CAPEX.

3.5.4 Net Cash flow Diagrams

Further, an economic spreadsheet was developed to evaluate the feasibility of the different scenarios. A depreciation rate of 20% and a tax rate of 28% was assumed. The accumulated net cash flow per year was graphed for each scenario to determine the break-even point (BEP). The BEP represents the point at which the net cash flow is positive, indicating the time frame required for the plant to start generating profits.

Chapter 4

Validation of Thermodynamic Model

In this chapter the validation of the thermodynamic model used in ProTreat® can be found for the two solvents used in this thesis, namely NaGly and aMDEA. Firstly, the model is described, before the procedure is presented. Lastly, the results from the validation is presented.

4.1 Deshmukh-Mather Model

The thermodynamic model used in ProTreat® is the Deshmukh-Mather model, which is based on the extended Debye-Huckel theory of electrolyte solutions to model equilibrium solubility of CO_2 and H_2S[76]. Murphrees efficiencies are not required in rate-based modeling, as it models true kinetics. The required parameters for ProTreat® include the equilibrium constants for chemical reactions, the Henry's law constants for CO_2 in solution, and the activity coefficients for the solvent and the solute species[77]. In 2010, OGT utilized the Deshmukh-Mather model as well as available VLE from BASF, and regressed it.

4.2 Procedure

To establish the correlation between the model utilized in ProTreat® and experimental data, a validation experiment was conducted by comparing the vapor-liquid equilibrium (VLE) curves generated in ProTreat® with the experimental data. As the VLE determines the operating characteristics of the process, a good agreement between the predicted and experimental values is desirable. To validate the model for NaGly, experimental data from Harris et al. (2008), Mondal et al. (2015) and Song et al. (2006) was used[78][79][80]. It is worth mentioning that this VLE data is not the same as the one employed in the regression of the ProTreat mode. Additionally, due to limited available experimental data for NaGly, VLE data for KGly from Portugal et al. (2009) was also used for comparison[81]. For aMDEA experimental data from Ghalib et al. (2017), Liu et al. (1999) and Dash et al. (2016) were utilized[82][6][83].

Equation 10 was used to calculate the absolute relative deviation (ARD) between the simulated value (x_{sim}) and experimental value (x_{exp}). Equation 11 was used to calculate the absolute

average relative deviation AARD:

$$\text{ARD} = \frac{|x_{\text{sim}} - x_{\text{exp}}|}{x_{\text{exp}}}, \tag{10}$$

$$\text{AARD}(\%) = \frac{\sum_1^n \text{ARD}}{n} \cdot 100 \tag{11}$$

To generate the VLE curves, the partial pressure of CO_2 was plotted as a function of the CO_2 loading (α) for varying temperatures and weight percentages. Parity plots, checking the agreement between the simulated and experimental datasets, were also generated.

4.3 Results

4.3.1 Absolute Average Relative Deviation

The AARD was calculated for each author and is presented in Table 13. The large AARD values for NaGly indicate that the model used in ProTreat® is not well aligned with the experimental data. Such large AARDs compromise the reliability and validity of the results using NaGly presented in this report. However, these experimental data were not used in ProTreat's model regression. Moreover, there is significant deviation between the experimental data points of the different authors, which may be due to variations in the execution of experiments, such as inconsistencies in solution preparation. This also raises some questions on the quality of the data itself. It can be observed that two AARD values are reported for Mondal et al. as two specific points contributed to most of the AARD of 270. These two points, with ARDs of 176 and 19 for T=323K are shown in Table 21. When excluding these points, the AARD is significantly reduced to 69%. Interestingly, Song et al.'s data has a higher relative deviation compared to Portugal et al's, which uses KGly as solvent.

The AARD values for aMDEA are significantly lower compared to those of NaGly, indicating a better alignment between the VLE data and the model. This is advantageous as it increases the reliability of the results. While there is a significant deviation in Dash et al's data, it is acknowledged in literature that there were issues with execution of the experiments (private communications with D.D Pinto, 15.04.2023).

Table 13: Calculated AARD values for NaGly and aMDEA

	Author	AARD[%]
NaGly		
	Harris et.al[80]	76
	Mondal et.al[79]	270 (69)
	Song et.al[78]	396
	Portugal et.al[81]	256
aMDEA		
	Dash et.al[82]	47
	Liu et.al[6]	22.5
	Derks et.al[5]	18.5

4.3.2 NaGly Results

VLE curves were generated for each of the weight percentages available from experimental data. The experimental data was plotted and color-coded according to temperature, with distinct symbols for each author. The VLE curves can be observed from Figure 11.

In Figure 11c, Figure 11d and Figure 11e it can be observed that the model is significantly deviating from Mondal's data at lower loadings, especially for α-values below 0.5. Despite the model being a better fit for higher α-values, it mostly underestimates the partial pressure of CO_2 when compared to experimental data. This can also be observed from Figure 12b, as most of the points are above the xy-line. Although, Mondal's data has the lowest AARD, at certain points the model overestimates over two orders of magnitude, which also can be observed in Appendix A.

In the case of 1 wt% (Figure 11a), it can observed that there is only data available for KGly, and that the data is not following a particular trend. This can be expected as the model is fitted to a different solvent. Also, the α-values from above 0.5 were not of much interest in this work given the absorption pressures investigated. However, it does state something about the models ability to predict the partial pressure. For 30 wt% KGly it can be observed that the partial pressure of CO_2 is underestimated for α-values between 0.1 and 0.5, but overestimating after 0.5. This might also be due to it being another solvent than the model is regressed to. However, from Figure 12c it can be observed that most of the datapoints are above the xy-line, indicating that the model mostly underestimates. Also, the deviation is increasing with increasing pressure.

Further, in Figure 11e it can be observed that the model is overestimating the partial pressure compared to Song et al.'s data, with remarkable deviations for α-values between 0.4 and 0.8.

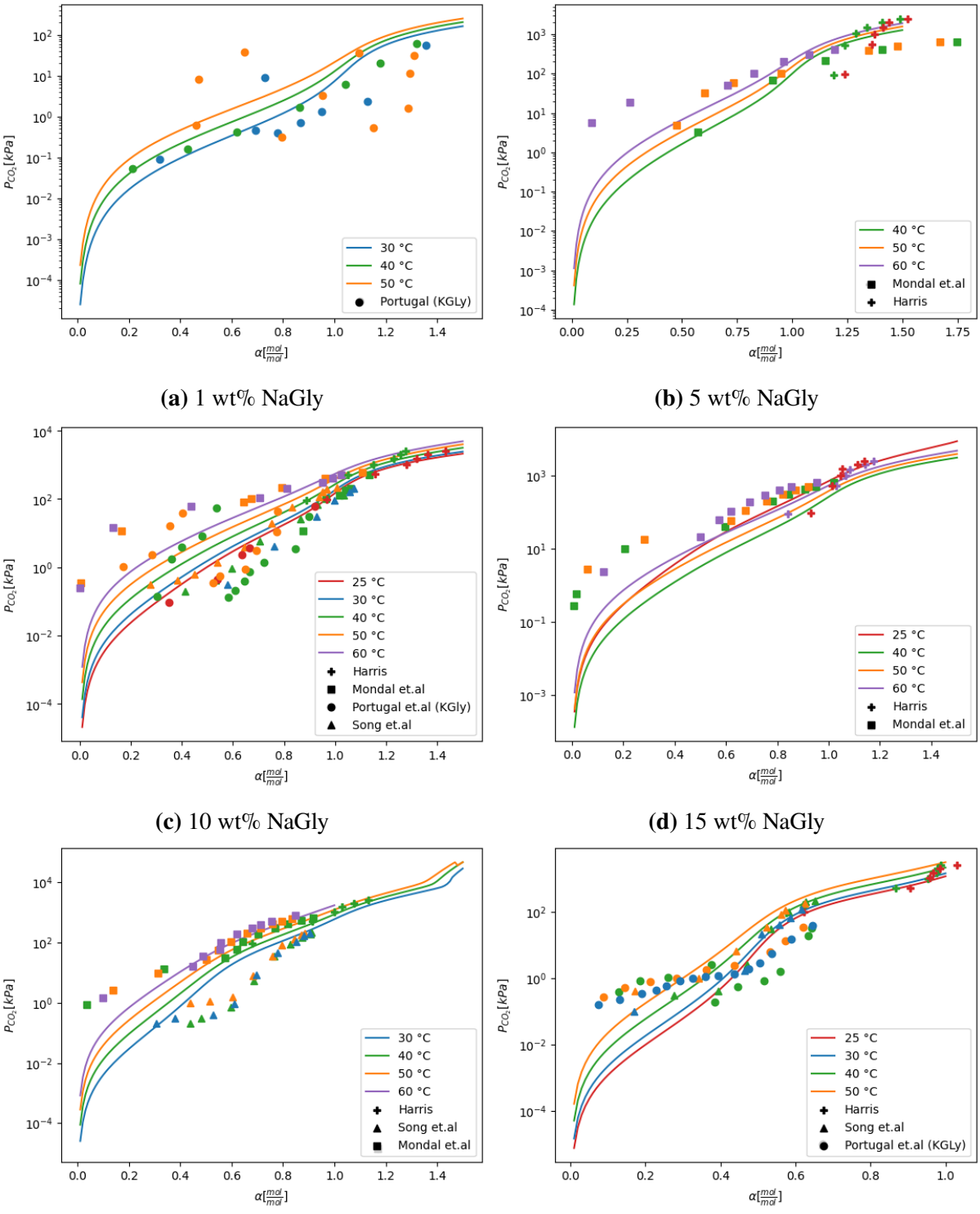

(a) 1 wt% NaGly

(b) 5 wt% NaGly

(c) 10 wt% NaGly

(d) 15 wt% NaGly

(e) 20 wt% NaGly

(f) 30 wt% NaGly

Figure 11: VLE curves for NaGly at different weight percentages generated for validation of thermodynamic model used in ProTreat®

This overestimation can also be observed from Figure 12d, following the same trend as data from Portugal et al., as most points are above the xy-line. For 10 and 30 wt% the model is a

better fit, which also can be observed from Appendix D when looking at the AARDs, as most of the total AARD is caused by the 20 wt% data set.

Harris's data covers a limited range of α-values, only between 0.8 and 1.4. The AARD value (Table 13) shows that the simulated vales are in reasonable agreement with the experimental values. However, Figure 12a shows that the points somewhat vertically aligned, possibly due to the experimental partial pressure being set during experiments, while measuring the loading. This can also be seen from Appendix C as the pressure is measured with a 500 kPa interval. Nevertheless, since the operating window for biogas will seldom reach α-values over 0.5 the implications of these results are somewhat limited.

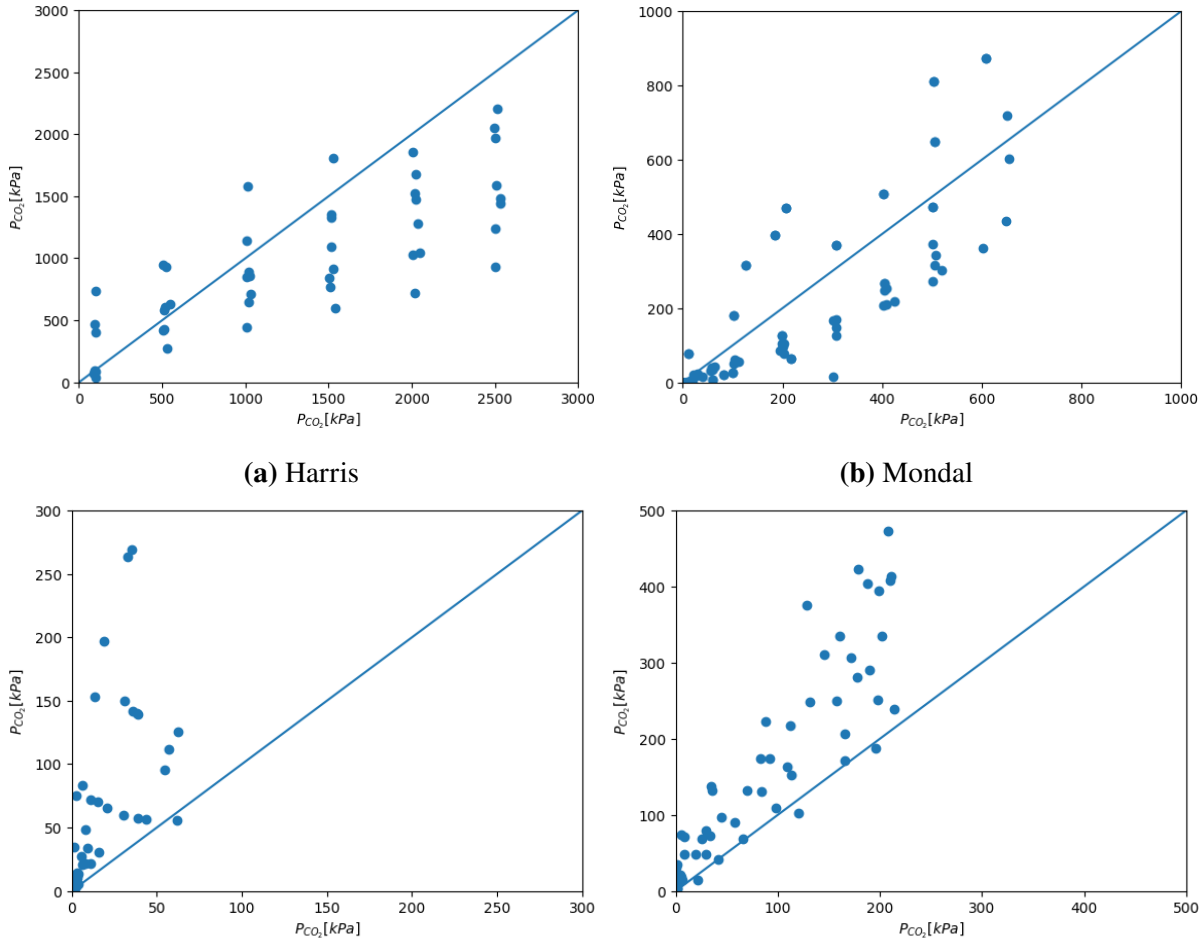

(a) Harris

(b) Mondal

(c) Portugal

(d) Song

Figure 12: Parity plots for the different authors

Based on the validation performed, it can be concluded that there is quite a discrepancy among the experimental data, and naturally the model is not in good agreement with the experimental data. In order to improve the data reliability, and consequently increase the accuracy of the model, further experimental campaigns should be carried out to minimize the deviation between the

experimental data and the simulation results. Further, additional datasets should be incorporated into ProTreat® to confirm the currently available model or develop the model further.

4.3.3 Activated MDEA Results

Further, VLE-validation using aMDEA was performed, which required conversion of some reported concentrations from molarities to weight percent. When converting from molarity to wt%, the density is a required parameter. This was assumed to be 1000 kg/m^3, as it was unknown for the different concentrations at the temperature which the solutions were prepared. It should be noted that this assumption could potentially introduce deviations between simulated and experimental values. The calculated weight percentages can be found in Appendix H.

From Figure 13a, Figure 13b as well as in Figure 36, the data suggests that the model is a better fit for temperatures 50 °C and 70 °C, compared to 90 °C, as the model overestimates all points for 90 °C. This trend is also apparent in Appendix E, for T=90 °C. As these are the only data points for higher temperatures using aMDEA, these findings suggest that the simulated results at higher temperatures, such as those from the stripper, may be less reliable. Additionally, Figure 14c shows that the model predictions are more accurate at lower partial pressures.

From Figure 13a and Figure 13e it appears that for α-values below 0.4, the model is slightly underestimating the pressure, while for α-values above 0.4 the model is slightly overestimating. This trend can also be observed in Figure 13f, but the shift occurs at a higher loading, around 0.7. Nevertheless, the model can be considered a satisfactory fit as the AARD is relatively small, and points close to the xy-line, at least for lower partial pressures, as seen in Figure 14a. However, the model tends to overestimate increasingly, as the CO_2 partial pressure increases. Derks' data only covers lower temperatures and pressures compared to the other authors, making it difficult to determine how it would perform in the actual process, where temperatures are significantly higher in certain parts.

From Figure 13c it can clearly be observed that the model is significantly underestimating the partial pressures at lower α-values. At α=0.2, the model is underestimating the partial pressure with two orders of magnitude, which is shown in Appendix G, Table 45, with high ARDs for lower loadings. Although the fit is better in Figure 13d and Figure 34, Figure 14b indicates that the model overestimates at higher partial pressures. It should be noted that experimental values at lower loadings are more difficult to measure, and usually carry a larger uncertainty.

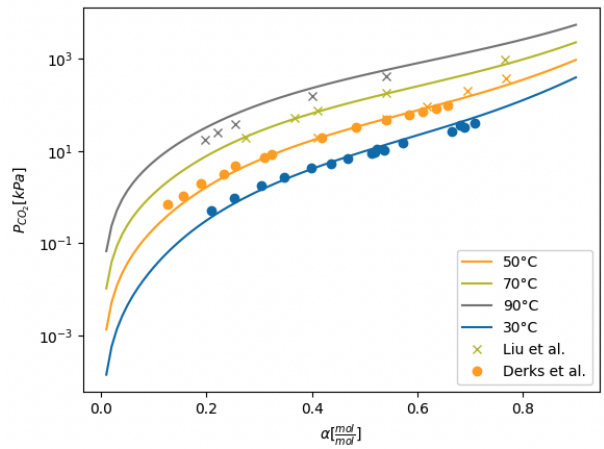

(a) 33 wt% MDEA, 6wt% PZ

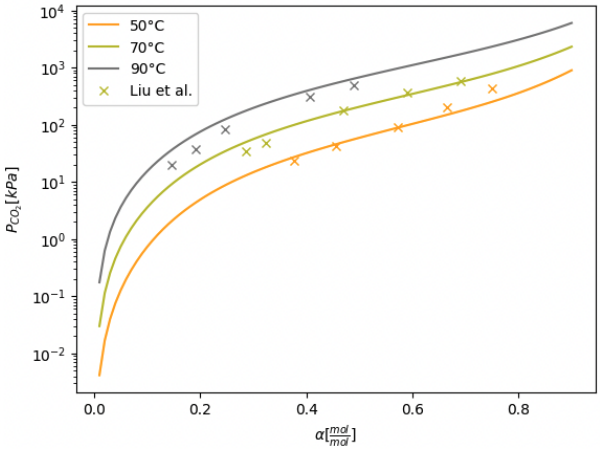

(b) 37 wt% MDEA, 3 wt% PZ

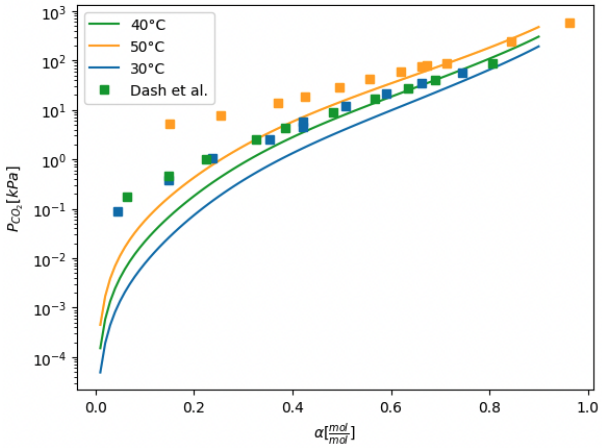

(c) 22 wt% MDEA, 8 wt% PZ

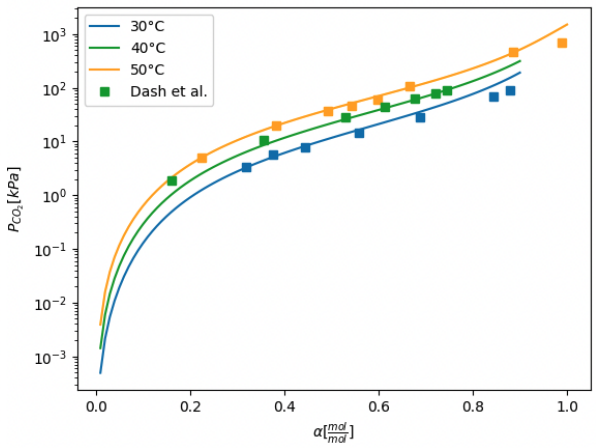

(d) 25 wt% MDEA, 5 wt% PZ

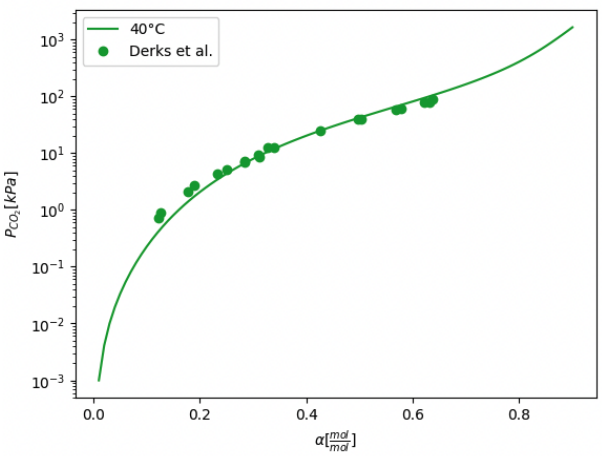

(e) 47 wt% MDEA, 6 wt% PZ

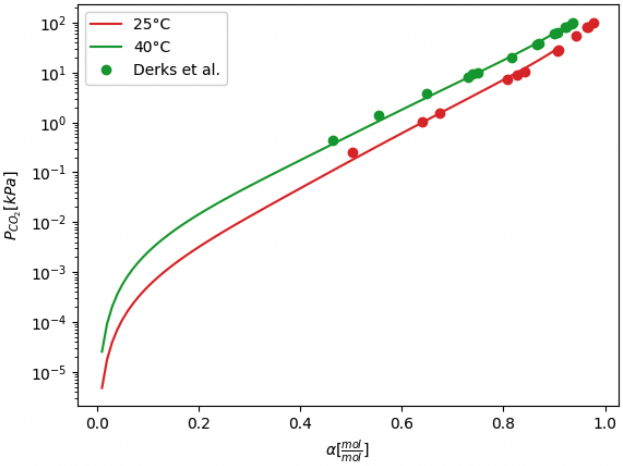

(f) 5% MDEA, 12 wt% PZ

Figure 13: VLE curves for aMDEA at different weight percentages generated for validation of thermodynamic model used in ProTreat®

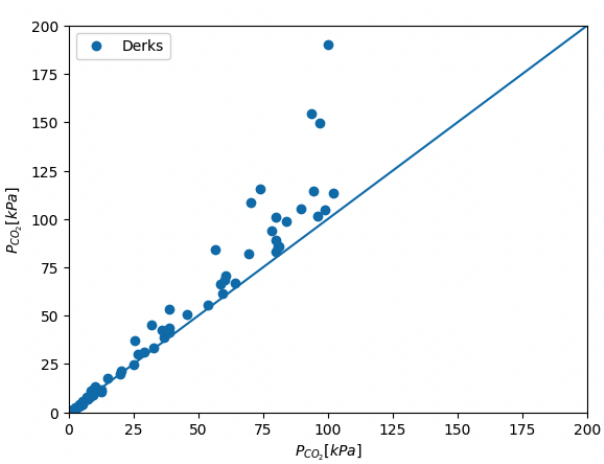

(a) Derks et al.

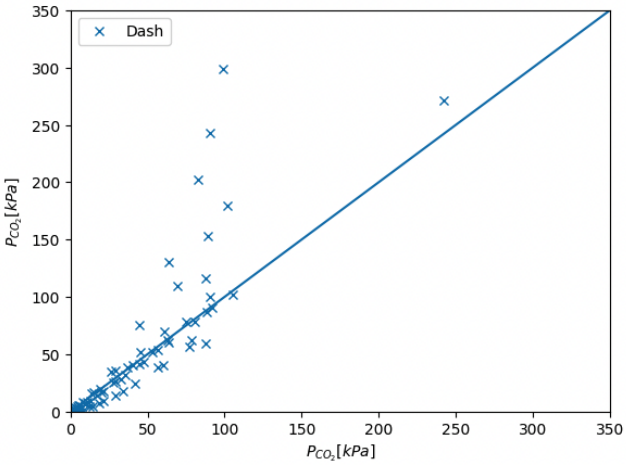

(b) Dash et al.

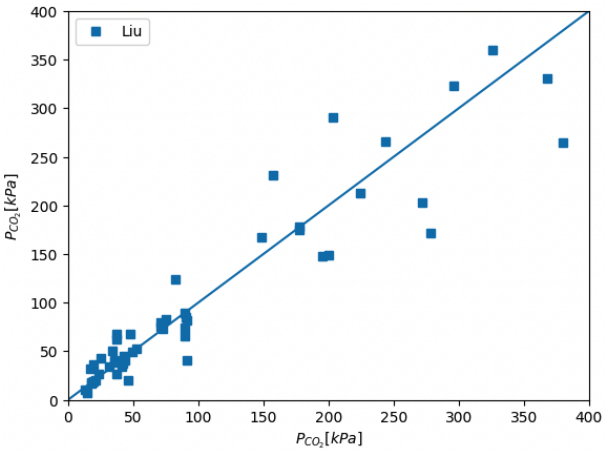

(c) Liu et al.

Figure 14: Parity plots for Derks, Dash and Liu

Except for the Dash et al.'s data the AARDs are below 23%, which is considered a strong alignment with the model. This is advantageous as it enhances the reliability of the upcoming results.

Chapter 5

Results and Discussion

This chapter presents the results and discussion of both simulations and experimental data. Further a comparison of the different solvents is presented, followed by the results from the economic analysis conducted.

5.1 Simulation results using NaGly

5.1.1 BaseCase

In Figure 15a the specific reboiler duty (SRD), defined as the required reboiler duty divided by the flow rate of CO_2 removed, is plotted against the liquid-to-gas ratio (L/G). The L/G represents the amount of solvent circulating in the system. It can be observed that at low L/G values, the SRD is high before rapidly decreasing. After reaching a minimum value, the SRD slowly increases as the L/G increases.

To maintain a constant capture efficiency at lower L/G-values, it is necessary to strip the solvent to a leaner loading to compensate for reduced amount of solvent in the system, as can be observed in Figure 15b. However, at higher solvent rates the reboiler duty is dominated by the heat required to increase the temperature and strip the larger amount of solvent.

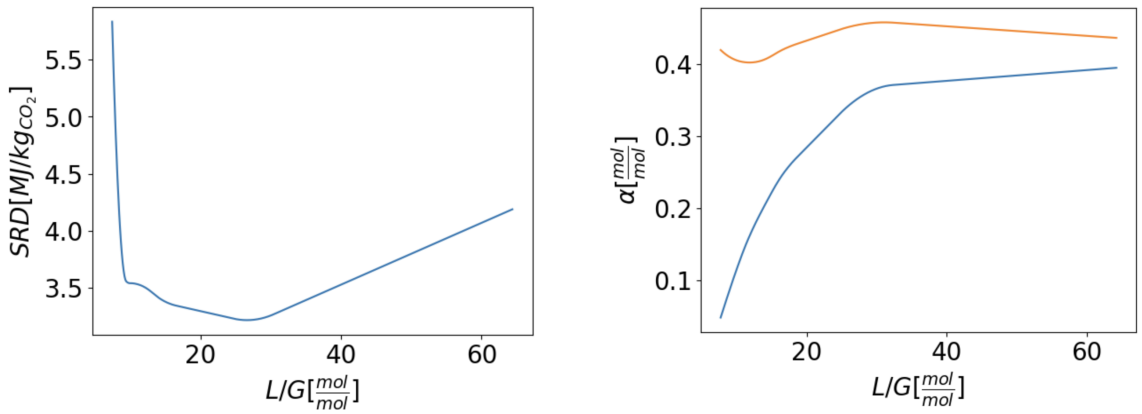

(a) SRD as a function of L/G for base case

(b) Lean and rich loadings for base case

Figure 15: SRD and loadings as a function of L/G for base case

The optimal point for the base case has an SRD is 3.19 MJ/kg CO_2 which occurs at a L/G-value of 28.4. This finding is consistent with previous studies by Ogava (2013) (3.3 MJ/kg CO_2) and Weiland (2010) (3 MJ/kg CO_2)[57][84], who also used 45 wt% NaGly in their simulations. Optimized Gas Treatment (2010) reported an even lower SRD of 2.24 MJ/kg CO_2 with 47 wt% NaGly[4]. However, the circulation rate corresponding to the minimum SRD is significantly lower for these cases, ranging from 1.1-24 L/m^3, compared to 28 L/m^3 reported in this study. This is expected as they simulated PCC processes, with a lower CO_2 concentration. Although the regeneration energy from simulations using the same software is within the same range, caution must be exercised due to the previously obtained validation results presented in Chapter 4. Rabensteiner et al. (2014), conducted the only experimental study, which resulted in regeneration energy requirements exceeding 5 MJ/kg CO_2. Considering the significantly higher energy requirements observed in the experimental studies, it is reasonable to expect that the regeneration energy requirements for this process also would fall within a higher range if implemented on pilot scale.

Figure 15b presents the lean and rich loadings plotted against the L/G ratio. As the L/G increases, the cyclic capacity decreases due to increase in the lean loading. However, the rich loading is expected to remain relatively constant, gradually decreasing only at higher L/G values. This behaviour is expected as the columns are designed such that the solvent is loaded to 90-95% of its equilibrium capacity, to maximize the use of the column. However, at higher L/G values, the amount of solvent exceeds the necessary amount to achieve this desired loading. Consequently, the rich loading starts to decrease.

However, the findings presented Figure 15b demonstrates an interesting pattern: the rich loading is initially declining before gradually increasing to its maximum value, before slowly declining again. It can be observed that the maximum rich loading occurs at the same L/G-value as the minimum SRD value. This behaviour can be explained by looking at the temperature profiles and CO_2 partial pressures through the absorber.

In Figure 16 the temperature profiles for the optimum case (orange graph) and for a case with lower circulation rate (blue graph) is presented. Segment 0 is at the top of the column, whilst segment 70 is at bottom. As can be observed the two temperature profiles exhibit significant differences. In the optimum case, temperatures do not exceed 50 °C, while in the other case, the temperature reaches values as high as 95 °C. These temperatures have the potential to cause desorption in the column, resulting in the unwanted release of CO_2 from the solvent in the absorber. The temperature increase is caused by the heat generated by the exothermic reaction between the AAS and CO_2, which is caused by high heat of absorption for NaGly as presented in Table 3. The differences in temperature profiles can be attributed to the varying amounts

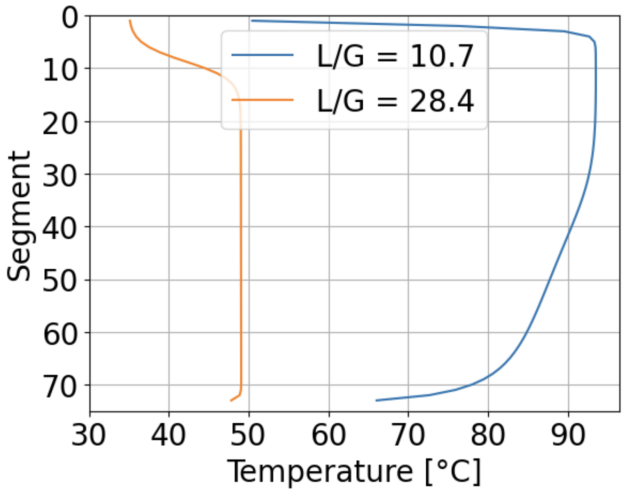

Figure 16: Absorber temperature profiles for two cases

of liquid available for heating in the absorber between the two scenarios. Further, it could explain why the rich loading does not reach its maximum value at lower L/G-values, as the CO_2 starts to desorb before the solvent has reached its desired loading. From Figure 17 the actual and equilibrium partial pressures for the two cases are presented. For the lower L/G case (Figure 17a), pinching occurs around segment 5, indicating that there is no driving force for further absorption throughout the rest of column, as the temperature is too high for absorption to occur.

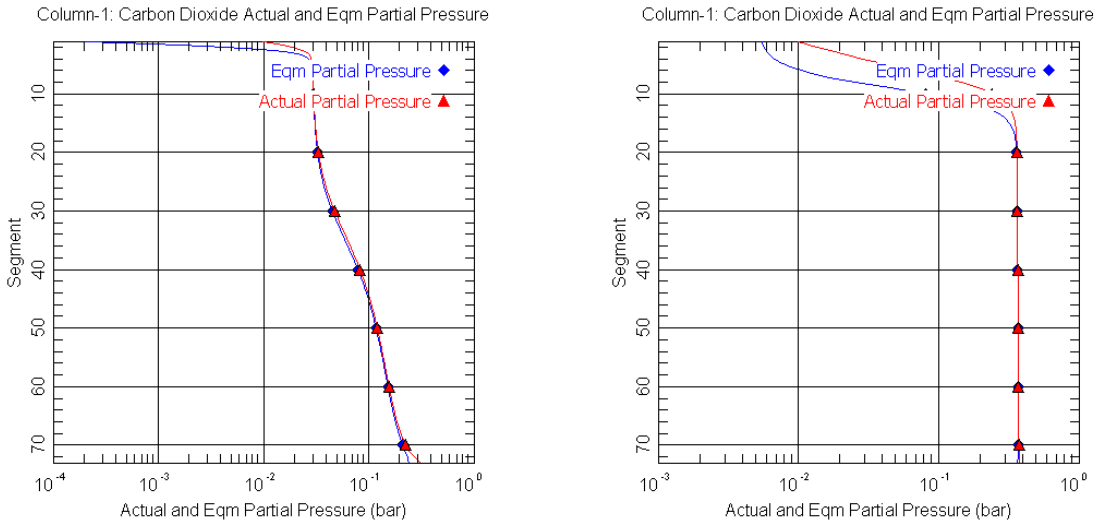

(a) For case with L/G= 10.7

(b) For optimum case

Figure 17: CO_2 actual and equilibrium partial pressure

However, as the L/G value increases, as for the optimal case, the absorber temperature decreases, and the pinch point occurs at a later stage in the column. This indicates that more CO_2 has been absorbed, resulting in an increased rich loading. Increasing the rich loading, minimizes

the regeneration energy requirements, which explains why the maximum rich loading occurs at the minimum SRD point. Ideally, pinching should not occur in the column, to ensure to optimal utilization of the solvent. Then a driving force for absorption is maintained across the entire column.

Nevertheless, operating with a L/G ratio of 28.4 entails large expenses connected to other operational costs, including pumping. Thus, it is desirable to reduce the circulation rate, while maintaining a low SRD. Therefore, different process modifications were implemented.

5.1.2 Intercooled Absorber

An IC was implemented to reduce the temperature in the absorber, to ensure absorption throughout the column, and to increase the rich loadings for lower L/G-values. When implementing ICs, there are various variables that need optimization, such as the positioning of the cooler. In Figure 18a the SRD plotted as a function of L/G can be observed for IC cases at different positions from the top of the absorber. For instance, the IC=2.5m case refers to the IC being placed 2.5 m from the top of the column.

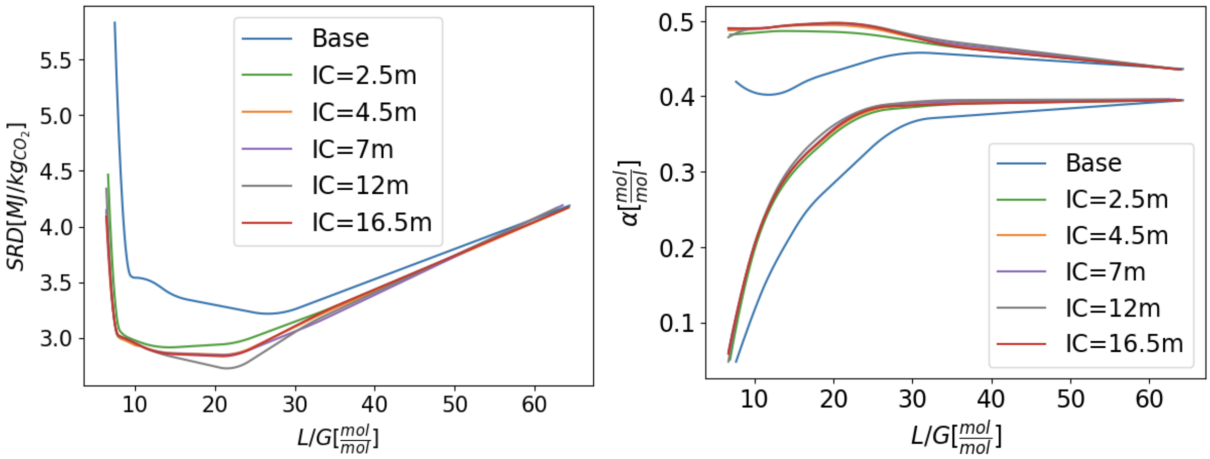

(a) SRD as a function of L/G for IC cases

(b) Lean and rich loadings for IC cases

Figure 18: SRD and loadings as function of L/G for IC cases and base case

The presented results in Figure 18a, indicate that all IC cases exhibit lower energy requirements compared to the base case. Additionally, the L/G values corresponding to the optimal points are all reduced compared to the base case. The minimum SRD of the IC cases is for the 12 m case, with a value of 2.7 MJ/kg CO_2 at L/G=23, which is a 15.4% decrease compared to base case. The second lowest SRD was for the 16 meter case, with an SRD of 2.83 MJ/kg CO_2 at L/G=25. According to literature, the energy savings achieved through the implementation of ICs can vary

significantly depending on the solvent used. To the extent of the author's knowledge, ICs has not been implemented to reduce energy requirements when using NaGly as solvent.

Further, from Figure 15b it can be observed that all IC cases reach higher rich loadings compared to the base case, which is in line with theoretical expectations. The presence of ICs facilitates higher rich loadings, by reducing the temperature and increasing the driving force for absorption. This decrease in temperature also leads to a reduced requirement of absorbent, resulting in lower energy demands in the stripper. The highest rich loading achieved with ICs was α=0.499, compared to α=0.46 for the base case. This is also consistent with theory as the maximum theoretical loading for NaGly is 0.5 at these pressures, due to the formation of carbamates and protonated AAS's. The rich loading increased 8.5%, which suggests that ICs can be an effective way of increasing the rich loading, while reducing the energy consumption. For the IC cases the rich loadings remain relatively constant until L/G value of 25, after which it starts to decrease. This is also where the minimum SRD value is reached for the IC cases according to Figure 18a. This indicates that once the minimum SRD value is reached, further increasing the solvent circulation rate no longer fully utilizes the absorption capacity of the solvent as there is an excess amount of solvent in the system.

The data indicates that among the IC cases, the 2.5m case exhibits the highest energy requirements. This finding is consistent with the observations made by Karimi et al. (2011) and Moullec & Kanniche (2011), who suggest that the positioning of an IC at the lower sections of the absorber leads to greater impact. However, it is worth noting that the energy demands of the other IC cases are relatively comparable, except for the 2.5m case, which stands out due to its higher energy requirements.

In all IC cases considered in this study, the fraction of liquid to be cooled was maintained at one, while the outlet temperature of the cooler was set to 25 °C. Although these variables should ideally be optimized for optimal results, this was not done due to time constraints. Nevertheless, considering the significant temperature increase, cooling to a low temperature was likely necessary in order to maintain a driving force for absorption throughout the column.

5.1.3 Lean Vapor Recompression

In Figure 19a the SRD as a function of L/G is presented for the base case and the LVR case. It can be observed that the LVR case does not reach high L/G-values, as the simulations ceased to converge at L/G-values above 16, due to potential flooding in the system. Therefore, the LVR

configuration was not fully investigated within the given time frame of the thesis.

The lean and rich loadings for the LVR case and the base case are presented in Figure 19b. The results indicate that the LVR configuration closely follows the base case, thus the configuration does not show the same effect on the rich loading as with IC. This is expected as a LVR configuration reduces the amount of liquid entering the reboiler, and improves heat usage, but does not directly impact the absorption process.

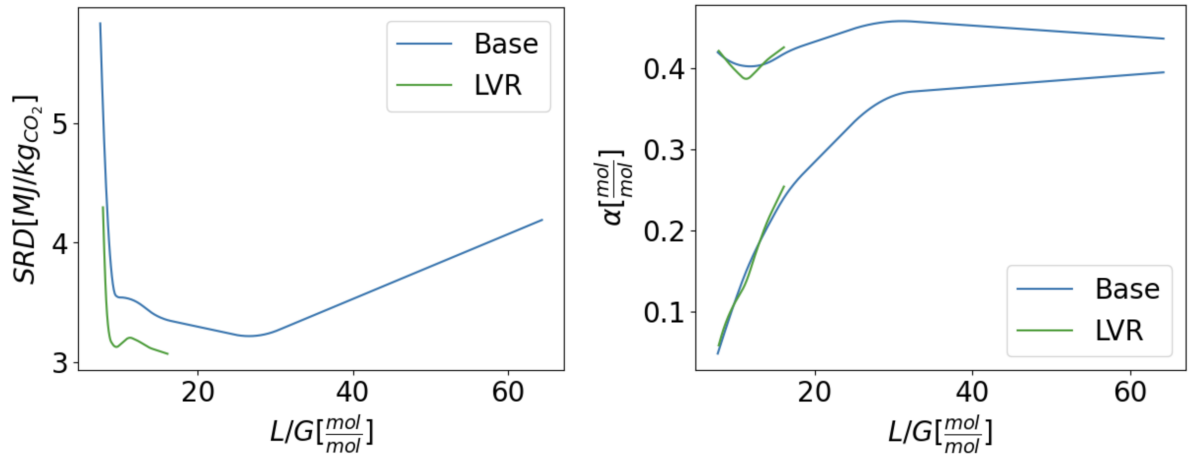

(a) SRD as a function of L/G for LVR and base case **(b)** Lean and rich loadings for LVR and base case

Figure 19: SRD and loadings for LVR case and base case

However, based on the simulations that have converged, the results indicate that the SRD values are lower compared to the base case. The declining trend of the graph at the endpoint, suggests that the minimum SRD of the LVR configuration may not have been reached. However, it is challenging to draw conclusions with incomplete simulations. If the end point is assumed to be the minimum SRD value, the LVR configuration reduces the SRD by 3.8% compared to the base case. This is because the vapor produced in the flash tank, mostly composed of CO_2 and H_2O, acts as a stripping steam, thus reducing the steam requirements from the reboiler. The reduction is smaller than Karimi et al. (2011), and Moullec & Kanniche (2011) reported when using MEA, which were between 7.78 and 9.36%.

Compared to the effect of an IC, the LVR configuration shows a smaller effect on the SRD. These findings contradict the results obtained by Kvamsdal et al. (2011), who reported that the LVR has a more pronounced effect on the SRD than the IC (IC)[(85)]. Nevertheless, it is possible that the effect could have been more prominent if the system had been properly optimized.

As mentioned earlier, Knudsen et al. (2011) reported that a LVR configuration have a more significant impact on solvents with higher energy requirements. The results of this study may

indicate that NaGly has high energy demands, similar to those of MEA. Consequently, LVR might have given a large energy penalty if implemented correctly. Furthermore, the combination of LVR with IC has been demonstrated to drastically reduce energy requirements for MEA [34], indicating the potential for further investigation of LVR in combination with intercooling. However, this was not investigated in this thesis.

5.1.4 Split absorber

The results from the split absorber case can be found in Figure 20. In practice, the system is identical to the base case. However the total height of the column was 20 meters, compared to 22 meters for the base case. From Figure 21a and Figure 21b it can be observed that the two graphs closely align with each other, indicating that the two-column system resembles the behaviour of the base case quite accurately. Based on the results, it can be concluded that the two additional meters of column height in the base case do not significantly limit the mass transfer, and could therefore be removed.

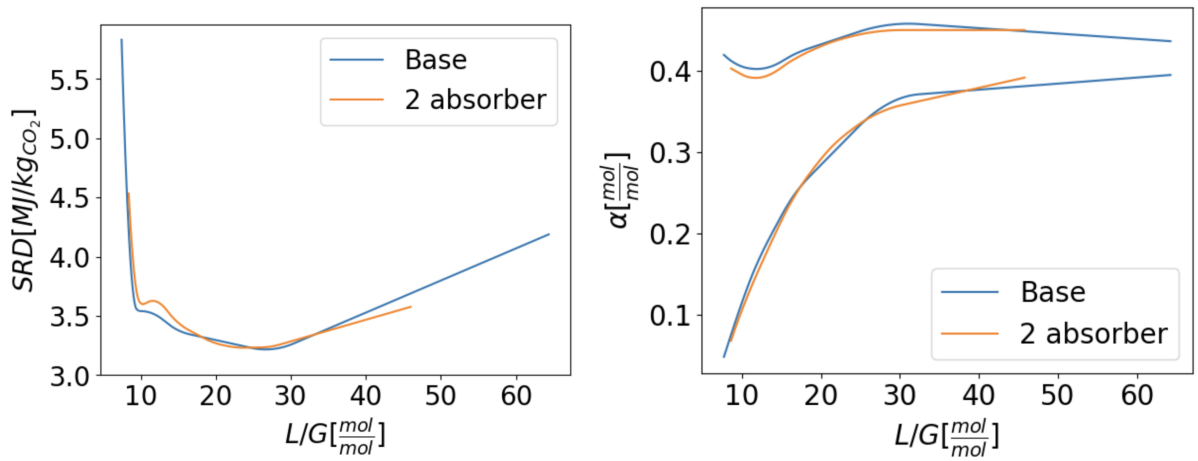

(a) SRD as a function of L/G for two absorber system and base case

(b) Lean and rich loadings for two absorber system and base case

Figure 20: Two absorber system SRD and loadings

Further, ICs were implemented in the split absorber system. Firstly, an IC was implemented in the second column (20-1) at 4 meters from the top. Secondly, ICs were implemented in both absorbers, both at 2.5 meters from the top. As shown in Figure 20a, ICs successfully reduced the specific energy requirements. As anticipated, two ICs performed better than one, which is also illustrated in Figure 21b, as the rich loading is higher with two ICs. One obvious explanation, is that the solvent is cooled to a lower temperature with two ICs, facilitating for a higher rich loading. A second explanation, could be the placing of the ICs. When having two ICs 2.5 m

from the top of both absorbers, this in reality means one at 2.5 m from the top, and one at 12.5 m from the top. As previously mentioned, positioning the IC in the lower part of the absorber, generally result in lower energy requirements. Furthermore, as the rich loadings increased with the use of ICs, the need for excessively lean loadings are reduced.

The rich loadings from both absorbers are combined before entering the heat exchanger. Upon closer examination of the individual rich loadings from the three cases (Figure 22), it is evident that the most significant increase in rich loading occurs when the IC is implemented in the first *(40-20)* absorber, thus in the lower part of the column. The rich loading for the second column with one IC (green dotted line), and rich loading of second column without IC (blue dotted line) show similar behaviour, which suggests that implementing an IC in the top half of the column, does not significantly affect the rich loading.

An interesting observation can be made when comparing these results to the single column with IC cases, from Chapter 5.1.2. In the 12-meter configuration the minimum SRD was 2.70 MJ/kg CO_2, whereas in this configuration the minimum SRD was 2.93 MJ/kg CO_2 with two ICs. Further, the highest rich loading value was 0.499, identical to that with one IC. This finding suggests that the IC located at the top is unnecessary, as the SRD is larger, and the rich loading can reach the same values without the additional IC.

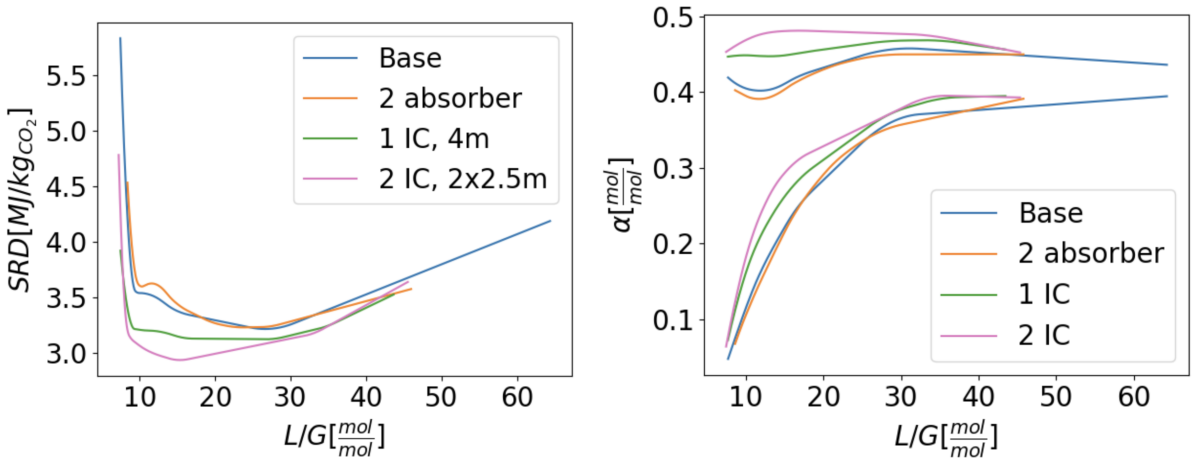

(a) SRD for two absorber system and base case **(b)** Loadings for two absorber system and base case

Figure 21: SRD and lean and rich loadings as a function of L/G for two absorber system and base case

In Figure 22, when examining the 1 IC case (indicated by the green lines), an interesting observation can be made. The rich loadings exhibit a crossover phenomenon. Initially, at lower L/G-values, a significant portion of the absorption occurs in the first column, which corresponds to a lower stage as indicated by the *40-20* graph positioned above the 20-1 graph. However,

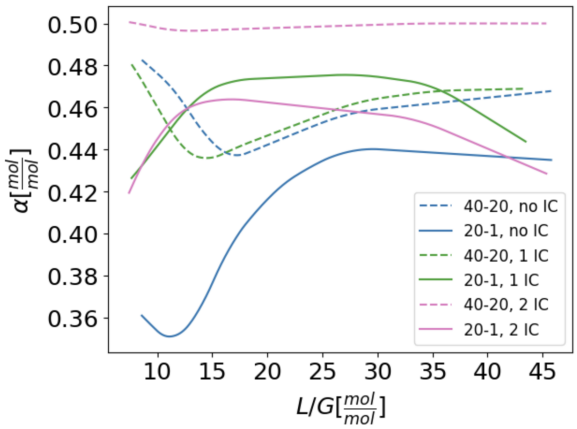

Figure 22: Separate rich loadings for the three different configurations

as the process continues, the graphs intersect, implying a shift towards a greater proportion of absorption occurring in the *20-1* column.

The results from the split absorber system do not demonstrate better performance compared to the base case, both with and without ICs. When considering the potential additional cost and increased complexity when implementing this system, it can be concluded that this configuration does not produce sufficient benefits to justify its adoption.

5.2 Experimental Results

As mentioned earlier precipitation experiments were conducted to find out if and when precipitation occurred for 45 wt% and 35 wt% NaGly. The experiments were carried out following the completion of simulations and validation procedures for NaGly.

5.2.1 45 wt% NaGly

A preliminary test was performed to determine the time taken for precipitation to occur with 45 wt% NaGly. The findings indicated that precipitation occurred only after 6 minutes, leading to the decision to sample the solution every minute. Appendix L, Table 49 and Table 50 presents the results of the two 45 wt% NaGly runs. In Figure 24a the loadings calculated based on weight increase over time is presented, and in Figure 24b the loadings based on the TOC results can be found. From Figure 24a it can be observed that there was a significant increase of the loading during the first 10 minutes, which gradually decelerated over time. From visual observations small particles were observed in the solution already after one minute, and the high temperature of the solution required careful sampling to prevent burning. However, the temperature was not monitored during the experiment. Notably, there are no TOC results after five minutes, as the solution's viscosity was too high for the TOC analysis. The solution solidified over time and failed to flow when turned upside down after 24 hours, as shown in Figure 23, thus releasing the solution from the glass bottle required heating. The highlighted value in Table 49, which is the orange dot in the lower right corner in Figure 24b, is incorrect as it is lower than the prior value, likely due to not obtaining the correct amount of sample as the solution had become too thick.

Figure 23: 45 wt% NaGly solution, 24 hours after ended experiment

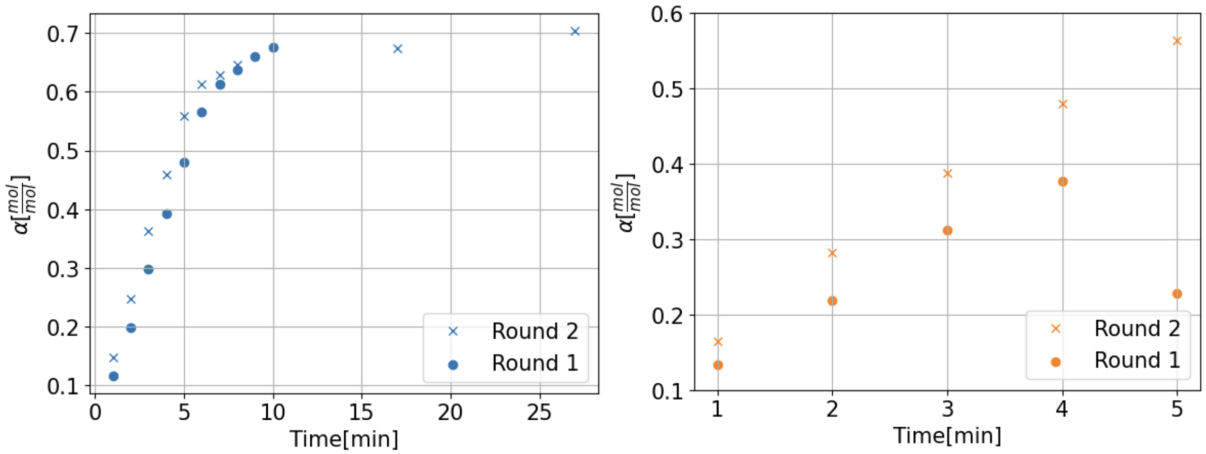

(a) Calculated loading based on weight increase

(b) Loadings based on TOC results

Figure 24: Loadings for 45 wt% NaGly

It is evident that the concentration of NaGly was too high to avoid precipitation, even at low loadings. However, it was when the loading reached 0.5, the solution turned white, and started thickening, which is at the point it has reached its maximum theoretical loading. The nature and composition of the precipitate was not investigated or determined. The precipitation results are consistent with those made by Aronu et al. (2013) when studying typical AASs[86]. Although, they investigated the precipitation behaviour of NaGly with concentrations starting from 53 wt% (5.5M) NaGly, the solution became white and viscous even at low CO_2 concentrations, but did also achieve high CO_2 loading. Moreover, the precipitate did not dissolve at 80 °C, and the authors were unable to strip it due to blockage of sintered gas lines caused by the precipitate. These findings contradict those of Rabensteiner et al,'s (2014) who did not report precipitation from a pilot study using 40 wt% NaGly[51]. One possible explanation for this difference could be the CO_2 concentration of the gas, as Rabensteiner utilized flue gas, while Aronu and this work utilized 100% CO_2 gas.

5.2.2 35% NaGly

Due to the rapid precipitation observed in the 45% NaGly case, it was decided to repeat the experiment with 35 wt% NaGly. For the first round, samples were taken every minute for the initial ten minutes, after which the sampling frequency was reduced as the solution remained clear throughout the experiment, allowing it to proceed for an hour. In the second round samples were only taken every ten minutes. The results for round 1 and 2 can be found in Table 51 and Table 52, respectively. Figure 25 presents the loadings based on the weight increase, and the

total organic carbon (TOC) results. It is clear from the figures that also at this concentration most of the absorption takes place during the first ten minutes. Interestingly, the loadings significantly exceeded the maximum theoretical loading of 0.5 without visible precipitation. However, precipitation occurred about an hour after the experiment ended. After 24 hours, the precipitation had settled as can be observed in Appendix L.2. The solution was less viscous compared with to the 45 wt% solutions, possibly because 35 wt% did not reach as high loadings. The results indicate that precipitation is strongly influenced by the solvent temperature.

The solubilization temperature for the 35 wt% solutions were determined by heating them until all precipitation had dissolved. For run 1, the precipitation dissolved at 78 °C, while for run 2 the temperature was 82 °C. These results suggest that the operational temperature for the absorber must be around 80 °C to prevent precipitation with 35 wt% NaGly. It is crucial to maintain a driving force for absorption and avoid desorption in the absorber. Operating the absorber at 80 °C, will lead to low absorption rate, due to equilibrium shifting to desorption of CO_2.

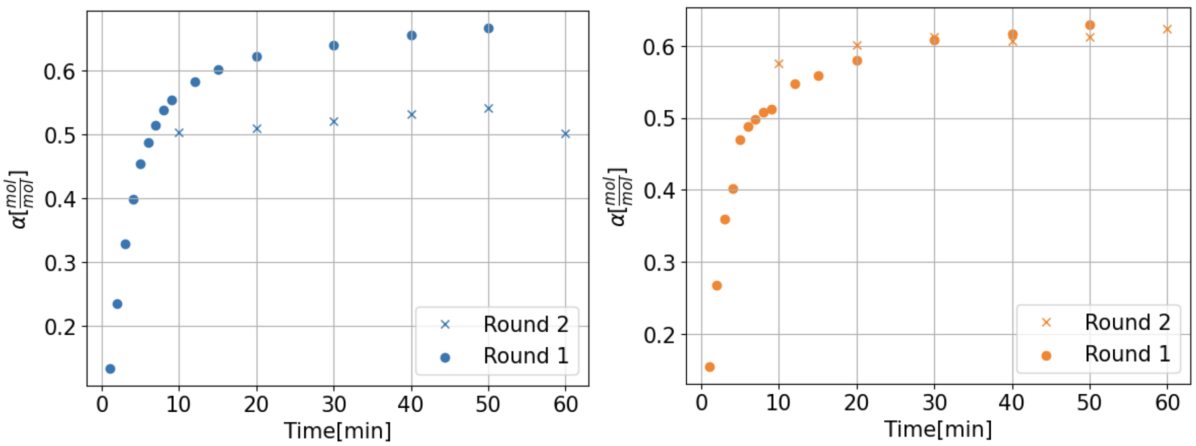

(a) Calculated loadings at 35 wt%

(b) TOC loadings at 35 wt%

Figure 25: Loadings for 35 wt% NaGly

There are various sources of uncertainties in the experiments. Firstly, preparation of solvent and sampling may have introduced some human errors, which could have affected the results. The concentration should have been verified by titration, but this was not feasible due to time constraints. Additionally, it was challenging to maintain a constant flow rate of CO_2 during the experiments, as the valve had to be turned on and off manually for each sampling, potentially impacting the absorption rate and leading to a wrong representation of how rapidly the loadings were achieved.

Considering the findings from the conducted experiments, it was determined to end simulations involving NaGly. The credibility of the simulation results is significantly compromised by the

experimental results, particularly those involving intercooling. This is primarily due to the high likelihood of precipitation at these temperatures, which would result in severe operational challenges such as pipe blockages.

To prevent precipitation, it is recommended to conduct additional experimental campaigns aimed at determining the optimal concentration for operating without the occurrence of precipitate formation. Although NaGly might have potential as a solvent for biogas upgrading, extensive research efforts are necessary to fully realize its potential in this regard.

5.3 Simulated results using aMDEA

The simulations conducted using aMDEA were based on the same base case depicted in Figure 9. However, previous simulation results from this thesis and earlier work by the author have consistently shown the need for ICs to facilitate absorption across the entire column, particularly due to the elevated temperatures involved. Consequently, all simulations involving aMDEA have one intercooler implemented in the lower section of the absorber.

In Figure 26a the SRD as a function of L/G is presented for the aMDEA and the optimal IC NaGly case. It is clear that there is a significant reduction in the SRD between the cases. Specifically, the aMDEA case achieved a minimum SRD of 1.72 MJ/kg CO_2 at a L/G-value of 7.9, while the optimal NaGly case with IC, had an SRD of 2.70 MJ/kg CO_2 at L/G-value of 23. This represents a 36 % decrease in reboiler duty between the two cases.

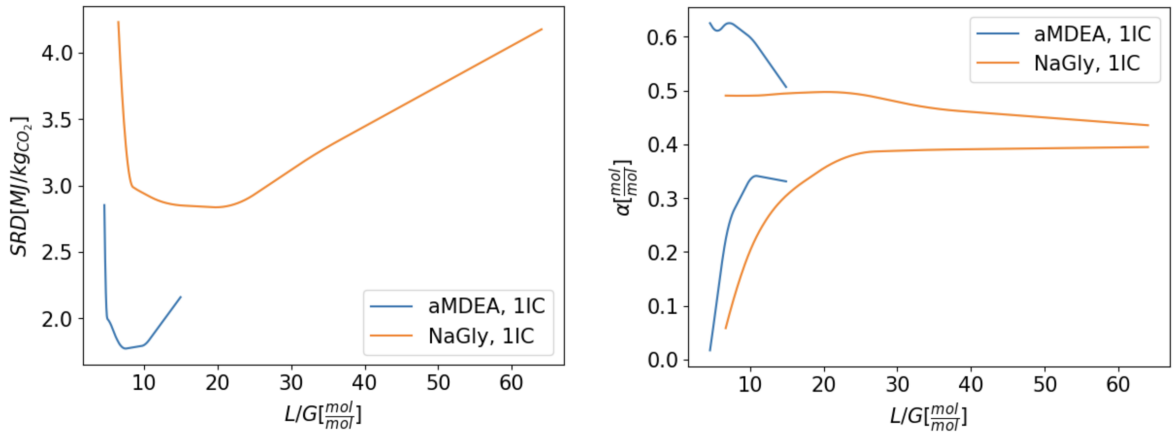

(a) SRD as a function of L/G for aMDEA and NaGly with 1 IC

(b) Lean and rich loadings aMDEA and NaGly with 1 IC

Figure 26: Comparison of aMDEA and NaGly SRD and loadings

The results show that using aMDEA as solvent leads to lower energy requirements, resulting in a more efficient system, and potentially lower operational costs related to the reboiler. The reduction in required circulation rate offers several benefits, including a reduced amount of solvent required and potential cost savings in terms of other operational expenses, such as pumping.

When comparing the SRD with previous research conducted on aMDEA, the findings exhibit considerable variations. The obtained SRD value is considerably lower than the result obtained by Khan et al. (2020), as their simulations, resulted in an SRD of 3.235 MJ/kg CO_2 [(65)]. However, with cold solvent split process modification the SRD was reduced to 2.78 MJ/kg CO_2. Zhao et

al. (2017) reported an SRD 2.24 MJ/kg CO_2, while Zhao et al. (2021) reported a significantly lower value of 0.617 MJ/kgCO_2 [87] [88], all for flue gas CO_2 capture. The differences may be caused by different MDEA/PZ ratios, different specifications, and parameters in the simulations.

From Figure 26b it can be observed that the rich loading in the aMDEA case exceeds 0.5. This is because MDEA, as a tertiary amine, and PZ as a di-amine, does not exhibit the theoretical maximum rich loading of 0.5, as NaGly does. Additionally, it can also be observed that the rich loading is decreasing quite rapidly, based on the initial observation. However, this perception is influenced on the zoom level of the graph, and when zoomed in the behaviour appears more aligned with theoretical expectations, which can be seen in Chapter 5.3.1.

In Figure 27a it can be observed from the temperature profile through the absorber, that the temperature reaches a maximum value of 55 °C, even with a shorter column (15 meters) than with NaGly (22 meters). This might be due to the difference in heat of absorption between the two solvents MDEA and NaGly, as can be seen in Table 3. One can observe that MDEA exhibits a considerably lower heat of absorption in comparison to NaGly, resulting in a distinct difference in temperatures within the absorber. Although PZ has a similar heat of absorption to NaGly, the concentration of PZ is significantly lower than the concentration of NaGly, thus the amount of heat generated from the reaction between PZ and CO_2 is smaller.

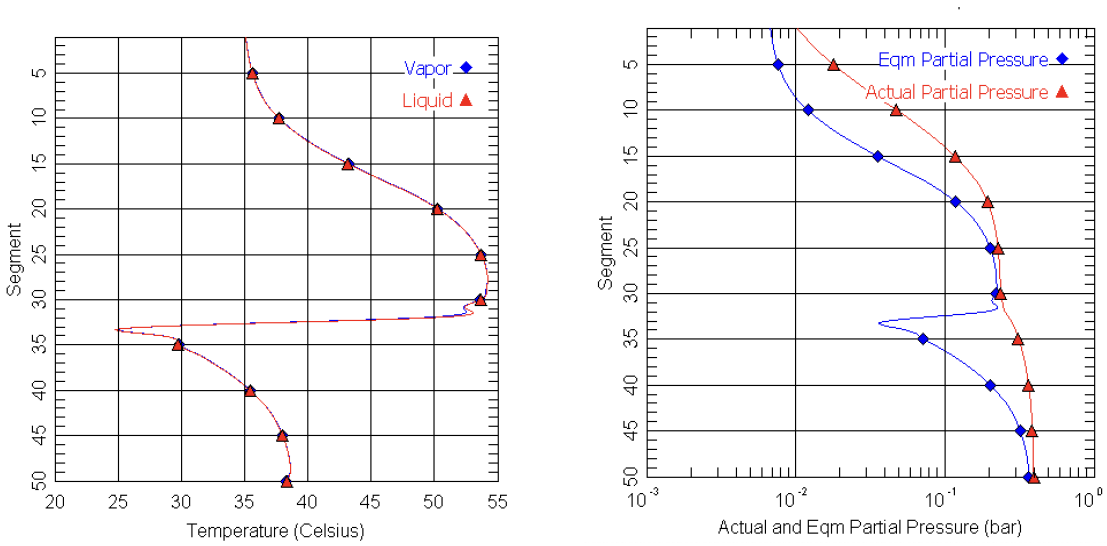

(a) SRD as a function of L/G for aMDEA and NaGly with 1 IC **(b)** Lean and rich loadings aMDEA and NaGly with 1 IC

Figure 27: Comparison of aMDEA and NaGly SRD and loadings

From Figure 27b it can be noted that that there is no pinching occurring in the system, indicating that a driving force for absorption is maintained throughout the column. The CO_2 equilibrium partial pressure is significantly reduced in the segment where the IC is positioned.

5.3.1 Pressurized Systems

Furthermore, the implementation of pressurized systems were explored, operating pressures at 3, 5, and 8 bara. As can be observed from Figure 28a the specific reboiler duty decreases with increasing pressure. The 1.05 bara case exhibited a minimum point of 1.72 MJ/kg CO_2 at a L/G-value of 7.9, while the 8 bara case showed a minimum point of 1.35 MJ/kg CO_2 at a L/G-ratio of 7.7. This represents a 21% decrease in the SRD between the two cases.

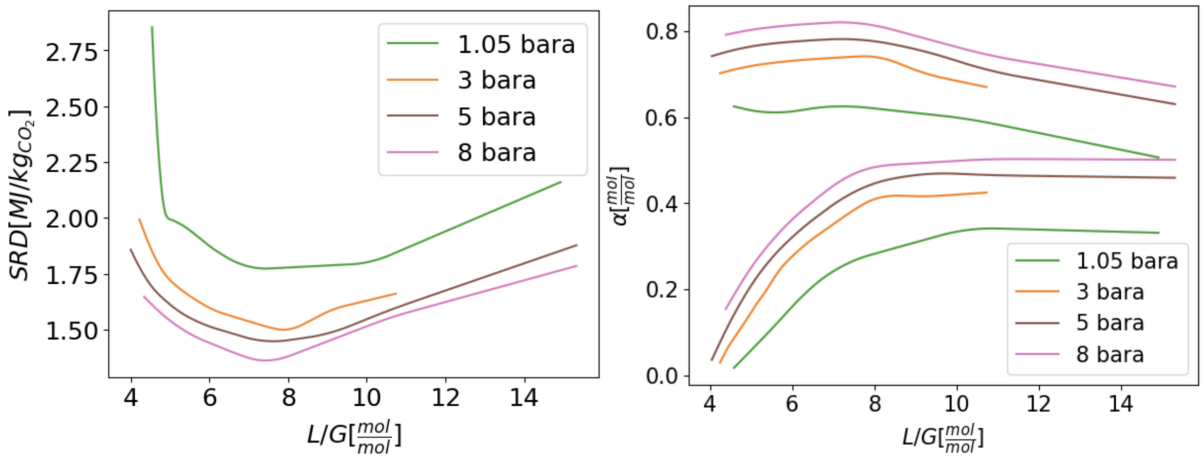

(a) SRD as a function of L/G for pressurized aMDEA cases

(b) Lean and rich loadings for pressurized aMDEA cases

Figure 28: IC SRD and loadings

The observed trend is consistent with theoretical expectations, as the solubility of CO_2 increases with increasing pressure, resulting in reduced solvent requirements [89]. Furthermore, the reaction rate between amines and CO_2 increases with increasing pressures, thus less energy is required to maintain the same level of CO_2 removal.

From Figure 28b the relationship between lean and rich loadings and the L/G-ratio can be observed. It can be observed that the rich loadings are increasing with increasing pressure. All cases exhibit the same trend, a relatively constant rich loading before gradually decreasing. As the solubility of CO_2 increases with increasing pressure, the amount of CO_2 that can be solubilised in the same amount of solvent increases. When the rich loading is increasing, the solvent does not have to be stripped to the same degree, thus less energy is required for stripping, which results in higher lean loadings. Actually, the cyclic capacities are somewhat constant for all cases, for instance the 1.05 bara case has a cyclic capacity of 0.334, while the 8 bara case has a cyclic capacity of 0.338. Khan et al. (2017) investigated the solubility of CO_2 in aMDEA at different pressures [90], and found that the rich loading increased with increasing pressure, but

decreased with increasing temperature. It is important to note that after compressing the inlet gas, it was cooled down to 35 °C, as the absorption process is largely temperature dependant. The temperature dependency was not investigated in this thesis due to time constraints.

5.4 Comparison of Solvents

In this thesis, simulations with NaGly and aMDEA have been conducted. However, from earlier work done by the author in the autumn of 2022, simulations using CESAR1 and MEA were conducted for the same system. In Figure 29a the SRD plotted against the L/G can be found for the different solvents. All simulations are done with one IC, placed in the lower half of the column.

Figure 29a clearly shows that the aMDEA exhibits the lowest energy requirements, followed by CESAR1. This finding is in line with theoretical expectations, considering aMDEA and CESAR1 are tertiary and sterically hindered amines, with PZ acting as a promoter. Tertiary and sterically hindered amines typically have higher absorption capacities due to their theoretical loading of one mole CO_2 per mole amine, thus higher rich loadings can be achieved, as can be observed from Figure 29. Consequently, these amines require less solvent, which is reflected in the lower L/G-values compared to NaGly and MEA. Additionally, their heat of reaction is lower than primary amines as they do not form carbamate, resulting in lower energy requirements for regeneration[91].

However, these amines suffer from low reactivity towards CO_2. The presence of PZ, a primary amine, enhances reactivity, and increases the stability of the solvent and the overall process efficiency[43]. Nonetheless, there are still some differences between aMDEA and CESAR1 in terms of energy requirements, likely attributed to their differences in heat of absorption (Table 3).

Addtionally, it can be observed that the MEA and NaGly cases are following each other closely, and from Table 14 it can be observed that the minimum SRDs are similar to each other. This finding has a positive implication for NaGly as it demonstrates that its energy requirements are comparable to those of MEA, while offering the advantages of an AAS, as discussed in Chapter 2.4.3. Since MEA and NaGly have a primary amine group, the heat of absorption is more or less the same, which can be seen from Table 3, which can imply that the regeneration energy requirements also are in the same range. The results are backed by Weiland[4], who also reports that the SRD is almost identical for 45 wt% NaGly and 30 wt% MEA.

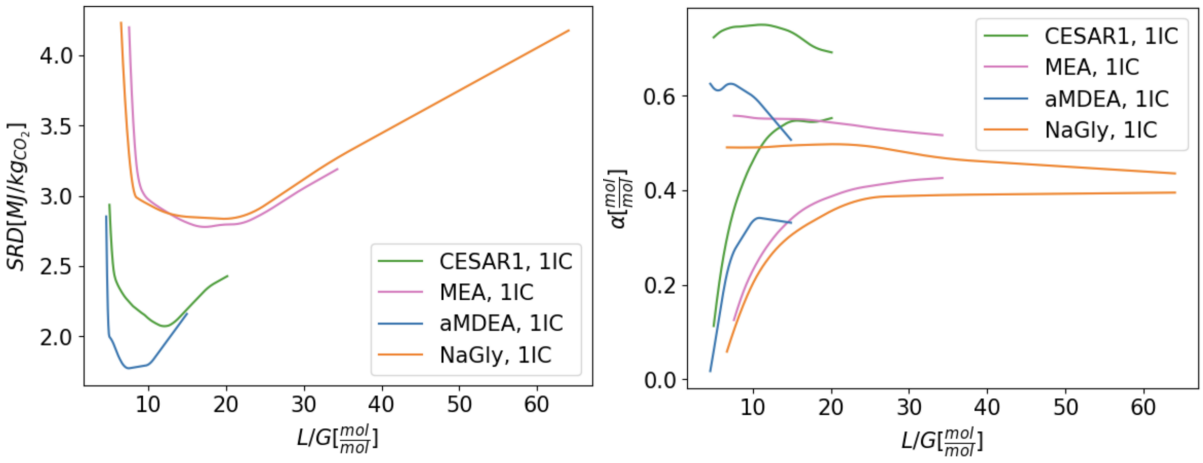

(a) SRD as a function of L/G for different solvents. **(b)** Lean and rich loadings for different solvents

Figure 29: Comparison of different solvents in terms of SRD and loadings vs. L/G ratio

However, it is important to acknowledge that the simulations conducted with NaGly, may not be directly used to design a process due to the possibility of precipitation formation according to the experimental results in Chapter 5.2. The experimental findings indicated that a NaGly concentration lower than 35 wt% was required to avoid precipitation. This requirement would increase the energy demands, as a larger quantity of solvent would be needed to achieve the same removal efficiency. Consequently, the comparability of NaGly and MEA, in terms of energy requirements, would likely no longer hold true.

Table 14: Information about minimal points of each solvent

Solvent	SRD [MJ/kg CO_2]	L/G [mol/mol]	Lean [mol/mol]	Rich [mol/mol]	Cyclic Capacity
aMDEA	1.716	7.90	0.302	0.636	0.334
CESAR1	2.063	12.28	0.532	0.750	0.218
MEA	2.768	17.53	0.373	0.594	0.221
NaGly	2.828	23.10	0.385	0.499	0.114

Analyzing the cyclic capacities presented in Table 14, it is clear that aMDEA exhibits the largest cyclic capacity, while NaGly has the lowest. A higher cyclic capacity implies that a greater amount of CO_2 can be captured by a specific quantity of absorbent[26]. Interestingly, despite the disparity in required solvent amounts, the cyclic capacities of MEA and CESAR1 are quite similar. However, the rich value of MEA (0.594) surpasses the theoretical maximum loading, which could be explained by the effect of pressure and physical solubility.

5.5 Economic Analysis

From Figure 29a it can be observed that the optimal solvent, in terms of regeneration energy requirements, is activated MDEA. Consequently, an economic analysis was performed using simulation results with aMDEA. As previously discussed, Figure 28a demonstrates further reduction in regeneration energy achieved through pressurized systems. The utilization of the 8 bara pressurized system, leads to a reduction in regeneration energy of approximately 22%, compared to the 1.05 bara case of aMDEA. However, due to the additional power requirements and extra process units associated with a pressurized system, the 1.05 bara case has also been optimized to compare the trade-off between regeneration energy savings and supplementary capital and operational costs.

5.5.1 Optimisation of Optimal Cases

Certain modifications in ProTreat® were necessary prior to conducting the economic analysis. As mentioned earlier in Chapter 3.5.1, the Sinnott & Towler book requires an S-value in order to calculate the cost of process equipment. The S-value corresponds to different parameters in the various process units, as can be seen in Table 10. To obtain these specific values from ProTreat®, certain process units had to be modelled differently.

All coolers, including the condenser, were transformed into heat exchangers to determine the necessary area, using water as cooling agent. The amount of cooling water required for each cooler was calculated based on Equation 12.

The reboiler was simulated as a heat exchanger with superheated steam (145 °C, 4 bara) and a following flash tank, rather than using ProTreat®'s in-built reboiler function. The mass stream of steam was found by the reboiler duty and specific enthalpy obtained from a steam table. The steam is assumed to be generated on-site, by combusting raw biogas.

The mass of pressure vessels for the absorber, stripper and flash tanks were calculated based on Equation 13, where L_c and D_c, is the length and diameter of the vessel, which are values obtained from ProTreat®. To account for spacers in the packing in the absorber and stripper, the heights were multiplied by 1.6.

Additional information about the modifications made and a flowsheet can be found in Appendix O.

5.5.2 CAPEX

The calculated S-values can be found in Table 68 for the 1.05 bara case, and in Table 67 for the 8 bara case. Based on the cost of each process unit, the total cost of equipment could be calculated, which can be found in Table 15. Further, the fixed capital costs were estimated using Equation 9.

Table 15: CAPEX for two optimum cases

Case	Equipment Cost, SS 2020 [Mill $]	Capital Cost, 2020 [Mill $]	Total CAPEX [Mill $]
1.05 bara	3.3	13.5	16.8
8 bara	3.6	15.2	18.8

By examining Table 15, it becomes apparent that the majority of the CAPEX comprises fixed capital costs. Additionally, it can be noted that the equipment cost is higher for the 8 bara case. Despite the absorber being smaller in the 8 bara scenario compared to the 1.05 bara case, the inclusion of an additional compressor and flash tank in the 8 bara configuration leads to increased expenses.

5.5.3 OPEX

The operational costs for 1.05 bara case and 8 bara case are presented in Table 16 and Table 17, respectively. The fixed operational costs comprise expenses related to operators and makeup amines. The variable costs include the power consumption by compressors, pumps and reboiler, as well as the cooling water requirements, and production of steam for the reboiler. It can be observed that the majority of the operational costs stem from makeup amines. Cooling water, sourced from seawater, is relatively inexpensive. A water temperature of 20 °C has been assumed, although it should be noted that if the plant was to operate in Norway, the temperature would be significantly lower during winter months.

5.5.4 Revenue

The revenue projections for the sale of biomethane can be found in Table 18. These estimates are derived from the Dutch TTF natural gas futures data for the first quarter of 2024[71]. It can be observed from Table 18 that the revenues are higher for the 1.05 bara case compared to the

Table 16: Operational costs for 1.05 bara case

Operational costs		Unit	Cost[$]	Unit Value	Mill $/year
	Operating hours	h/year	8000		
Fixed					
	Operators	$/operator year	60000	3	0.18
	Amines makeup	MDEA [$/ton]	56760	1.6	0.9
		PZ [$/ton]	75570	0.64	0.5
Variable					
	Power	$/MWh	145.2		0.007
		MWh/year	48.9		
	Cooling water	$/m^3	0.02		
		m^3/year	390009		0.078
	Steam	$/MWh	35.2	4458	0.16
Total					1.825

Table 17: Operational costs for 8 bara case

Operational costs		Unit	Cost[$]	Unit Value	Mill $/year
	Operating hours	h/year	8000		
Fixed					
	Operators	$/operator year	60000	3	0.18
	Amines makeup	MDEA [$/ton]	56760	1.24	0.70
		PZ [$/ton]	75570	0.46	0.35
Variable					
	Power	$/MWh	145.2		0.28
		MWh/year	1921		
	Cooling water	$/m^3	0.02		
		m^3/year	460080		0.09
	Steam	$/MWh	35.2	3251	0.12
Total					1.72

8 bara case. This difference can be attributed to the significantly larger methane slip in the 8 bara case, which is five times higher than that of 1.05 case. Although the methane slip only is 0.0009% of the methane entering in 1.05 bara case, and 0.0045% in the 8 bara case, this constitutes 1.003 ton/year and 5.075 ton/year for the two cases, respectively. This is consistent with theory as CH_4 solubility increases with increasing pressure. While most of the CH_4 slip originates from the condensed CO_2 stream, there are also some contributions from the liquid fractions in the flash tanks. The methane loss represents a substantial loss in potential revenue, and further investigation is needed to explore ways to mitigate these losses.

Table 18: Revenue from biomethane sale

		1.05 bara case	8 bara case
Sales Price	\$/MWh	60	60
Gas flow rate	m^3/h	931	863
Calorific value	MJ/m^3	36	36
MW		9.31	8.7
MWh		74480	69600
Revenue [Mill\$/year]		4.47	4.14

5.5.5 Net Cash Flow Diagram

As previously mentioned, the economic analysis considered the potential influence of subsidies and the revenue generated from the sale of carbon credits. Net cash flow diagrams were constructed to assess the break-even point under different scenarios. For these calculations, a depreciation rate of 20% and a tax percentage of 28% were utilized.

In the first case, no subsidies or carbon credit sale was considered, and the net cash flow diagrams for the two cases can be observed in Figure 30. The 1.05 case has a payback time of around eight years, while 8 bara case requires nine years to break-even. The estimated return on invest (ROI) is approximately 16% for the 1.05 bara case, and 13% for the 8 bara case. Investments with shorter payback periods, of three to five years, are considered advantageous as they provide a faster return on investment (private communications with D.D Pinto, 15.05.23). Nonetheless, it is important to note that the payback period can vary considerably based on the plant's scale and prevailing market conditions. While these options may not align with the 3-5 year time frame, they can generate profits throughout the plant's lifespan, rendering them financially advantageous.

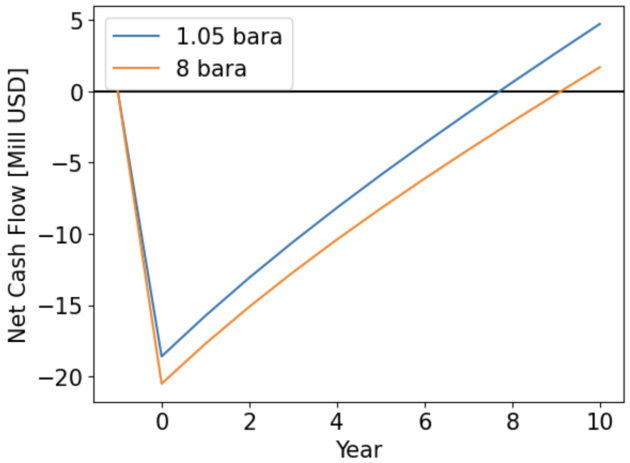

Figure 30: Break-even diagram of 1.05 bara and 8 bara case, no subsidies

However, it is crucial to take into account that in order for the gas to be injected into the gas grid, it must adhere to specific pressure requirements. In the scenario involving 8 bara, the need for compression at a later stage would be reduced, potentially narrowing the economic disparity between the two cases. However, these investigations fall outside the scope of the project.

Further, a case with different percentages of subsidies are presented in Figure 31. From Figure 31a, it can be observed that the introduction of 45% subsidies on CAPEX reduces the payback time from eight to five years. This brings the break-even point to a more favourable time frame. For the 8 bara case, with 45% subsidies, the payback time is reached in slightly less than six years. However, it is important to note that a 45% subsidy represents the maximum level of subsidies available for plants promoting renewable energy sources in Norway, which could possibly be difficult to obtain.

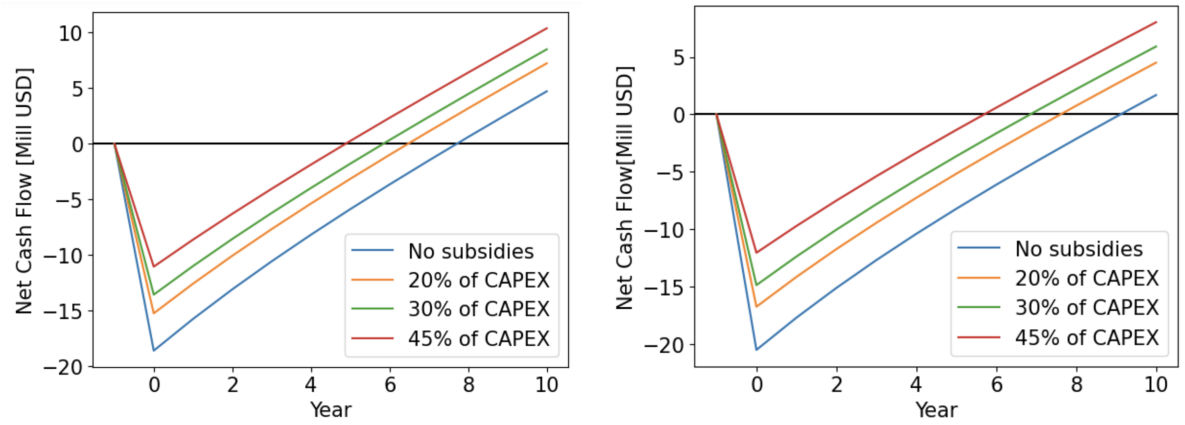

(a) Break-even diagram for 1.05 case with subsidies **(b)** Break-even diagram for 8 case with subsidies

Figure 31: Break-even diagrams for 1.05 and 8 bara case with and without subsidies

When considering sale of carbon credits, the revenue and thereby the slope of the graph increases. The assumed price for carbon credits is set to \$99/ton CO_2 [73]. Different scenarios have been examined, where 10, 25, 50 and 100% of the captured and stored CO_2 is sold as carbon credits. From Figure 32 it can be observed that the payback time is reduced by approximately two years in both cases when 100% of the captured CO_2 is sold as carbon credits. The impact is more significant for the 8 bara case, due to its steeper slope, which reflects the larger total investment involved. It should be noted that this analysis is simplistic as it does not include costs associated with conditioning the CO_2, transporting and storing it.

Finally, a case was examined where a combination of carbon credit sale and subsidies was considered. Due to time constraints, only one combination of sale and subsidy percentage was investigated. In Figure 33, the two graphs with 100% sale, and 45% subsidies are presented. These represent the maximum support available, and it can be observed that the payback times

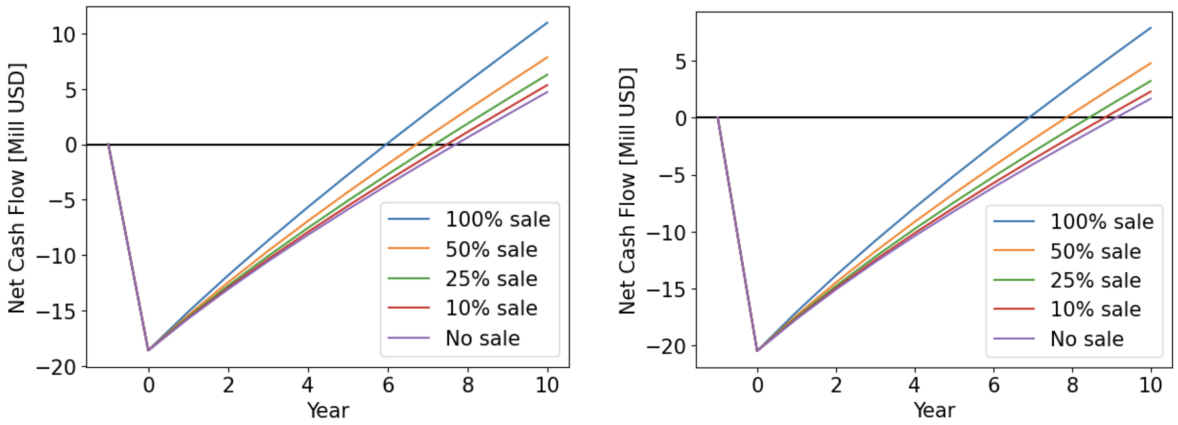

(a) Break-even diagram for 1.05 bara case

(b) Break-even diagram for 8 bara case

Figure 32: Break-even diagrams for 1.05 and 8 bara case with various percentages of carbon credit sale

are significantly reduced compared to the no subsidies and no sale cases. For the 1.05 bara case the break-even point is reduced from eight to three years, while for the 8 bara case, it is reduced from nine years to four years. Both cases fall within the desired range of break-even period, suggesting that they can be considered financially favourable.

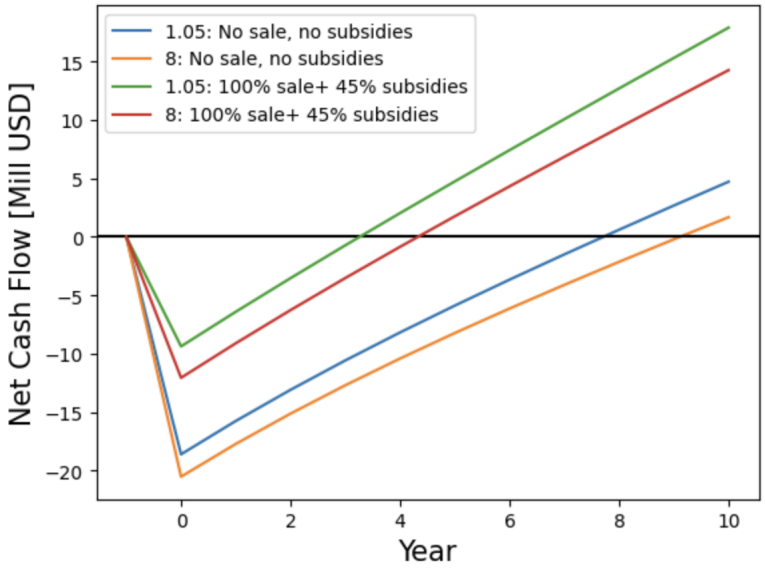

Figure 33: Break even diagrams with no subsidies and no credit sale, and maximum subsidies and credit sale

An effective approach to mitigate climate change is to increase the price of emitting CO_2. By creating a financial incentive, businesses and consumers are encouraged to move from carbon-based to renewable energy sources. Although the carbon price is relatively high in Europe, it remains significantly lower in other regions across the globe. Discussions during the climate summit of 2022 (COP 27) highlighted the need to raise the global average carbon price to at least

$75 by 2030[92], in order to prevent relocating of carbon-intensive processes to other regions with lower carbon prices.

However, according to a report from the ”Getting to Zero Coalition”, the carbon price could potentially reach up to $360/ton CO_2, at full decarbonisation by 2050. This number is 3.5 times higher than the carbon price used in these calculations, and would result in a payback time of less than four years, without accounting for potential subsidies. It is evident that both subsidies and carbon pricing play a significant role in shaping investment decisions. However, providing precise numerical figures is challenging due to the considerable fluctuation experienced by these factors.

5.5.6 Uncertainties

The economic analysis conducted in this thesis provides estimations rather than precise numbers that can be applied to real-world scenarios. While it offers insights into different situations, it is important to exercise caution in relying solely on the exact numbers presented. In this section, various uncertainties are discussed associated with the analysis.

The CAPEX values are based on the 2021 CEPCI index, as later CEPCI indexes are not confirmed. However, it is important to note that the prevailing trend suggests an increase in the index, indicating a likelihood of higher total CAPEX. The cost of power and cooling water can vary significantly depending on the geographical location of the plant. Even within Norway, energy prices exhibit large variations across different regional zones. Simulations should be adjusted to reflect specific plant locations, and the corresponding temperature of cooling water. Both energy and biomethane prices are dynamic and can fluctuate significantly throughout the year. This variability can result in the plant reaching the payback time earlier or later than initially estimated.

Furthermore, there are other uncertainties to consider, such as potential variations in demand, amine prices, labor costs, and actual production capacity. Although quantifying the uncertainties associated with these factors is challenging, it is important to identify and assess them when conducting an economic analysis, as they can have significant impact of the plant’s financial performance and viability. Lastly, assuming that the biogas is already purified from all other contaminants before entering the plant will result in an elevated production cost of biomethane, ultimately resulting in a prolonged payback time.

Chapter 6

Conclusions

This master thesis aimed to investigate different solvents for chemical scrubbing in biogas upgrading, focusing on their regeneration energy requirements and process design. Specifically, the potential of using NaGly, an AAS, as a solvent was explored and compared with simulations using aMDEA. The simulation results were compared to earlier obtained results using CESAR1 and MEA. An economic analysis was conducted on the most favourable solvent and design.

Prior to simulations, a validation of the thermodynamic model in ProTreat® was conducted for NaGly and aMDEA. The results revealed a poor fit between the data sets and the model when using 45 wt% NaGly, indicating unreliable results. However, the experimental data was also in disagreement which raised questions regarding the quality of the experiments itself. Nevertheless, satisfactory results were obtained for aMDEA, with AARDs ranging from 19 to 47%.

Simulation results indicated that the NaGly base case exhibited high specific regeneration energy requirements and high solvent circulation rates. Various process modifications were implemented in order to mitigate these requirements. The intercooled absorber showed the most favourable results, reducing the SRD by 15.4% compared to the base case. However, precipitation experiments conducted with NaGly in the laboratory, demonstrated that 45 wt% NaGly precipitates rapidly, even at low CO_2 loadings, compromising the reliability of the simulation results. Also, 35 wt% NaGly precipitates at ambient temperatures.

The simulation results using aMDEA with intercooled absorber, showed a significantly lower regeneration energy requirement compared to NaGly. Pressurized systems with 3, 5 and 8 bara, showed that the 8 bara case had the lowest regeneration energy requirements, due to the increased solubility at higher pressures.

In comparison to the previously obtained results of CESAR1 and MEA, energy demands of MEA and NaGly were found to be similar. However, as precipitation occurred at these concentrations, the energy requirements will increase when operating at a non-precipitate concentration of NaGly. On the other hand, activated MDEA exhibited a 20% lower energy requirement compared to CESAR1, possibly attributed to the difference in heat of absorption.

An economic analysis was conducted for the 1.05 bara case and the 8 bara case using aMDEA with intercooling. The 8 bara case demonstrated higher CAPEX costs and methane losses, resulting in a nine-year payback time compared to eight years for the 1.05 bara case. Potential subsidies and carbon credit sales were evaluated, demonstrating that with maximum support, the payback time could be reduced to three and four years for the 1.05 bara case and the 8 bara case, respectively. However, it is important to note that there are significant uncertainties associated with these numbers due to various assumptions made.

In summary, the findings of this thesis indicate that NaGly currently has limited potential as a solvent for chemical scrubbing in biogas upgrading. Tertiary and sterically hindered amines, on the other hand, demonstrate substantially lower energy requirements compared to primary amines. However, it is important to note that the use of an intercooled absorber is proven necessary due to the high temperatures in the absorber caused by the high concentration of CO_2 present in biogas.

6.1 Recommendations for further work

Recommendations for further work include executing more experimental campaigns on the VLE behaviour of CO_2 and NaGly, as well as developing the model used in ProTreat®. Additionally, the precipitation behaviour of NaGly at different concentrations should be thoroughly investigated. Determining the concentration range at which precipitation occurs and understanding at which concentrations one can operate at is crucial. Further, exploring the potential of using blends of amino acid salts, including secondary and tertiary structures, in combination with promoters such as PZ. This could help reduce the energy requirements associated with NaGly and potentially improve its performance as a solvent in biogas upgrading.

Considering the IC modification using aMDEA as the most promising design, it is advisable to optimize the IC configuration in terms of its fraction and temperature. Additionally, it would be valuable to explore the potential of combining process modifications, such as the use of LVR and IC, and assess whether the associated additional costs are justified from an economic standpoint.

References

[1] Hannah Ritchie, Max Roser, and Pablo Rosado. Co_2 and greenhouse gas emissions. *Our World in Data*, 2020.

[2] IEA Bioenergy. Iea bioenergy task 37. country report summaries 2019. *Pariisi, Ranska: IEA*, 2020.

[3] Rimika Kapoor, Pooja Ghosh, Madan Kumar, and Virendra Kumar Vijay. Evaluation of biogas upgrading technologies and future perspectives: a review. *Environmental Science and Pollution Research*, 26:11631–11661, 2019.

[4] Ralph H Weiland, Nathan A Hatcher, and Jaime L Nava. Post-combustion co2 capture with amino-acid salts. *GPA Eur*, 22:24, 2010.

[5] P.W.J. Derks, J.A. Hogendoorn, and G.F. Versteeg. Experimental and theoretical study of the solubility of carbon dioxide in aqueous blends of piperazine and n-methyldiethanolamine. *The Journal of Chemical Thermodynamics*, 42(1):151–163, 2010.

[6] Hua-Bing Liu, Cheng-Fang Zhang, and Guo-Wen Xu. A study on equilibrium solubility for carbon dioxide in methyldiethanolamine piperazine water solution. *Industrial & Engineering Chemistry Research*, 38(10):4032–4036, 1999.

[7] Andrew Dessler. *Introduction to Climate Change*. Cambridge University Press, 2012.

[8] European Commision. Causes of climate change. https://climate.ec.europa.eu/climate-change/causes-climate-change_en. Accessed 11.05.2023.

[9] United Nations in Western Europe. Guterres: The ipcc report is a code red for humanity. Accessed 15.10.2022.

[10] United Nations, Climate Change. What is the Kyoto Protocol. https://unfccc.int/kyoto_protocol. Accessed: 2023-02-13.

[11] United Nations, Climate Change. The Paris Agreement. What is the Paris Agreement? https://tinyurl.com/2fdrs4zh. Accessed: 2023-02-13.

[12] Hannah Ritchie. Which sources does our global energy come from? how much is low-carbon? *Our World in Data*, 2021.

[13] Federico Capra, Federico Fettarappa, Francesco Magli, Manuele Gatti, and Emanuele Martelli. Biogas upgrading by amine scrubbing: solvent comparison between mdea and mdea/mea blend. *Energy Procedia*, 148:970–977, 2018. ATI 2018 - 73rd Conference of the Italian Thermal Machines Engineering Association.

[14] P. Greene. Basics of biogas upgrading. https://www.biocycle.net/basics-biogas-upgrading/, 2018. Accessed 13.10.2022.

[15] Anneli Petterson and Arthur Wellinger. Biogas upgrading technologies, developments and innovation. 2009.

[16] Olumide Wesley Awe, Yaqian Zhao, Ange Nzihou, Doan Pham Minh, and Nathalie Lyczko. A review of biogas utilisation, purification and upgrading technologies. *Waste and Biomass Valorization*, 8:267–283, 2017.

[17] Neutrium. Wobbe index. https://neutrium.net/properties/wobbe-index/, 2016. Accessed 23.11.2022.

[18] International Energy Agency. An introduction to biogas and biomethane. https://www.iea.org/reports/outlook-for-biogas-and-biomethane-prospects-for-organic-growth/an-introduction-to-biogas-and-biomethane. Accessed 18.03.2023.

[19] Allegue and Hinge. Report - biogas and bio-syngas upgrading, 2012.

[20] Fredric Bauer, Tobias Persson, Christian Hulteberg, and Daniel Tamm. Biogas upgrading–technology overview, comparison and perspectives for the future. *Biofuels, Bioproducts and Biorefining*, 7(5):499–511, 2013.

[21] European Commission. Methane emissions. https://energy.ec.europa.eu/topics/oil-gas-and-coal/methane-emissions_en. Accessed:02.06.23.

[22] Alexander Ryhl Ammongas. Methane leakage from biogas upgrading technologies. Accessed 12.05.2023.

[23] European Commission. Eu emissions trading system (eu ets). https://climate.ec.europa.eu/eu-action/eu-emissions-trading-system-eu-ets_en, note=Accessed 10.05.2023.

[24] European Biogas Association. Short-, mid- and longterm strategies to speed up biomethane deployment in europe.

[25] RR Bottoms. Process for separating acidic gases. *USA Patent US*, 1783901, 1930.

[26] G. Puxty and M. Maeder. The fundamentals of post-combustion capture. *Absorption-Based Post-Combustion Capture of Carbon Dioxide*, pages 13–33, 1 2016.

[27] Gary Rochelle, S. Bishnoi, S. Chi, H. Dang, and J. Santos. Research needs for co2 capture from flue gas by aqueous absorption/stripping. *Research Report for P.O.: No. DE-AF26-99FT01029 of U.S. Department of Energy*, 01 2001.

[28] Y. Le Moullec and T. Neveux. 13 - process modifications for co2 capture. In Paul H.M. Feron, editor, *Absorption-Based Post-combustion Capture of Carbon Dioxide*, pages 305–340. Woodhead Publishing, 2016.

[29] Mehdi Karimi, Magne Hillestad, and Hallvard F. Svendsen. Investigation of intercooling effect in co2 capture energy consumption. *Energy Procedia*, 4:1601–1607, 2011. 10th International Conference on Greenhouse Gas Control Technologies.

[30] Jorge M. Plaza, Eric Chen, and Gary T. Rochelle. Absorber intercooling in co2 absorption by piperazine-promoted potassium carbonate. *AIChE Journal*, 56(4):905–914, 2010.

[31] Y. Le Moullec and M. Kanniche. Screening of flowsheet modifications for an efficient monoethanolamine (mea) based post-combustion co2 capture. *International Journal of Greenhouse Gas Control*, 5(4):727–740, 2011.

[32] Jacob N. Knudsen, Jimmy Andersen, Jørgen N. Jensen, and Ole Biede. Evaluation of process upgrades and novel solvents for the post combustion co2 capture process in pilot-scale. *Energy Procedia*, 4:1558–1565, 2011. 10th International Conference on Greenhouse Gas Control Technologies.

[33] Mehdi Karimi, Magne Hillestad, and Hallvard F Svendsen. Capital costs and energy considerations of different alternative stripper configurations for post combustion co2 capture. *Chemical engineering research and design*, 89(8):1229–1236, 2011.

[34] Zeinab Amrollahi, Paul Andreas Marchioro Ystad, Ivar S. Ertesvåg, and Olav Bolland. Optimized process configurations of post-combustion co2 capture for natural-gas-fired power plant – power plant efficiency analysis. *International Journal of Greenhouse Gas Control*, 8:1–11, 2012.

[35] Jochen Oexmann and Alfons Kather. Minimising the regeneration heat duty of post-combustion co2 capture by wet chemical absorption: The misguided focus on low heat of absorption solvents. *International Journal of Greenhouse Gas Control*, 4(1):36–43, 2010.

[36] Arthur L. Kohl and Richard B. Nielsen. Chapter 2 - alkanolamines for hydrogen sulfide and carbon dioxide removal. In Arthur L. Kohl and Richard B. Nielsen, editors, *Gas Purification (Fifth Edition)*, pages 40–186. Gulf Professional Publishing, Houston, fifth edition edition, 1997.

[37] Fatemeh Yazdipour, Mehdi Amouei Torkmahalleh, Mohammadmahdi Kamyabi, and Rahmat Sotudeh-Gharebagh. On solvent losses in amine absorption columns. *ACS Sustainable Chemistry & Engineering*, 10(34):11154–11164, 2022.

[38] Thu Nguyen, Marcus Hilliard, and Gary T. Rochelle. Amine volatility in co2 capture. *International Journal of Greenhouse Gas Control*, 4(5):707–715, 2010.

[39] C. Gouedard, D. Picq, F. Launay, and P.-L. Carrette. Amine degradation in co2 capture. i. a review. *International Journal of Greenhouse Gas Control*, 10:244–270, 2012.

[40] Eirik F. da Silva, Herman Kolderup, Earl Goetheer, Kai W. Hjarbo, Arjen Huizinga, Purvil Khakharia, Ilse Tuinman, Thor Mejdell, Kolbjørn Zahlsen, Kai Vernstad, Astrid Hyldbakk, Torunn Holten, Hanne M. Kvamsdal, Peter van Os, and Aslak Einbu. Emission studies from a co2 capture pilot plant. *Energy Procedia*, 37:778–783, 2013. GHGT-11 Proceedings of the 11th International Conference on Greenhouse Gas Control Technologies, 18-22 November 2012, Kyoto, Japan.

[41] Hammad Majeed and Hallvard F. Svendsen. Effect of water wash on mist and aerosol formation in absorption column. *Chemical Engineering Journal*, 333:636–648, 2018.

[42] Odd Gunnar Brakstad Andy Bootha, Eirik da Silvaa. Environmental impacts of amines and their degradation products:current status and knowledge gaps. 2010.

[43] Francis Bougie and Maria C. Iliuta. Sterically hindered amine-based absorbents for the removal of co2 from gas streams. *Journal of Chemical & Engineering Data*, 57(3):635–669, 2012.

[44] The activator mechanism of piperazine in aqueous methyldiethanolamine solutions. *Energy Procedia*, 114:2078–2087, 2017. 13th International Conference on Greenhouse Gas Control Technologies, GHGT-13, 14-18 November 2016, Lausanne, Switzerland.

[45] Fred Closmann, Thu Nguyen, and Gary T Rochelle. Mdea/piperazine as a solvent for co2 capture. *Energy Procedia*, 1(1):1351–1357, 2009.

[46] G Puxty and M Maeder. The fundamentals of post-combustion capture. In *Absorption-Based Post-Combustion Capture of Carbon Dioxide*, pages 13–33. Elsevier, 2016.

[47] Hans-Ulrik Lingelem. Process optimization of biogas upgrading with amp using pilot plant data and simulations with aspen plus. Master's thesis, NTNU, 2016.

[48] M. Reddy. amino acids. https://www.britannica.com/science/amino-acid, note =Accessed 23.02.2023, 2022.

[49] Magdalena Elzbieta Majchrowicz. Amino acid salt solutions for carbon dioxide capture. 11 2014.

[50] Ho-Jun Song, Seungmoon Lee, Kwinam Park, Joonho Lee, Dal Chand Spah, Jin-Won Park, and Thomas P. Filburn. Simplified estimation of regeneration energy of 30 wt % sodium glycinate solution for carbon dioxide absorption. *Industrial & Engineering Chemistry Research*, 47(24):9925–9930, 2008.

[51] Markus Rabensteiner, Gerald Kinger, Martin Koller, Günter Gronald, Sven Unterberger, and Christoph Hochenauer. Investigation of the suitability of aqueous sodium glycinate as a solvent for post combustion carbon dioxide capture on the basis of pilot plant studies and screening methods. *International Journal of Greenhouse Gas Control*, 29:1–15, 2014.

[52] Benedicte Mai Lerche. Co2 capture from flue gas using amino acid salt solutions. 2012.

[53] P. S. Kumar, J. A. Hogendoorn, P. H. M. Feron, and G. F. Versteeg. Equilibrium solubility of co2 in aqueous potassium taurate solutions: Part 1. crystallization in carbon dioxide loaded aqueous salt solutions of amino acids. *Industrial & Engineering Chemistry Research*, 42(12):2832–2840, 2003.

[54] Robert J. Hook. An investigation of some sterically hindered amines as potential carbon dioxide scrubbing compounds. *Industrial & Engineering Chemistry Research*, 36(5):1779–1790, 1997.

[55] Eva Sanchez Fernandez, Katarzyna Heffernan, Leen V. van der Ham, Marco J. G. Linders, Emma Eggink, Frank N. H. Schrama, D. W. F. Brilman, Earl L. V. Goetheer, and Thijs J. H. Vlugt. Conceptual design of a novel co2 capture process based on precipitating amino acid solvents. *Industrial & Engineering Chemistry Research*, 52(34):12223–12235, 2013.

[56] Shuiping Yan, Qingyao He, Shuaifei Zhao, Hong Zhai, Minhui Cao, and Ping Ai. Co2 removal from biogas by using green amino acid salts: Performance evaluation. *Fuel processing technology*, 129:203–212, 2015.

[57] Ralph H Weiland, Nathan A Hatcher, and Jaime L Nava. Benchmarking solvents for carbon capture. *Proceeding of Distillation and Absorption*, pages 12–15, 2010.

[58] Seungmoon Lee, Ho-Jun Song, Sanjeev Maken, Seung-Kwan Yoo, Jin-Won Park, Seon-wook Kim, Jae Goo Shim, and Kyung-Ryong Jang. Simulation of co 2 removal with aqueous sodium glycinate solutions in a pilot plant. *Korean Journal of Chemical Engineering*, 25:1–6, 2008.

[59] Stefania Moiolia, Gabriele Lodia, Laura A Pellegrinia, Minh T Hob, and Dianne E Wileyb. Amino acid based solvent vs. traditional amine solvent: a comparison. *CHEMICAL ENGINEERING*, 69, 2018.

[60] Quanzhen Huang, Saloni Bhatnagar, Joseph E. Remias, John P. Selegue, and Kunlei Liu. Thermal degradation of amino acid salts in co2 capture. *International Journal of Greenhouse Gas Control*, 19:243–250, 2013.

[61] Elisabeth Fleury, Jean Kittel, Bruno Vuillemin, Roland Oltra, and Francois Ropital. Corrosion in amine solvents used for the removal of acid gases. In *Eurocorr 2008*, 2008.

[62] Seongyeon Ahn, Ho-Jun Song, Jin-Won Park, Ji Hyun Lee, In Young Lee, and Kyung-Ryong Jang. Characterization of metal corrosion by aqueous amino acid salts for the capture of co 2. *Korean Journal of Chemical Engineering*, 27:1576–1580, 2010.

[63] A. Benamor and M.K. Aroua. Modeling of co2 solubility and carbamate concentration in dea, mdea and their mixtures using the deshmukh–mather model. *Fluid Phase Equilibria*, 231(2):150–162, 2005.

[64] Engineering Toolbox (2003). Heat Exchangers - Heat Transfer Coefficients. https://www.engineeringtoolbox.com/heat-transfer-coefficients-exchangers-d_450.html. Accessed: 2023-05-22.

[65] Bilal Alam Khan, Asad Ullah, Muhammad Wajid Saleem, Abdullah Nawaz Khan, Muhammad Faiq, and Mir Haris. Energy minimization in piperazine promoted mdea-based co2 capture process. *Sustainability*, 12(20), 2020.

[66] Ray Sinnott and Gavin Towler. *Chemical engineering design: Fifth Edition*. Butterworth-Heinemann, 2009.

[67] Ray Sinnott and Gavin Towler. Chapter 6 - costing and project evaluation. In Ray Sinnott and Gavin Towler, editors, *Chemical Engineering Design (Sixth Edition)*, Chemical Engineering Series, pages 275–369. Butterworth-Heinemann, sixth edition edition, 2020.

[68] Solomon Aforkoghene Aromada and Lars Øi. Simulation of improved absorption configurations for co2 capture. In *Proceedings of the 56th Conference on Simulation and Modelling (SIMS 56), October, 7-9, 2015, Linköping University, Sweden*, number 119, pages 21–29. Linköping University Electronic Press, 2015.

[69] João Gomes, Samuel Santos, and João Bordado. Choosing amine-based absorbents for co2 capture. *Environmental Technology*, 36(1):19–25, 2015. PMID: 25409579.

[70] H Haugen, A Anundskås, N Edrup, A Schaatun, G Glittum, R Skagestad, and A Mathisen. Co2 fangst av utslipp fra industrianlegg. *Porsgrunn, Norway, Tel-Tek report*, (2109020), 2009.

[71] ICE Endex. Dutch ttf natural gas futures. https://www.theice.com/products/27996665/Dutch-TTF-Natural-Gas-Futures/data?marketId=5493476&span=2. Accessed 11.05.2023.

[72] International Energy Agency. An introduction to biogas and biomethane. https://www.iea.org/reports/outlook-for-biogas-and-biomethane-prospects-for-organic-growth/an-introduction-to-biogas-and-biomethane. Accessed 24.04.2023.

[73] Statista. European union emission trading system (eu-ets) carbon pricing from january 2022 to april 2023. "https://www.statista.com/statistics/1322214/carbon-prices-european-union-emission-trading-scheme/. Accessed 11.05.2023.

[74] Innovasjon Norge. Statsstøtteregelverket - støtte til investeringer for å fremme fornybare energikilder. https://www.innovasjonnorge.no/no/tjenester/finansiering2/statsstotteregelverket/stotte-til-investeringer-for-fornybare-kilder-gber-art.-41/, 2023. Accessed 25.04.2023.

[75] Innovasjon Norge. Statsstøtteregelverket - støtte til investeringer i gjenvinning og gjenbruk av avfall. https://www.innovasjonnorge.no/no/tjenester/finansiering2/statsstotteregelverket/stotte-til-investeringer-i-gjenvinning-og-gjenbruk-av-avfall-gber-art.-47/, 2023.

[76] R.D. Deshmukh and A.E. Mather. A mathematical model for equilibrium solubility of hydrogen sulfide and carbon dioxide in aqueous alkanolamine solutions. *Chemical Engineering Science*, 36(2):355–362, 1981.

[77] Marcin Stec, Lucyna Wiec law-Solny, Andrzej Wilk, and Adam Tatarczuk. Modelling co2 solubility in aqueous amine solutions using deshmukh mather model. 05 2013.

[78] Ho Jun Song, Seungmoon Lee, Sanjeev Maken, Jong Jin Park, and Jin Won Park. Solubilities of carbon dioxide in aqueous solutions of sodium glycinate. *Fluid Phase Equilibria*, 246:1–5, 8 2006.

[79] Bikash K. Mondal, Syamalendu S. Bandyopadhyay, and Amar N. Samanta. Vle of co2 in aqueous sodium glycinate solution – new data and modeling using kent–eisenberg model. *International Journal of Greenhouse Gas Control*, 36:153–160, 5 2015.

[80] Faisal Harris, Kiki Adi Kurnia, M.Ibrahim A. Mutalib, and Murugesan Thanapalan. Solubilities of carbon dioxide and densities of aqueous sodium glycinate solutions before and after co2 absorption. *Journal of Chemical amp; Engineering Data*, 54:144–147, 12 2008.

[81] A. F. Portugal, J. M. Sousa, F. D. Magalhães, and A. Mendes. Solubility of carbon dioxide in aqueous solutions of amino acid salts. *Chemical Engineering Science*, 64, 2009.

[82] Sukanta Kumar Dash and Syamalendu S. Bandyopadhyay. Studies on the effect of addition of piperazine and sulfolane into aqueous solution of nmethyldiethanolamine for co2 capture and vle modelling using enrtl equation. *International Journal of Greenhouse Gas Control*, 44:227–237, 2016.

[83] Lubna Ghalib, Brahim Si Ali, Wan Mohd Ashri, Shaukat Mazari, and Idris Mohamed Saeed. Modeling the effect of piperazine on co2 loading in mdea/pz mixture. *Fluid Phase Equilibria*, 434:233–243, 2017.

[84] T. Ogawa. Carbon dioxide capture and utilization for gas engine. *Energy and Power Engineering*, 5(10):587–590, 2013.

[85] Hanne M. Kvamsdal, Geir Haugen, Hallvard F. Svendsen, Andrew Tobiesen, Hari Mangalapally, Ardi Hartono, and Thor Mejdell. Modelling and simulation of the esbjerg pilot plant using the cesar 1 solvent. *Energy Procedia*, 4:1644–1651, 2011. 10th International Conference on Greenhouse Gas Control Technologies.

[86] Ugochukwu E. Aronu, Arlinda F. Ciftja, Inna Kim, and Ardi Hartono. Understanding precipitation in amino acid salt systems at process conditions. *Energy Procedia*, 37:233–240, 2013. GHGT-11 Proceedings of the 11th International Conference on Greenhouse Gas Control Technologies, 18-22 November 2012, Kyoto, Japan.

[87] Bingtao Zhao, Tongbo Fang, Weifeng Qian, Jinpeng Liu, and Yaxin Su. Process simulation, optimization and assessment of post-combustion carbon dioxide capture with piperazine-activated blended absorbents. *Journal of Cleaner Production*, 282:124502, 2021.

[88] Bin Zhao, Fangzheng Liu, Zheng Cui, Changjun Liu, Hairong Yue, Siyang Tang, Yingying Liu, Houfang Lu, and Bin Liang. Enhancing the energetic efficiency of mdea/pz-based co2 capture technology for a 650mw power plant: Process improvement. *Applied Energy*, 185:362–375, 2017.

[89] Jesse W Mason and Barnett F Dodge. *Equilibrium absorption of carbon dioxide by solutions of the ethanolamines*. PhD thesis, Verlag nicht ermittelbar, 1936.

[90] Saleem Nawan Khan, Sintayehu Mekuria Hailegiorgis, Zakaria Man, and Azmi Mohd Shariff. High pressure solubility of carbon dioxide (co2) in aqueous solution of piperazine (pz) activated n-methyldiethanolamine (mdea) solvent for co2 capture. *AIP Conference Proceedings*, 2017.

[91] Milad Narimani, Sepideh Amjad-Iranagh, and Hamid Modarress. Performance of tertiary amines as the absorbents for co2 capture: Quantum mechanics and molecular dynamics studies. *Journal of Natural Gas Science and Engineering*, 47:154–166, 2017.

[92] Reuters. EXCLUSIVE COP27: IMF chief says $75/ton carbon price needed by 2030. https://www.reuters.com/business/cop/exclusive-cop27-imf-chief-says-75ton-carbon-price-needed-by-2030-2022-11-07/. Accessed: 2023-05-21.

Appendix

A Mondal et al. VLE

Table 19: 5 wt% Mondal

T= 313.15 K				T=323.15 K				T=333.15 K			
α	P_{exp}	P_{sim}	ARD	α	P_{exp}	P_{sim}	ARD	α	P_{exp}	P_{sim}	ARD
0.57	3.24	2.73	0.16	0.48	4.91	2.88	0.41	0.09	5.68	0.10	0.98
0.91	69.11	37.98	0.45	0.60	32.38	6.69	0.79	0.26	18.80	1.11	0.94
1.15	210.93	378.35	0.79	0.73	59.45	16.20	0.73	0.71	49.75	24.88	0.50
1.41	403.38	1024.67	1.54	0.95	103.93	92.63	0.11	0.83	100.66	56.33	0.44
1.75	649.82	2005.28	2.09	1.35	396.09	1067.70	1.70	0.96	202.37	160.34	0.21
				1.48	508.94	1499.95	1.95	1.08	301.29	385.79	0.28
				1.67	653.53	2180.97	2.34	1.19	404.35	736.77	0.82

Table 20: 10 wt% Mondal

T= 313.15 K				T=323.15 K				T=333.15 K			
α	P_{exp}	P_{sim}	ARD	α	P_{exp}	P_{sim}	ARD	α	P_{exp}	P_{sim}	ARD
0.88	11.53	77.50	5.72	0.01	0.34	0.00	1.00	0.00	0.24	0.00	1.00
0.96	101.58	181.36	0.79	0.16	11.16	0.18	0.98	0.13	14.73	0.26	0.98
1.02	126.65	315.41	1.49	0.64	80.74	20.64	0.74	0.44	59.64	7.92	0.87
1.04	184.40	396.49	1.15	0.67	100.15	26.28	0.74	0.71	106.37	59.64	0.44
1.06	207.65	469.11	1.26	0.79	217.30	64.32	0.70	0.81	198.81	125.88	0.37
1.14	503.28	810.23	0.61	0.96	404.00	268.20	0.34	0.95	307.02	370.63	0.21
				1.02	501.13	472.45	0.06	0.99	402.61	508.37	0.26
				1.11	608.35	873.47	0.44	1.02	504.12	648.48	0.29

Table 21: 15 wt% Mondal

T= 313.15 K				T=323.15 K				T=333.15 K			
α	P_{exp}	P_{sim}	ARD	α	P_{exp}	P_{sim}	ARD	α	P_{exp}	P_{sim}	ARD
0.01	0.28	6.3E-05	1.00	0.06	2.82	0.02	176.88	0.12	2.40	0.21	0.91
0.02	0.59	3.1E-04	1.00	0.28	18.38	0.91	19.15	0.50	21.07	21.70	0.03
0.21	10.06	0.12	0.99	0.62	59.90	34.79	0.72	0.57	62.78	41.45	0.34
0.60	39.84	15.82	0.60	0.68	111.19	55.84	0.99	0.62	104.31	60.11	0.42
0.78	203.46	76.38	0.62	0.76	203.55	105.02	0.94	0.69	197.77	104.74	0.47
0.84	307.49	126.78	0.59	0.82	307.87	169.33	0.82	0.75	301.44	166.31	0.45
0.91	424.85	219.27	0.48	0.87	408.53	254.43	0.61	0.81	403.89	247.57	0.39
0.95	504.21	316.20	0.37	0.92	501.67	373.09	0.34	0.85	506.09	343.43	0.32
1.02	653.90	601.46	0.08					0.95	649.68	718.69	0.11

Table 22: 20 wt% Mondal

T= 313.15 K				T=323.15 K				T=333.15 K			
α	P_{exp}	P_{sim}	ARD	α	P_{exp}	P_{sim}	ARD	α	P_{exp}	P_{sim}	ARD
0.04	0.84	1.3E-03	1.00	0.14	2.61	0.09	0.97	0.10	1.43	0.10	0.93
0.34	13.16	0.77	0.94	0.31	9.74	1.42	0.85	0.45	16.33	18.83	0.15
0.58	30.19	24.42	0.19	0.50	26.81	18.42	0.31	0.49	35.27	29.66	0.16
0.62	57.90	40.27	0.30	0.55	55.27	31.74	0.43	0.55	57.52	60.42	0.05
0.64	102.27	50.42	0.51	0.60	104.62	54.28	0.48	0.56	98.78	63.05	0.36
0.70	194.04	85.52	0.56	0.66	200.77	96.83	0.52	0.62	193.06	110.74	0.43
0.77	301.25	14.16	0.95	0.71	306.59	148.88	0.51	0.68	298.18	183.83	0.38
0.82	402.89	206.86	0.49	0.76	409.15	208.93	0.49	0.71	398.12	233.57	0.41
0.87	519.92	301.15	0.42	0.80	501.29	273.28	0.45	0.76	509.54	320.09	0.37
0.92	648.60	434.87	0.33	0.84	601.39	362.70	0.40	0.85	773.50	604.56	0.22

B Portugal et al. VLE

Table 23: 1 wt% Portugal

T= 303.15 K				T=313.15 K				T=323.15 K			
α	P_{exp}	P_{sim}	ARD	α	P_{exp}	P_{sim}	ARD	α	P_{exp}	P_{sim}	ARD
0.32	0.09	0.05	0.42	0.21	0.05	0.05	0.15	0.65	0.62	2.01	2.24
0.73	0.46	0.74	0.62	0.43	0.16	0.26	0.66	1.10	8.32	48.46	4.82
1.13	9.09	34.01	2.74	0.62	0.41	0.82	1.02	1.29	38.80	139.03	2.58
0.69	4.02	0.60	0.85	0.86	1.65	3.82	1.31	0.47	0.31	0.72	1.33
0.78	0.69	1.03	0.49	1.04	6.05	20.48	2.39	0.95	3.22	14.35	3.46
0.87	1.29	1.97	0.53	1.18	20.85	65.24	2.13	1.29	36.10	141.63	2.92
0.95	2.33	4.09	0.75	1.32	62.45	125.30	1.01	0.46	0.53	0.68	0.29
1.36	57.20	112.12	0.96					0.79	1.61	4.66	1.89
								1.15	11.20	71.65	5.40
								1.31	31.00	149.48	3.82

Table 24: 10 wt% Portugal

T= 298.15 K				T=313.15 K				T=323.15 K			
α	P_{exp}	P_{sim}	ARD	α	P_{exp}	P_{sim}	ARD	α	P_{exp}	P_{sim}	ARD
0.03	0.95	0.17	0.82	0.30	0.14	0.43	2.08	0.35	1.03	1.77	0.71
0.05	4.28	1.53	0.64	0.61	1.70	8.65	4.09	0.52	2.31	8.21	2.55
0.06	23.20	4.11	0.82	0.67	3.75	13.61	2.63	0.69	15.80	30.46	0.93
0.07	36.20	5.38	0.85	0.72	7.96	21.35	1.68	0.78	38.90	57.49	0.48
0.09	616.00	55.96	0.91	0.90	54.70	95.88	0.75	0.17	0.35	0.20	0.42
				0.36	0.13	0.82	5.29	0.28	0.56	0.84	0.50
				0.40	0.20	1.24	5.14	0.40	0.89	2.85	2.20
				0.48	0.39	2.70	5.96	0.55	3.01	10.15	2.37
				0.54	0.72	4.51	5.28	0.65	10.80	22.00	1.04
				0.58	1.34	6.82	4.09	0.77	43.70	56.18	0.29
				0.65	3.44	11.56	2.36				
				0.85	30.50	59.43	0.95				

Table 25: 30 wt% Portugal

T= 303.15 K				T=313.15 K				T=323.15 K			
α	P_{exp}	P_{sim}	ARD	α	P_{exp}	P_{sim}	ARD	α	P_{exp}	P_{sim}	ARD
0.08	0.16	0.00	0.99	0.19	0.37	0.04	0.88	0.09	0.27	0.02	0.94
0.13	0.23	0.00	0.98	0.38	0.82	1.43	0.74	0.14	0.51	0.06	0.88
0.19	0.35	0.02	0.96	0.45	1.03	6.74	5.55	0.21	0.77	0.22	0.72
0.23	0.43	0.03	0.93	0.56	2.49	75.47	29.31	0.28	0.98	0.74	0.24
0.26	0.57	0.05	0.91	0.13	0.19	0.01	0.92	0.36	1.78	3.10	0.74
0.29	0.84	0.10	0.88	0.26	0.53	0.17	0.68	0.44	2.37	13.54	4.71
0.33	0.99	0.18	0.82	0.39	0.81	1.80	1.22	0.53	6.05	83.71	12.84
0.36	1.11	0.36	0.68	0.52	1.56	34.38	21.04	0.57	13.50	152.92	10.33
0.39	1.20	0.73	0.39	0.63	18.80	197.21	9.49	0.62	35.00	269.13	6.69
0.44	1.36	2.04	0.50	0.66	32.60	263.51	7.08				
0.48	1.93	5.67	1.94								
0.51	2.94	12.82	3.36								
0.54	5.36	27.19	4.07								
0.59	15.20	70.05	3.61								
0.65	38.10	139.81	2.67								

C Harris et al. VLE

Table 26: 5 wt% Harris

T= 298.15 K				T=313.15 K			
α	P_{exp}	P_{sim}	ARD	α	P_{exp}	P_{sim}	ARD
1.24	98.00	403.88	0.76	1.19	92.00	464.86	4.05
1.36	547.00	626.71	0.13	1.24	514.00	585.40	0.14
1.38	1022.00	648.66	0.58	1.29	1029.00	709.98	0.31
1.44	1511.00	765.32	0.97	1.34	1503.00	837.95	0.44
1.41	2020.00	718.73	1.81	1.41	2007.00	1027.62	0.49
1.53	2500.00	930.50	1.69	1.49	2503.00	1239.99	0.50

Table 27: 10 wt% Harris

T= 298.15 K				T=313.15 K			
α	P_{exp}	P_{sim}	ARD	α	P_{exp}	P_{sim}	ARD
0.97	98.00	736.07	0.87	0.89	91.00	86.51	0.05
1.16	522.00	932.23	0.44	1.05	512.00	430.03	0.16
1.28	1009.00	1137.52	0.11	1.15	1018.00	886.25	0.13
1.32	1517.00	1351.62	0.12	1.23	1515.00	1328.76	0.12
1.36	2024.00	1675.88	0.21	1.26	2022.00	1474.93	0.27
1.43	2498.00	2049.99	0.22	1.28	2505.00	1588.81	0.37

Table 28: 15 wt% Harris

T= 298.15 K				T=313.15 K			
α	P_{exp}	P_{sim}	ARD	α	P_{exp}	P_{sim}	ARD
0.93	98.00	133.67	0.27	0.84	91.00	125.64	0.38
1.01	526.00	329.34	0.60	1.03	520.00	655.59	0.26
1.05	1002.00	460.72	1.17	1.07	1017.00	894.11	0.12
1.05	1536.00	496.94	2.09	1.08	1504.00	1007.90	0.33
1.11	2035.00	805.01	1.53	1.14	2038.00	1485.07	0.27
1.14	2521.00	952.63	1.65	1.18	2499.00	1786.75	0.29

Table 29: 20 wt% Harris

T= 298.15 K				T=313.15 K			
α	P_{exp}	P_{sim}	ARD	α	P_{exp}	P_{sim}	ARD
0.70	98.00	40.23	1.44	0.68	90.00	71.07	0.21
0.94	528.00	275.43	0.92	0.91	508.00	420.04	0.17
0.99	1010.00	441.95	1.29	1.00	1009.00	851.75	0.16
1.02	1541.00	593.84	1.59	1.03	1516.00	1092.56	0.28
1.12	2038.00	1278.93	0.59	1.08	2019.00	1520.68	0.25
1.13	2531.00	1441.72	0.76	1.13	2513.00	2205.61	0.12

Table 30: 30 wt% Harris

T= 298.15 K				T=313.15 K			
α	P_{exp}	P_{sim}	ARD	α	P_{exp}	P_{sim}	ARD
0.62	98.00	86.18	0.14	0.58	91.00	96.80	0.06
0.91	516.00	609.66	0.15	0.87	508.00	944.19	0.86
0.96	1026.00	859.15	0.19	0.95	1011.00	1576.46	0.56
0.97	1526.00	915.98	0.67	0.98	1525.00	1804.33	0.18
0.99	2049.00	1045.08	0.96	0.98	2003.00	1852.18	0.08
1.03	2534.00	1484.66	0.71	0.99	2501.00	1965.66	0.21

D Song et al. VLE

Table 31: 10 wt% Song

T= 303.15 K				T=313.15 K				T=323.15 K			
α	P_{exp}	P_{sim}	ARD	α	P_{exp}	P_{sim}	ARD	α	P_{exp}	P_{sim}	ARD
0.58	0.30	3.37	10.24	0.41	0.20	1.43	6.15	0.28	0.30	0.78	1.60
0.76	4.00	16.63	3.16	0.53	0.40	4.35	9.88	0.38	0.40	2.36	4.91
0.93	29.90	79.40	1.66	0.60	0.90	7.62	7.46	0.45	0.60	4.36	6.27
1.00	92.20	174.39	0.89	0.71	5.70	18.79	2.30	0.54	1.40	9.20	5.57
1.06	160.10	334.55	1.09	0.86	25.20	68.97	1.74	0.65	3.90	21.51	4.51
1.08	199.10	394.81	0.98	0.93	69.50	132.18	0.90	0.75	19.40	47.89	1.47
				1.04	128.00	375.05	1.93	0.83	58.10	89.75	0.54
				1.05	178.50	422.44	1.37	0.94	111.70	217.60	0.95
				1.06	208.00	473.12	1.27	0.95	157.30	249.18	0.58
								0.97	189.40	290.76	0.54
								1.01	209.60	408.34	0.95

Table 32: 20 wt% Song

T= 303.15 K				T=313.15 K				T=323.15 K			
α	P_{exp}	P_{sim}	ARD	α	P_{exp}	P_{sim}	ARD	α	P_{exp}	P_{sim}	ARD
0.31	0.20	0.17	0.17	0.44	0.20	3.57	16.87	0.44	1.00	3.68	2.68
0.38	0.30	0.53	0.76	0.48	0.30	7.04	22.46	0.51	1.10	10.98	8.98
0.53	0.40	6.57	15.42	0.60	0.70	31.00	43.28	0.61	1.50	34.19	21.79
0.61	0.90	20.87	22.18	0.69	5.40	73.56	12.62	0.68	7.90	71.69	8.07
0.70	8.60	48.55	4.64	0.76	34.90	137.96	2.95	0.76	36.00	131.87	2.66
0.78	44.70	96.53	1.16	0.83	87.90	222.75	1.53	0.80	83.10	173.62	1.09
0.85	108.70	163.80	0.51	0.87	145.90	311.07	1.13	0.84	131.10	248.74	0.90
0.88	165.70	206.85	0.25	0.91	187.90	403.89	1.15	0.87	171.40	306.41	0.79
0.90	197.50	251.12	0.27	0.91	211.10	413.49	0.96	0.88	201.50	335.57	0.67

Table 33: 30 wt% Song

T= 303.15 K				T=313.15 K				T=323.15 K			
α	P_{exp}	P_{sim}	ARD	α	P_{exp}	P_{sim}	ARD	α	P_{exp}	P_{sim}	ARD
0.17	0.10	0.01	0.90	0.28	0.30	0.23	0.25	0.17	0.40	0.11	0.74
0.46	1.70	4.19	1.47	0.40	0.40	2.17	4.42	0.34	1.00	2.14	1.14
0.51	21.60	14.60	0.32	0.47	2.50	12.43	3.97	0.44	6.40	14.40	1.25
0.56	41.20	41.73	0.01	0.53	29.80	48.38	0.62	0.52	33.20	73.05	1.20
0.59	66.10	68.00	0.03	0.58	97.80	108.57	0.11	0.56	84.00	131.26	0.56
0.62	120.30	101.79	0.15	0.62	165.40	171.84	0.04	0.57	113.10	152.92	0.35
				0.63	195.80	187.27	0.04	0.62	177.90	280.29	0.58
				0.65	213.50	239.08	0.12				

E Liu et al. VLE

Table 34: 1.5 wt% PZ+ 18.2 wt% MDEA

T= 323.15 K				T=343.15 K			
α	P_{exp}	P_{sim}	ARD	α	P_{exp}	P_{sim}	ARD
0.47	21.18	20.40	0.04	0.39	35.43	40.24	0.14
0.59	44.00	40.92	0.07	0.49	71.29	75.70	0.06
0.70	89.44	74.66	0.17	0.64	148.80	167.45	0.13
0.85	271.90	203.09	0.25	0.81	418.80	427.17	0.02
0.98	669.40	639.44	0.04	0.88	688.80	644.90	0.06

Table 35: 3 wt% PZ+ 16.1 wt% MDEA

T= 323.15 K				T=343.15 K			
α	P_{exp}	P_{sim}	ARD	α	P_{exp}	P_{sim}	ARD
0.50	17.78	16.94	0.05	0.35	17.60	18.54	0.05
0.61	41.14	34.73	0.16	0.43	32.07	33.96	0.06
0.71	89.43	65.16	0.27	0.56	71.26	79.93	0.12
0.94	509.40	390.62	0.23	0.76	243.80	265.59	0.09
0.96	586.90	472.11	0.20	0.79	296.30	322.77	0.09

Table 36: 4.6 wt% PZ+ 56.8 wt% MDEA

T= 323.15 K				T=343.15 K			
α	P_{exp}	P_{sim}	ARD	α	P_{exp}	P_{sim}	ARD
0.32	42.51	37.67	0.11	0.19	35.83	38.48	0.07
0.42	91.15	81.98	0.10	0.25	75.61	82.47	0.09
0.65	326.20	359.57	0.10	0.40	203.10	290.53	0.43
0.71	508.70	535.71	0.05	0.53	460.60	672.25	0.46
0.76	753.70	836.68	0.11	0.59	713.10	973.48	0.37

Table 37: 13.4 wt% PZ+ 44.7 wt% MDEA

T= 323.15 K				T=343.15 K			
α	P_{exp}	P_{sim}	ARD	α	P_{exp}	P_{sim}	ARD
0.35	14.34	6.70	0.53	0.25	13.16	9.92	0.25
0.45	46.49	20.11	0.57	0.32	37.35	26.25	0.30
0.53	91.15	40.82	0.55	0.54	224.70	212.63	0.05
0.65	278.30	171.15	0.39	0.64	479.70	505.48	0.05
0.75	678.30	752.52	0.11	0.67	667.20	701.71	0.05

Table 38: 3 wt% PZ+ 37.5 wt% MDEA

T= 323.15 K				T=343.15 K				T=363.15 K			
α	P_{exp}	P_{sim}	ARD	α	P_{exp}	P_{sim}	ARD	α	P_{exp}	P_{sim}	ARD
0.38	23.95	27.19	0.14	0.29	33.86	50.16	0.48	0.15	19.88	36.74	0.85
0.46	42.97	45.32	0.05	0.32	48.08	67.94	0.41	0.19	37.54	67.72	0.80
0.57	90.11	89.10	0.01	0.47	178.00	174.52	0.02	0.25	82.54	124.17	0.50
0.67	200.10	149.07	0.26	0.59	368.00	330.37	0.10	0.41	312.50	405.54	0.30
0.75	422.60	251.40	0.41	0.69	573.00	555.83	0.03	0.49	482.50	640.45	0.33

Table 39: 6 wt% PZ+ 33.4 wt% MDEA

T= 323.15 K				T=343.15 K				T=363.15 K			
α	P_{exp}	P_{sim}	ARD	α	P_{exp}	P_{sim}	ARD	α	P_{exp}	P_{sim}	ARD
0.41	18.98	18.33	0.03	0.27	19.24	20.01	0.04	0.20	17.37	31.57	0.82
0.54	49.60	49.53	0.00	0.37	52.64	49.08	0.07	0.22	25.37	42.56	0.68
0.62	90.17	85.04	0.06	0.41	73.14	70.09	0.04	0.25	37.19	62.64	0.68
0.69	195.10	147.96	0.24	0.54	177.80	173.58	0.02	0.40	157.20	231.15	0.47
0.77	380.10	265.08	0.30	0.77	935.30	749.18	0.20	0.54	412.20	564.64	0.37

F Derks et al. VLE

Table 40: 2.8M MDEA + 0.7M PZ

T= 303.15 K				T=323.15 K			
α	P_{exp}	P_{sim}	ARD	α	P_{exp}	P_{sim}	ARD
0.21	0.51	0.36	0.29	0.13	0.68	0.41	0.40
0.25	0.96	0.73	0.24	0.16	1.05	0.75	0.29
0.30	1.75	1.45	0.17	0.19	2.00	1.42	0.29
0.35	2.61	2.43	0.07	0.23	3.19	2.76	0.13
0.40	4.16	4.08	0.02	0.26	4.68	3.73	0.20
0.44	5.23	5.71	0.09	0.31	6.99	7.19	0.03
0.47	6.80	7.63	0.12	0.32	8.37	8.26	0.01
0.51	8.65	11.09	0.28	0.42	19.70	19.96	0.01
0.54	10.20	13.45	0.32	0.48	32.80	33.27	0.01
0.52	9.40	11.55	0.23	0.54	45.80	50.70	0.11
0.52	10.70	12.02	0.12	0.58	60.30	68.58	0.14
0.57	15.20	17.89	0.18	0.61	69.50	82.24	0.18
0.66	25.70	36.93	0.44	0.64	84.00	98.73	0.18
0.68	36.10	42.52	0.18	0.66	94.50	114.66	0.21
0.69	32.10	45.48	0.42				
0.71	38.90	53.53	0.38				
0.76	56.40	84.35	0.50				
0.79	73.70	115.52	0.57				
0.78	70.40	108.74	0.54				
0.82	93.80	154.67	0.65				
0.82	96.90	149.80	0.55				
0.84	100.10	190.25	0.90				

Table 41: 0.5M MDEA + 1.5M PZ

T= 303.15 K				T=323.15 K			
α	P_{exp}	P_{sim}	ARD	α	P_{exp}	P_{sim}	ARD
0.50	0.25	0.18	0.30	0.47	0.45	0.37	0.17
0.64	1.02	0.99	0.03	0.56	1.38	1.07	0.23
0.68	1.55	1.53	0.01	0.65	3.76	3.15	0.16
0.81	7.15	7.79	0.09	0.74	9.24	8.87	0.04
0.83	9.02	9.92	0.10	0.73	8.10	8.01	0.01
0.84	10.60	12.37	0.17	0.75	9.70	9.83	0.01
0.91	26.80	29.99	0.12	0.82	20.10	21.55	0.07
0.91	29.10	31.41	0.08	0.87	36.90	38.70	0.05
0.94	53.70	55.66	0.04	0.87	38.80	41.25	0.06
0.97	81.10	85.58	0.06	0.90	59.20	61.51	0.04
0.97	80.10	89.24	0.11	0.91	64.10	66.92	0.04
0.98	102.00	113.21	0.11	0.92	79.80	83.27	0.04
				0.92	80.80	85.81	0.06
				0.93	96.00	101.71	0.06
				0.94	98.80	104.99	0.06

Table 42: 4M MDEA + 0.6M PZ

T= 313.15 K			
α	P_{exp}	P_{sim}	ARD
0.12	0.72	0.43	0.40
0.13	0.90	0.46	0.49
0.18	2.07	1.41	0.32
0.19	2.70	1.72	0.36
0.23	4.36	3.40	0.22
0.25	5.24	4.36	0.17
0.28	7.00	6.57	0.06
0.28	7.33	6.65	0.09
0.31	9.38	8.88	0.05
0.31	8.65	9.07	0.05
0.33	12.60	10.57	0.16
0.34	12.80	11.90	0.07
0.43	25.30	24.94	0.01
0.50	39.00	41.70	0.07
0.50	39.00	43.42	0.11
0.57	58.40	66.20	0.13
0.58	60.40	70.66	0.17
0.62	78.50	93.80	0.19
0.63	80.00	100.99	0.26
0.64	89.70	105.19	0.17

G Dash et al. VLE

Table 43: 28 wt% MDEA + 2wt% PZ Dash

T= 303.15 K				T=313.15 K				T=323.15 K			
α	P_{exp}	P_{sim}	ARD	α	P_{exp}	P_{sim}	ARD	α	P_{exp}	P_{sim}	ARD
0.32	3.29	3.25	0.01	0.16	1.85	1.04	0.44	0.22	5.06	5.03	0.01
0.38	5.62	5.16	0.08	0.36	10.55	8.59	0.19	0.38	19.54	19.78	0.01
0.44	7.80	8.26	0.06	0.53	28.86	25.98	0.10	0.49	36.66	38.67	0.05
0.56	14.69	16.47	0.12	0.61	44.97	41.60	0.08	0.54	45.32	51.58	0.14
0.69	28.91	35.71	0.24	0.68	63.37	60.23	0.05	0.60	60.55	69.35	0.15
0.84	69.09	109.37	0.58	0.72	80.31	78.32	0.02	0.67	105.53	101.70	0.04
0.88	88.93	153.15	0.72	0.74	91.70	90.82	0.01	0.89	472.77	450.10	0.05
0.89	101.77	179.22	0.76					0.99	685.55	1341.40	0.96

Table 44: 25 wt% MDEA + 5wt% PZ Dash

T= 303.15 K				T=313.15 K				T=323.15 K			
α	P_{exp}	P_{sim}	ARD	α	P_{exp}	P_{sim}	ARD	α	P_{exp}	P_{sim}	ARD
0.30	1.18	0.94	0.20	0.15	0.42	0.19	0.55	0.11	1.01	0.21	0.79
0.45	4.49	4.51	0.01	0.29	2.81	1.86	0.34	0.25	4.47	2.47	0.45
0.61	13.41	15.90	0.19	0.43	9.68	7.29	0.25	0.31	7.49	4.73	0.37
0.71	26.34	34.64	0.31	0.53	20.24	16.57	0.18	0.38	12.93	9.40	0.27
0.80	44.46	75.52	0.70	0.62	35.44	31.47	0.11	0.45	21.49	17.28	0.20
0.86	63.36	129.91	1.05	0.68	52.76	51.49	0.02	0.51	32.49	27.88	0.14
0.90	82.46	201.95	1.45	0.74	74.99	78.28	0.04	0.58	47.24	43.12	0.09
0.91	90.49	242.64	1.68	0.77	90.27	100.39	0.11	0.61	56.73	53.76	0.05
0.93	99.29	298.59	2.01					0.63	62.67	62.48	0.00
0.89	101.77	179.22	0.76					0.99	685.55	1341.40	0.96

Table 45: 22 wt% MDEA + 8wt% PZ Dash

T= 303.15 K				T=313.15 K				T=323.15 K			
α	P_{exp}	P_{sim}	ARD	α	P_{exp}	P_{sim}	ARD	α	P_{exp}	P_{sim}	ARD
0.04	0.09	0.00	0.99	0.06	0.18	0.01	0.96	0.15	5.37	0.17	0.97
0.15	0.37	0.03	0.93	0.15	0.45	0.07	0.85	0.26	7.77	1.00	0.87
0.24	1.08	0.14	0.87	0.23	1.00	0.28	0.72	0.37	13.99	4.20	0.70
0.35	2.51	0.76	0.70	0.33	2.52	1.17	0.53	0.43	18.82	7.42	0.61
0.42	4.49	1.69	0.62	0.38	4.23	2.37	0.44	0.50	28.78	14.28	0.50
0.42	5.68	1.70	0.70	0.48	9.15	6.44	0.30	0.56	42.13	24.17	0.43
0.51	12.15	4.07	0.66	0.57	17.22	13.94	0.19	0.62	60.09	40.72	0.32
0.59	21.02	8.94	0.57	0.64	27.67	25.10	0.09	0.66	77.29	56.59	0.27
0.66	34.37	17.34	0.50	0.69	40.15	40.17	0.00	0.67	78.30	62.54	0.20
0.75	56.69	38.08	0.33	0.81	87.76	115.70	0.32	0.71	88.32	86.73	0.02
0.79	87.95	59.39	0.32					0.84	242.09	271.88	0.12
								0.96	593.96	966.54	0.63

H Conversion molarity to wt%

Table 46: Conversion from molarity to wt% for Derks et al.[5] and Liu et al.[6]

1.55 M PZ	13.35 wt%
3.75M MDEA	44.7 wt%
0.53 M PZ	4.57wt%
4.77 M MDEA	56.84 wt%
0.35 M PZ	3.01 wt%
3.15 M MDEA	37.53 wt%
1.35 M MDEA	16.09 wt%
0.7 M PZ	6.03 wt%
2.8 M MDEA	33.36 wt%
1.5 M PZ	12.92 wt%
0.5 M MDEA	5.96 wt%

I Additional VLE plots

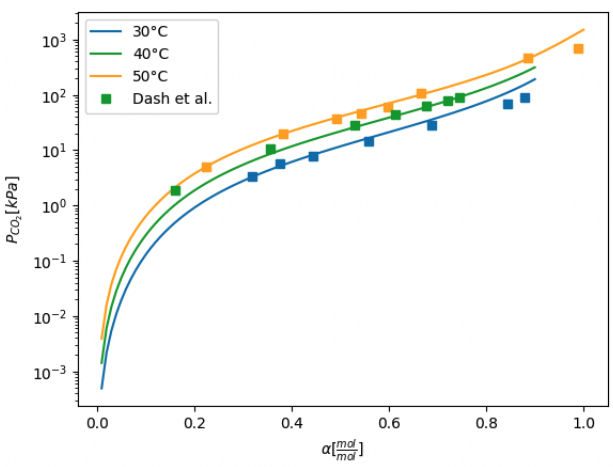

Figure 34: 28 wt% MDEA + 2wt% PZ

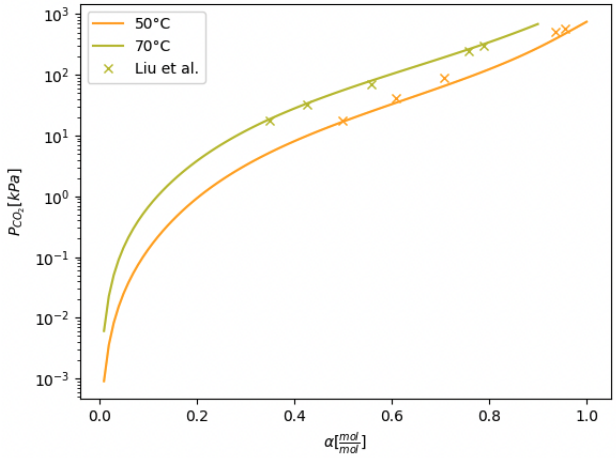

Figure 35: 16 wt% MDEA + 3 wt% PZ

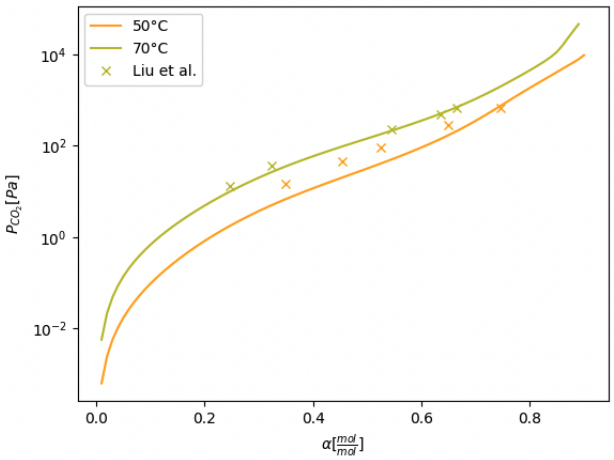

Figure 36: 44 wt% MDEA + 13 wt% PZ

J Additional parity plots

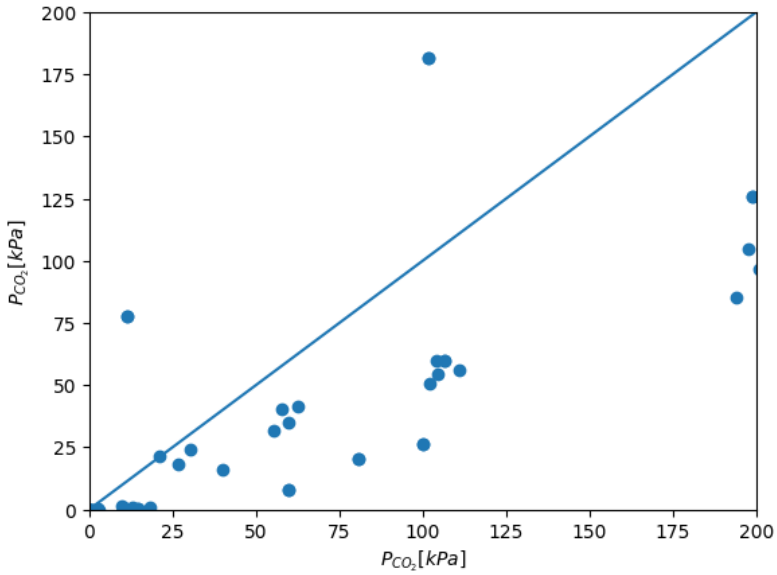

Figure 37: Parity plot for Mondal data zoomed in

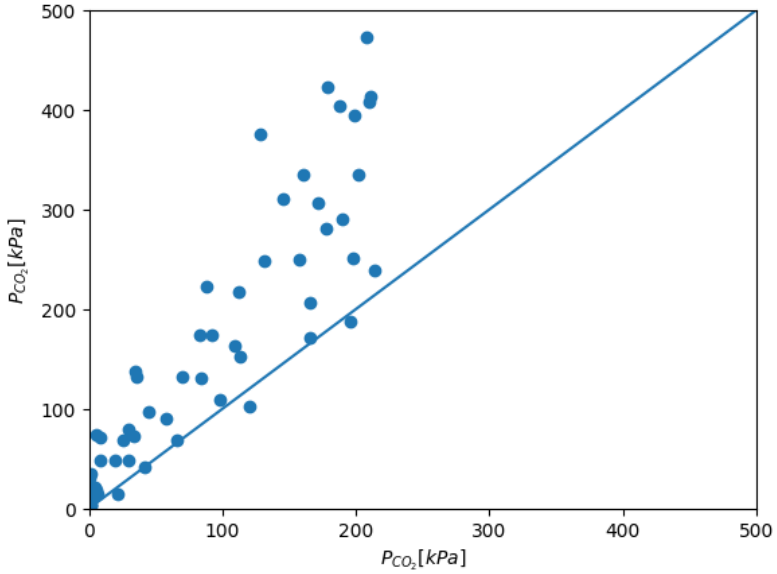

Figure 38: Parity plot for Song data zoomed in

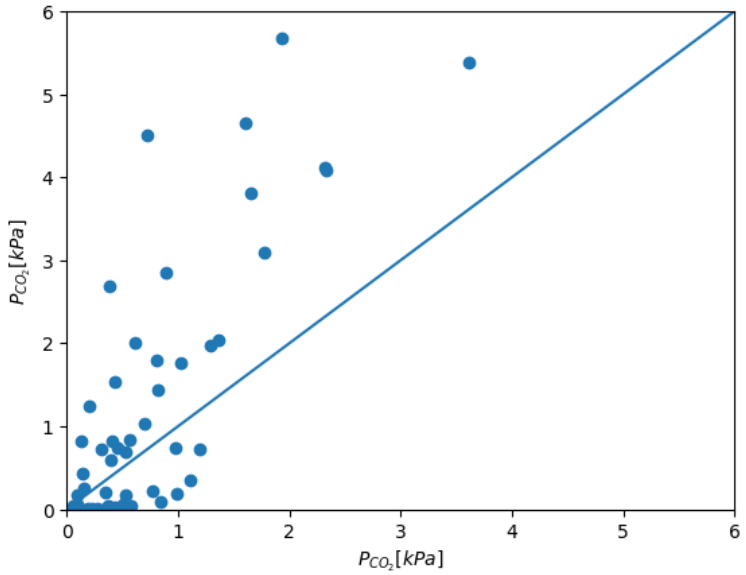

Figure 39: Parity plot for Portugal data zoomed in

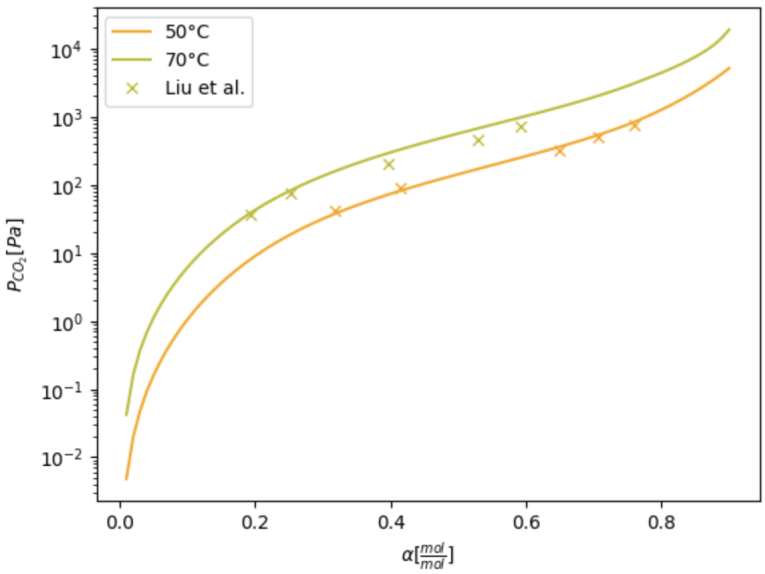

Figure 40: 56 wt% MDEA, 4 wt% PZ

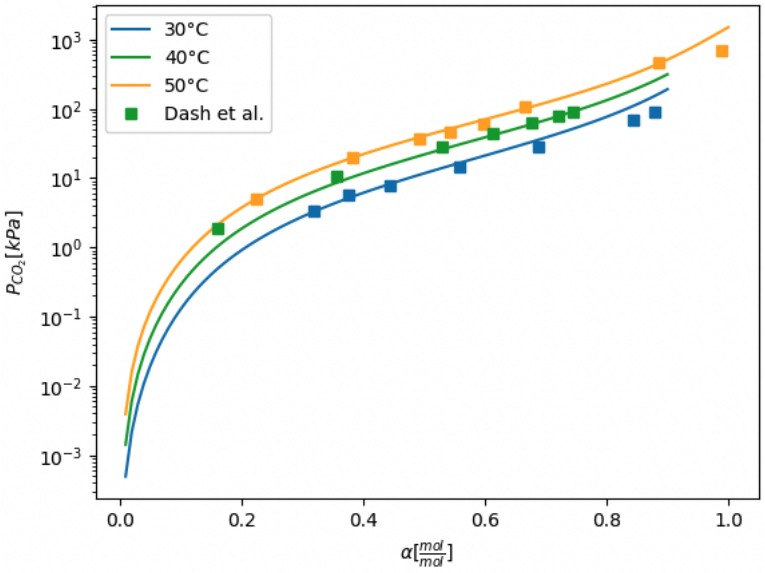

Figure 41: 28% MDEA, 2wt% PZ

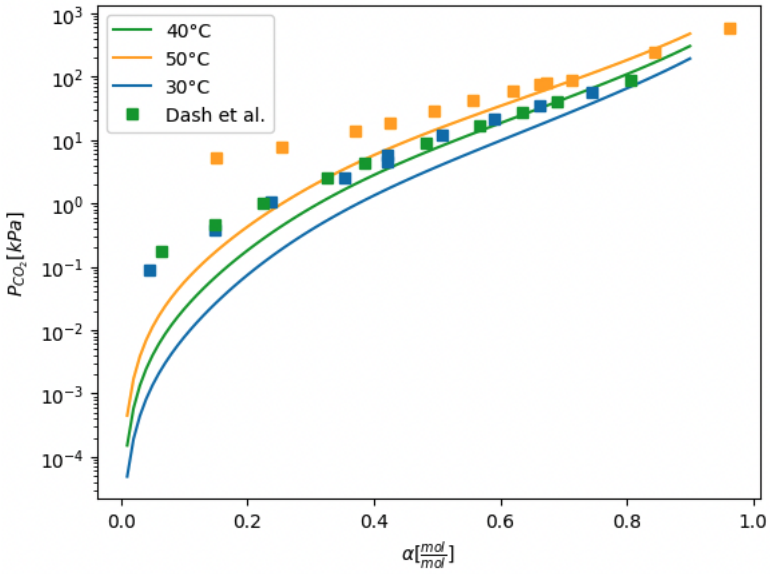

Figure 42: 22 wt% MDEA, 8 wt% PZ

K Flowsheets for process modifications

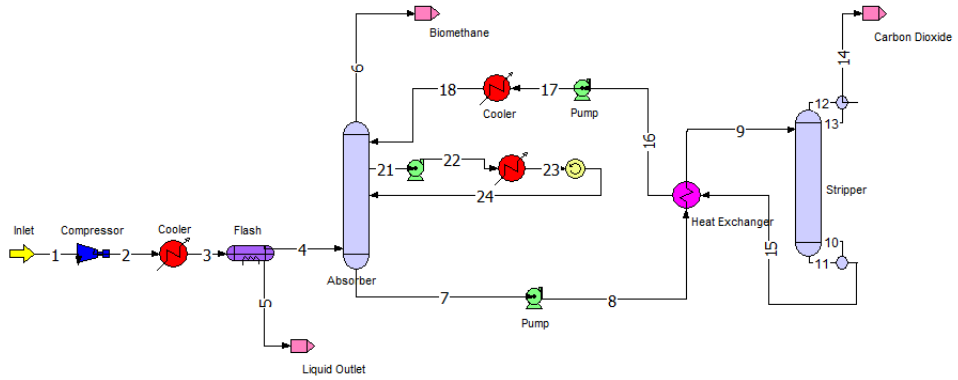

Figure 43: Flowsheet with 1 IC

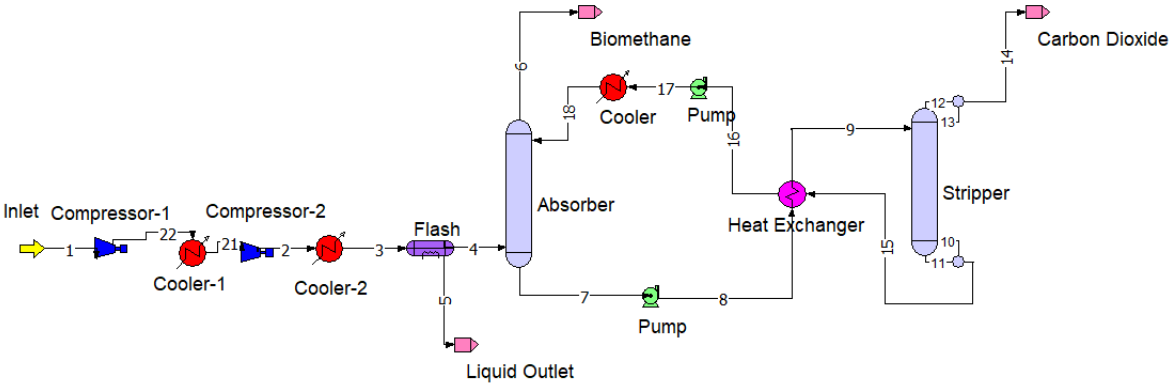

Figure 44: Two compressors in series with intercooling

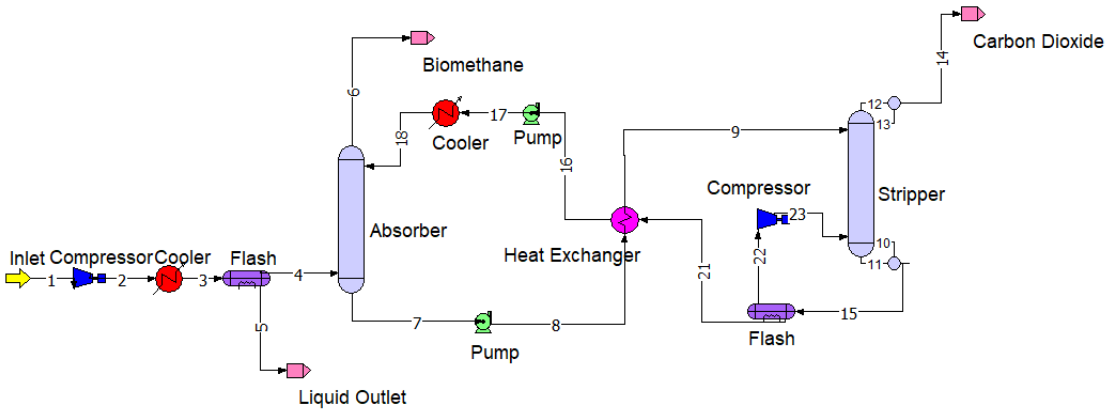

Figure 45: Flowsheet for lean vapor recompression

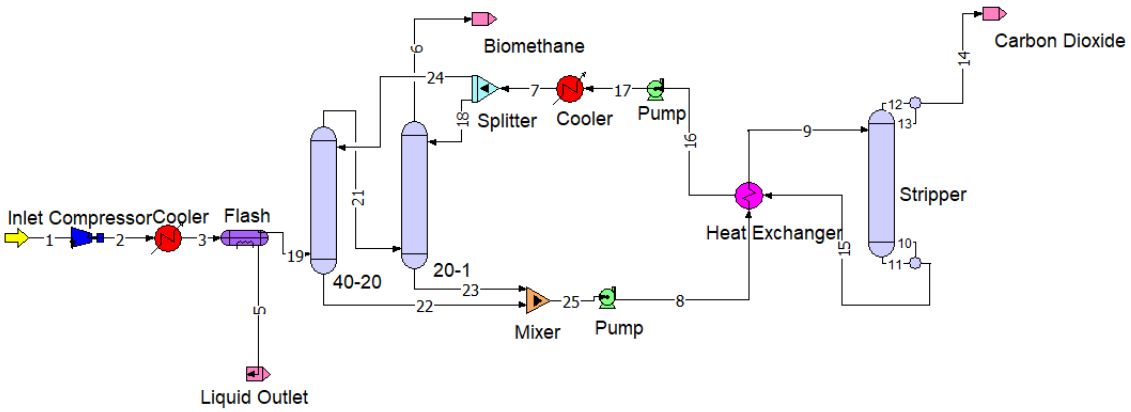

Figure 46: Flowsheet of split absorber

L Experimental data

L.1 Weight of chemicals for different solutions

The exact weight of chemicals used in the 35 wt% experiment can be found in Table 47.

Table 47: Weight of chemicals for solution preparation, 45wt%

45 wt%	Theoretical[g]	Experimental[g]	
		1	2
Glycine	34.803	34.73	34.79
NaOH	18.543	18.48	18.50
H_2O	46.650	46.64	46.61

The exact weight of chemicals used in the 35 wt% experiment can be found in Table 48

Table 48: Weight of chemicals for solution preparation, 35wt%

35 wt%	Theoretical[g]	Experimental[g]	
		1	2
Glycine	14.424	14.45	14.53
NaOH	58.51	58.51	58.56
H_2O	27.073	27.03	27.01

L.2 Visual Experimental

Figure 47: Precipitation in 35 wt% flasks left for 24h

L.3 Experimental results 45 wt%

Table 49: Experimental results from 45 wt%, round 1

No.	Time [min]	Weight increase [g]	Calc. CO_2 loading [mol/mol]	TOC loading [mol/mol]	Visual observation
1	1	1.815	0.116	0.134	Blank
2	2	1.243	0.198	0.219	Small particles
3	3	1.493	0.298	0.312	Small particles
4	4	1.326	0.392	0.377	Evidently particles
5	5	1.191	0.480	0.228	Foggy white
6	6	1.128	0.565	-	White and cloudy
7	7	0.582	0.613	-	White and cloudy
8	8	0.258	0.638	-	Thick white slurry
9	9	0.072	0.660	-	Thick white slurry
10	10	0.025	0.677	-	Thick white slurry

Table 50: Experimental results from 45 wt%, round 2

No.	Time [min]	Weight increase [g]	CO_2 loading [mol/mol]	TOC [ppm CO_2]	Visual observation
1	1	2.308	0.147	0.165	Blank
2	2	1.523	0.248	0.282	Small particles
3	3	1.685	0.363	0.387	Small particles
4	4	1.301	0.458	0.480	Evidently particles
5	5	1.358	0.559	0.563	Foggy white
6	6	0.665	0.614	-	White and cloudy
7	7	0.068	0.630	-	White and cloudy
8	8	0.046	0.646	-	Thick white slurry
9	17	0.138	0.674	-	Thick white slurry
10	27	0.07	0.704	-	Thick white slurry

L.4 Experimental results 35 wt%

Table 51: Experimental results from 35 wt%, round 1

No.	Time [min]	Δ Weight [g]	Calc. CO_2 loading [mol/mol]	TOC CO_2 loading [mol/mol]	Visual Observation
1	1	2.094	0.134	0.154	blank
2	2	1.54	0.236	0.268	blank
3	3	1.355	0.328	0.359	blank
4	4	0.97	0.398	0.402	blank
5	5	0.735	0.455	0.470	blank
6	6	0.373	0.487	0.488	blank
7	7	0.295	0.516	0.497	blank
8	8	0.203	0.538	0.508	blank
9	9	0.105	0.554	0.512	blank
10	12	0.26	0.583	0.547	blank
11	15	0.13	0.602	0.559	blank
12	20	0.142	0.622	0.580	blank
13	30	0.11	0.641	0.609	blank
14	40	0.043	0.656	0.616	blank
15	50	0	0.668	0.630	blank

Table 52: Experimental results from 35 wt%, round 2

No.	Time [min]	Δ Weight [g]	Calc. CO_2 loading [mol/mol]	TOC CO_2 loading [mol/mol]	Visual Observation
1	10	7.872	0.503	0.576	blank
2	20	0.001	0.510	0.601	blank
3	30	0.037	0.521	0.612	blank
4	40	0.043	0.553	0.607	blank
5	50	0.019	0.541	0.612	blank
6	60	0.009	-	0.623	blank

M NaGly simulations results

Table 53: Simulation results for base case

Boilup ratio	Reb. duty [MJ]	L/G	SRD [MJ/kg CO_2]	Lean [mol/mol]	Rich [mol/mol]
0.005	1.248	64.694	4.171	0.395	0.436
0.010	0.955	28.364	3.170	0.368	0.460
0.050	1.023	14.622	3.383	0.231	0.415
0.075	1.059	13.024	3.502	0.193	0.401
0.100	1.091	11.948	3.604	0.159	0.388
0.115	1.113	11.348	3.656	0.141	0.383
0.125	1.100	10.697	3.620	0.129	0.387
0.135	1.077	9.986	3.554	0.120	0.395
0.150	1.045	9.078	3.472	0.103	0.406
0.175	1.031	8.050	3.437	0.074	0.417
0.200	1.126	7.778	3.611	0.066	0.420
0.225	1.129	7.598	3.772	0.059	0.422
0.250	1.139	7.491	3.795	0.054	0.423
0.300	1.548	7.273	5.169	0.045	0.425

Table 54: Simulation results for IC=12m

Boilup ratio	Reb. duty [MJ]	L/G	SRD [MJ/kg CO_2]	Lean [mol/mol]	Rich [mol/mol]
0.005	1.223	62.919	4.154	0.396	0.437
0.008	0.939	32.208	3.128	0.395	0.476
0.010	0.850	22.920	2.702	0.385	0.499
0.020	0.857	15.805	2.819	0.328	0.496
0.030	0.866	13.258	2.861	0.293	0.494
0.050	0.885	11.063	2.928	0.249	0.491
0.075	0.903	9.790	2.978	0.212	0.488
0.100	0.913	8.951	3.015	0.182	0.486
0.125	0.919	8.262	3.038	0.153	0.484
0.135	0.922	8.015	3.039	0.142	0.485
0.150	0.912	7.558	3.025	0.125	0.488
0.175	0.905	6.914	3.009	0.090	0.491
0.200	0.934	6.472	3.114	0.066	0.493
0.225	1.027	6.374	3.424	0.060	0.493
0.250	1.124	6.307	3.745	0.054	0.492

Table 55: Simulation results for IC=4.5m

Boilup ratio	Reb. duty [MJ]	L/G	SRD [MJ/kg CO_2]	Lean [mol/mol]	Rich [mol/mol]
0.005	1.230	63.668	4.134	0.395	0.436
0.008	0.964	33.706	3.208	0.391	0.469
0.010	0.853	23.220	2.844	0.383	0.495
0.030	0.867	13.258	2.867	0.294	0.494
0.050	0.887	11.086	2.927	0.248	0.491
0.075	0.903	9.782	2.982	0.212	0.488
0.100	0.913	8.951	2.899	0.182	0.486
0.125	0.924	8.299	3.045	0.153	0.484
0.150	0.921	7.595	3.050	0.121	0.483
0.175	0.914	6.914	3.036	0.088	0.487
0.200	0.955	6.523	3.178	0.065	0.489
0.250	1.147	6.344	3.821	0.053	0.489

Table 56: Simulation results for IC=7m

Boilup ratio	Reb. duty [MJ]	L/G	SRD [MJ/kg CO_2]	Lean [mol/mol]	Rich [mol/mol]
0.005	1.233	63.670	4.178	0.396	0.436
0.008	0.953	32.959	3.126	0.393	0.472
0.010	0.858	23.071	2.840	0.386	0.498
0.030	0.868	13.273	2.864	0.293	0.494
0.050	0.886	11.071	2.928	0.249	0.491
0.075	0.903	9.790	2.979	0.212	0.488
0.100	0.913	8.959	3.013	0.182	0.486
0.125	0.919	8.270	3.037	0.153	0.484
0.150	0.917	7.581	3.038	0.123	0.486
0.175	0.909	6.921	3.018	0.091	0.490
0.200	0.941	6.487	3.135	0.066	0.491
0.225	1.037	6.397	3.452	0.059	0.492
0.250	1.130	6.315	3.764	0.054	0.492

Table 57: Simulation results for IC=2.5m

Boilup ratio	Reb. duty [MJ]	L/G	SRD [MJ/kg CO_2]	Lean [mol/mol]	Rich [mol/mol]
0.050	1.238	64.417	4.159	0.395	0.435
0.008	0.978	34.455	3.248	0.390	0.466
0.010	0.886	23.145	2.947	0.379	0.485
0.030	0.879	13.632	2.907	0.291	0.487
0.050	0.893	11.235	2.953	0.248	0.487
0.075	0.905	9.842	2.992	0.211	0.486
0.100	0.915	8.988	3.023	0.182	0.484
0.125	0.927	8.337	3.050	0.153	0.482
0.150	0.929	7.640	3.071	0.120	0.480
0.200	1.000	6.666	3.309	0.062	0.480
0.250	1.212	6.517	3.997	0.051	0.480

Table 58: Simulation results for IC=2.5m

Boilup ratio	Reb. duty [MJ]	L/G	SRD [MJ/kg CO_2]	Lean [mol/mol]	Rich [mol/mol]
0.050	1.238	64.417	4.158	0.395	0.435
0.008	0.978	34.455	3.249	0.390	0.466
0.010	0.859	23.100	2.828	0.385	0.499
0.030	0.868	13.288	2.859	0.293	0.494
0.050	0.888	11.101	2.925	0.249	0.491
0.075	0.907	9.827	2.978	0.212	0.489
0.100	0.918	8.988	3.017	0.182	0.486
0.125	0.920	8.277	3.036	0.153	0.484
0.150	0.912	7.565	3.024	0.126	0.489
0.200	0.933	6.472	3.108	0.066	0.493
0.250	1.120	6.292	3.736	0.054	0.493

Table 59: Simulation results for 2 absorber system. no IC

Boilup ratio	Reb. duty [MJ]	L/G	SRD [MJ/kg CO_2]	Lean [mol/mol]	Rich [mol/mol]
0.006	1.070	46.061	3.571	0.392	0.450
0.020	0.986	27.637	3.234	0.352	0.450
0.017	0.983	23.031	3.229	0.323	0.441
0.024	0.996	19.960	3.271	0.294	0.431
0.050	1.042	15.467	3.423	0.230	0.409
0.075	1.077	13.690	3.550	0.192	0.396
0.100	1.109	12.526	3.660	0.158	0.382
0.125	1.088	10.881	3.599	0.130	0.389
0.150	1.074	9.557	3.564	0.103	0.399
0.175	1.144	8.970	3.801	0.086	0.401
0.200	1.252	8.693	4.160	0.076	0.402
0.250	1.478	8.323	4.913	0.063	0.404

Table 60: Simulation results for 2 absorber system. IC=4

Boilup ratio	Reb. duty [MJ]	L/G	SRD [MJ/kg CO_2]	Lean [mol/mol]	Rich [mol/mol]
0.007	1.067	43.727	3.517	0.395	0.456
0.008	0.983	35.114	3.236	0.393	0.469
0.010	0.945	28.189	3.123	0.372	0.468
0.030	0.946	16.152	3.130	0.282	0.451
0.050	0.966	13.399	3.192	0.239	0.445
0.075	0.969	11.351	3.205	0.204	0.449
0.100	0.971	10.149	3.202	0.175	0.450
0.125	0.974	9.253	3.228	0.146	0.449
0.150	0.977	8.429	3.232	0.114	0.449
0.250	1.280	7.405	4.240	0.063	0.447

Table 61: Simulation results for 2 absorber system. 2 IC=2.5m

Boilup ratio	Reb. duty [MJ]	L/G	SRD [MJ/kg CO_2]	Lean [mol/mol]	Rich [mol/mol]
0.007	1.110	45.630	3.629	0.393	0.452
0.008	0.956	33.471	3.172	0.396	0.476
0.025	0.885	15.430	2.926	0.306	0.482
0.050	0.909	11.882	3.000	0.247	0.478
0.075	0.926	10.496	3.055	0.209	0.474
0.100	0.939	9.613	3.101	0.179	0.469
0.125	0.953	8.928	3.144	0.149	0.464
0.150	0.965	8.248	3.183	0.115	0.458
0.175	1.010	7.724	3.335	0.086	0.455
0.200	1.111	7.531	3.669	0.075	0.454
0.250	1.330	7.311	4.394	0.062	0.452
0.300	1.552	7.161	5.138	0.053	0.451

Table 62: Simulation results for LVR

Boilup ratio	Reb. duty [MJ]	L/G	SRD [MJ/kg CO_2]	Lean [mol/mol]	Rich [mol/mol]
0.030	0.930	16.152	3.070	0.255	0.426
0.050	0.946	13.917	3.118	0.210	0.410
0.075	0.961	12.478	3.176	0.171	0.395
0.100	0.972	11.287	3.211	0.134	0.384
0.125	0.937	9.528	3.110	0.105	0.401
0.150	0.965	8.561	3.212	0.083	0.412
0.175	1.067	8.234	3.552	0.073	0.416
0.200	1.178	8.023	3.924	0.066	0.419
0.250	1.408	7.760	4.685	0.056	0.422
0.200	1.111	7.531	3.669	0.075	0.454
0.250	1.330	7.311	4.394	0.062	0.452

N Activated MDEA simulations results

Table 63: 1.05 bara case

Boilup ratio	Reb. duty [MJ]	L/G	SRD [MJ/kg CO_2]	Lean [mol/mol]	Rich [mol/mol]
0.024	0.650	14.983	2.151	0.331	0.505
0.030	0.545	10.271	1.796	0.343	0.597
0.040	0.521	7.896	1.716	0.302	0.636
0.050	0.536	7.169	1.768	0.260	0.629
0.075	0.561	6.292	1.853	0.192	0.619
0.100	0.579	5.842	1.915	0.147	0.610
0.125	0.599	5.517	1.978	0.109	0.603
0.150	0.608	5.228	2.004	0.070	0.610
0.175	0.606	4.646	2.003	0.029	0.624
0.200	0.673	4.556	2.236	0.020	0.626
0.250	0.828	4.512	2.753	0.016	0.627

Table 64: 3 bara case

Boilup ratio	Reb. duty [MJ]	L/G	SRD [MJ/kg CO_2]	Lean [mol/mol]	Rich [mol/mol]
0.010	0.882	45.872	2.935	0.429	0.486
0.025	0.500	10.775	1.657	0.425	0.669
0.028	0.480	9.236	1.592	0.415	0.700
0.030	0.452	8.158	1.492	0.419	0.742
0.330	0.458	7.697	1.504	0.398	0.742
0.050	0.481	6.170	1.587	0.295	0.733
0.075	0.508	5.402	1.672	0.216	0.725
0.100	0.525	5.028	1.731	0.127	0.720
0.125	0.540	4.791	1.777	0.131	0.716
0.200	0.623	4.202	2.051	0.020	0.701

Table 65: 5 bara case

Boilup ratio	Reb. duty [MJ]	L/G	SRD [MJ/kg CO_2]	Lean [mol/mol]	Rich [mol/mol]
0.019	0.565	15.392	1.869	0.459	0.629
0.023	0.480	10.774	1.588	0.465	0.707
0.025	0.450	9.235	1.478	0.472	0.755
0.030	0.435	7.611	1.437	0.441	0.785
0.050	0.465	5.803	1.533	0.311	0.775
0.075	0.491	5.064	1.620	0.226	0.767
0.100	0.510	4.737	1.680	0.176	0.761
0.12	0.524	4.521	1.725	0.139	0.757
0.150	0.536	4.325	1.766	0.102	0.752
0.200	0.589	3.968	1.942	0.021	0.740

Table 66: 8 bara case

Boilup ratio	Reb. duty [MJ]	L/G	SRD [MJ/kg CO_2]	Lean [mol/mol]	Rich [mol/mol]
0.017	0.537	15.392	1.779	0.501	0.670
0.022	0.470	10.774	1.555	0.503	0.743
0.027	0.410	7.696	1.346	0.485	0.823
0.030	0.414	7.196	1.367	0.459	0.822
0.050	0.451	5.510	1.488	0.324	0.811
0.100	0.497	4.510	1.639	0.182	0.796
0.125	0.510	4.310	1.683	0.145	0.791

O Optimized flowsheet

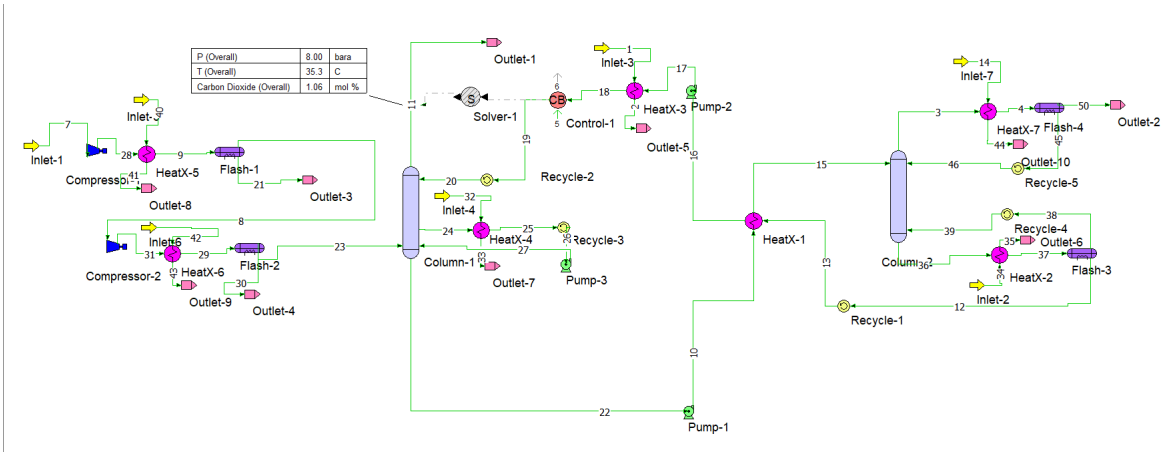

Figure 48: Flowsheet for optimized case, showing 8 bara case

P CAPEX

Table 67: S-values for 8 bara case

Process Unit	Name				
Heat Exchangers		area[m^2]			
	HX1 - real	134.8			
	HX2 - lean	3.3			
	HX3 - reboiler	9.6			
	HX4 - IC	35.0			
	HX5 - inlet 1	3.0			
	HX6 - inlet 2	2.8			
	HX7 - condenser	1.5			
Shell mass		d[m]	L[m]	t_w[m]	mass[kg]
	Absorber	0.7	11.2	0 .008	1576
	Absorber, sump	0.7	4.5	0.008	633
	Stripper	0.5	6.4	0.01	804
	Sump, stripper	0.5	9	0.001	1130.4
	Flash 1 - inlet 1	0.168	0.589	0.008	19.9
	Flash 2 - inlet 2	0.14	0.48	0.008	13.0
	Flash 3 - reboiler	0.97	3.40	0.01	827.5
	Flash 4 - condenser	0.13	0.46	0.01	16.6
Packing		Height[m]	Area [m^2]	Volume [m^3]	
	Absorber	7	0.39	2.7	
	Stripper	4	0.2	0.79	
Compressors		Flow m^3			
	Compressor 1 - inlet 1	1500			
	Compressor 2 - inlet 2	1500			
Pumps		Power [kW]			
	Pump 1 - rich	1.1			
	Pump 2 - lean	3.6			
	Pump 3	0.0015			

Table 68: S-values for 1.05 bara case

Process Unit	Name				
Heat Exchangers		area[m^2]			
	HX1 - real	178.1			
	HX2 - lean heater	0.30			
	HX3 - reboiler	24.8			
	HX4 -IC	45.1			
	HX5 - inlet	0.36			
	HX6 - condenser	4.3			
Shell mass		d[m]	L[m]	t_w[m]	mass[kg]
	Absorber	0.7	19.2	0.008	2701
	Absorber, sump	0.7	5.2	0.008	732
	Stripper	0.5	6.4	0.01	804
	Sump, stripper	0.5	10.5	0.01	1319
	Flash 1 - inlet	0.072	0.252	0.008	3.64
	Flash 2 - condenser	0.21	0.734	0.01	38.7
Packing		Height [m]	Area [m^2]	Volume [m^3]	
	Absorber	12	0.39	4.62	
	Stripper	4	0.2	0.79	
Compressors		Flow m^3			
	Compressor 1 - inlet	1500			
Pumps		Power [kW]			
	Pump 1 - Rich	2.8			
	Pump 2 - Lean	0.124			
	Pump 3 - IC	0.568			

P.1 Fixed capital cost

Table 69: Fixed Capital Costs

Case	ISBL	OSBL	D&E	X	FCC
1.05	8.44	1.27	2.91	0.84	14.36
8	9.50	1.42	3.28	0.95	15.15

P.2 Coolers

$$Q = mC_p\Delta T \tag{12}$$

The ΔT used was 10°C, with 20°C of the cooling water and a Cp of 4186.8 J/kg-K, and Q was obtained from ProTreat. The heat transfer coefficient used was U=800 W/m^{2}K.

P.3 Absorber, stripper and flash tanks

$$\text{Shell mass} = \pi L_c D_c t_w \rho \tag{13}$$

P.4 Reboiler

Specific enthalpy for steam was obtained from a steam table for 145 °C, 4 bara was 2738 kJ/kg. The mass stream of steam was calculated based on the required reboiler duty and the specific enthalpy.

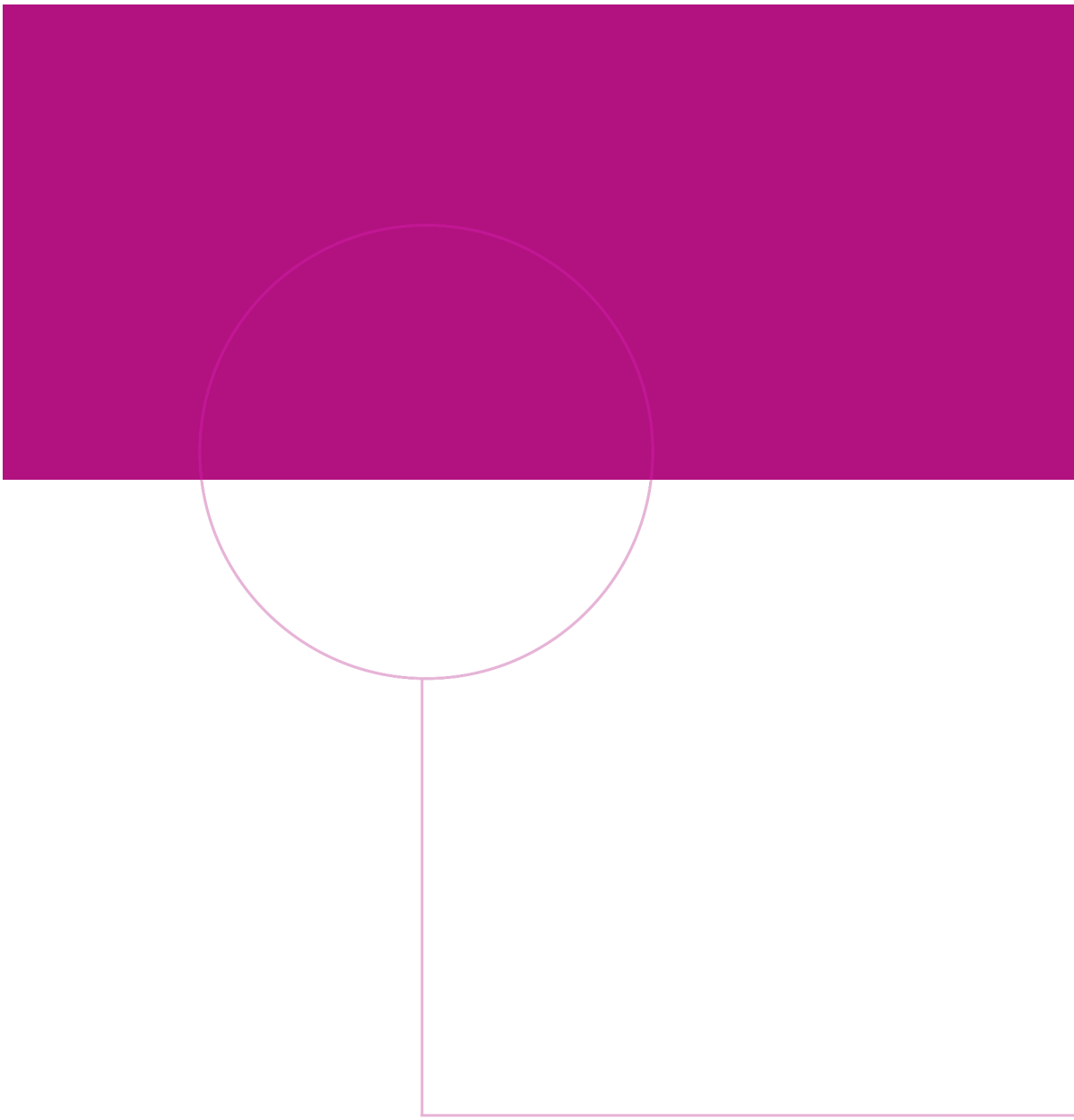

NTNU

Norwegian University of
Science and Technology